

Portland State University

PDXScholar

Dissertations and Theses

Dissertations and Theses

10-27-2008

Methodology for Developing a Functional Multiscale Architecture Model System Towards Future Integrated Circuits

Yamini Yadov

Portland State University

Follow this and additional works at: https://pdxscholar.library.pdx.edu/open_access_etds



Part of the [Electrical and Computer Engineering Commons](#)

Let us know how access to this document benefits you.

Recommended Citation

Yadov, Yamini, "Methodology for Developing a Functional Multiscale Architecture Model System Towards Future Integrated Circuits" (2008). *Dissertations and Theses*. Paper 6053.

<https://doi.org/10.15760/etd.7923>

This Dissertation is brought to you for free and open access. It has been accepted for inclusion in Dissertations and Theses by an authorized administrator of PDXScholar. Please contact us if we can make this document more accessible: pdxscholar@pdx.edu.

METHODOLOGY FOR DEVELOPING A FUNCTIONAL MULTISCALE
ARCHITECTURE MODEL SYSTEM TOWARDS FUTURE INTEGRATED
CIRCUITS

by

YAMINI YADAV

A dissertation submitted in partial fulfillment of the
requirements for the degree of


DOCTOR OF PHILOSOPHY
in
ELECTRICAL AND COMPUTER ENGINEERING


Portland State University
2009

DISSERTATION APPROVAL

The abstract and dissertation of Yamini Yadav for the Doctor of Philosophy in Electrical and Computer Engineering were presented October 27, 2008, and accepted by the dissertation committee and the doctoral program.

COMMITTEE APPROVALS:

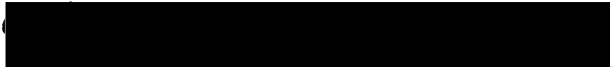

Shalini Prasad, Chair


Xiaoyu Song



James Morris


Branimir Pejcinovic


Graham Howard


Elizabeth ~~Wosley~~-George
Representative of the Office of Graduate Studies

DOCTORAL PROGRAM APPROVAL:


Malgorzata Chrzanowska-Jeske, Director
Electrical and Computer Engineering
Ph.D. Program

ABSTRACT

An abstract of the dissertation of Yamini Yadav for the Doctor of Philosophy in Electrical and Computer Engineering presented October 27, 2008.

Title: Methodology for Developing a Functional Multiscale Architecture Model System towards Future Integrated Circuits.

Detection of the biochemical species in the environmental pollution, industrial emission monitoring, medical diagnosis, public security, agriculture and a variety of industries has resulted in the emerging need for a generation of high density nanostructured sensor arrays. The fundamental two terminal and three terminal device components because of their potential for specificity eventually have to be integrated into miniaturized and portable nanoarray sensors. One of the key components in these nanosensors is the development of building functional building blocks that improve device performance capabilities. This research is focused on methodology for developing fundamental, functional, multiscale architecture model system for generating high density nanoscale two terminal structures for future integrated circuits for sensor applications. The key idea is to design and characterize a nanomaterial junction array that can demonstrate diode like electrical behavior. A hybrid methodology for fabricating this basic nanoelectronic building block, its performance capabilities and its limitations is presented. A soft lithography and standard photolithography techniques are integrated in assembling nanomaterial composites of

p- and n- type material to form a junction, which are characterized by using standard electrical characterization methods.

ACKNOWLEDGEMENTS

Since 2006, it has been three years in Portland State University; journey to accomplish my dreams was exciting and adventurous. This adventurous journey would have been impossible without immeasurable support and help from my professors and colleagues who were my companions in my voyage.

First, I would like to sincerely thank Prof. Shalini Prasad, my advisor who gave me the honor to work with her at BMNL. Without her direction and unconditional support, it would have been impossible to complete my program. She continually stimulated my analytical thinking, helped me cultivate research aptitude, and greatly assisted me with scientific writing to convey my research in most logical and thoughtfully organized manner. She always encouraged me to perform a step beyond my capability for my research. I highly appreciate the opportunity to present my work at various international and regional conferences and the work on my dissertation serves as a great foundation for my career goals. It has been a continual learning experience working with her for last three years. Dr. Prasad thank you for everything I learnt from you.

I would also like to express my gratitude to my co-advisor Prof. Xiaoyu Song for his generous time and encouragement that helped me achieves all hurdles throughout my Ph. D. program successfully. He constantly provided guidelines in my research. I would also like to thank Prof. James Morris for his assistance, generosity, and advice, he provided time to time. It was great pleasure and a learning experience to work with

him. He gave me my first break to write the chapters in his book. I am also thankful to him for allowing me to use his laboratory resources and equipments.

I also thank Prof. Branimir Pejcinovic who agreed to participate in the examining committee and for his valuable advice on concepts of device analysis and simulation. Thank you for being approachable and accommodative. I am also very grateful for having an exceptional doctoral committee and wish to thank Prof. Elizabeth Wosley_George and Prof. Graham Howard for their continual support and encouragement. My gratitude is also due to Prof. Sanchez who assisted me to use his laboratory resources and always gave valuable inputs to my research.

Thanks to Brent for tolerating my incessant visits and being ever patient while answering all my recursive questions on university rules and policies. I am very grateful to all my colleagues at BMNL. The atmosphere has always been a perfect source of motivation. I enjoyed excellent working climate and many fruitful discussions. I also enjoyed nice evenings out with my colleague Bhuwan, Prasanna, Manish, Vindya and Vinu after lab meeting every week. I will always have these as my special memories. I also thank Sailaja and Mohan who were always willing to help and discuss topics in my research. In addition, I would like to show my appreciation to my friend Shashi in Texas for his creative skills in art and graphics who gave priceless ingenious suggestions to my presentations and conference posters. Finally, I express my gratitude to all the people whose anonymous contributions were significant to this dissertation and I extend my thanks to all the people whose names are not mentioned.

Last but not the least; I would like to thank my family members for their ongoing support, patience, and encouragement throughout the PhD program.

TABLE OF CONTENTS

ACKNOWLEDGEMENTS	i
LIST OF TABLES	viii
LIST OF FIGURES.....	ix
LIST OF ABBREVIATIONS	xiii
CHAPTER 1.....	1
DISSERTATION OBJECTIVE.....	1
1.1 Innovative contributions.....	2
1.2 Applications	3
1.3 Analytical and experimental contributions	4
1.4 Material System	5
1.5 Motivation	5
1.6 Current Limitations and Key Innovations.....	7
CHAPTER 2.....	11
INTRODUCTION.....	11
2.1 Role of nanomaterials	11
2.2 Nanodevice architecture.....	12
2.3 Architectural model system.....	14
2.4 Lithography	15
2.4.1 Introduction	15
2.4.2 Photolithography	16
Photoresists	18
Coating process.....	21

Exposure	23
Development.....	24
Post-exposure baking.....	25
Etching and resist stripping.....	25
2.4.3 Electron beam lithography	25
2.4.4 Soft lithography	28
Micro-transfer molding (μ TM)	30
Micromolding in capillaries (MIMIC).....	31
Micro-replica molding (REM).....	33
2.5 Patterning and alignment techniques	36
2.5.1 Langmuir Blodgett method.....	36
2.5.2 Superlattices nanowires pattern transfer (SNAP).....	37
2.5.3 Atomic force microscopy	38
2.5.4 Electrophoresis	39
2.5.5 Fluidic alignment.....	40
2.6 Nanomaterials	41
2.6.1 Carbon nanotube.....	41
Properties of CNTs	41
Uses of carbon nanotubes	43
Classification of CNTs.....	45
2.6.2 Nanowires.....	47
2.6.3 Molecular semiconductors.....	48
2.7 Method for synthesis of extrinsic nanomaterials	51

2.7.1 Ion Implantation	51
2.7.2 Surface diffusion	55
2.7.3 Electrostatic and chemical doping	56
CHAPTER 3.....	58
MATERIALS AND METHODS	58
3.1 Synthesis of extrinsic nanomaterials	59
3.2 Microelectrode array	66
3.3 Mask design for microelectrode array fabrication	70
3.4 Stamp fabrication	75
3.5 Patterning nanomaterials	77
3.6 Instrumentation	79
CHAPTER 4.....	84
RESULTS AND DISCUSSION	84
4.1 Microelectrode array characterization.....	84
4.2 PDMS stamp characterization.....	90
4.3 Patterned CNT characterization	93
4.4 CNT device characterization.....	97
4.4.1 Multiwalled carbon nanotube device.....	98
4.4.2 Single walled carbon nanotube device	105
4.5 Modeling Results	110
CHAPTER 5.....	120
CONCLUSION AND FUTURE WORK.....	120

REFERENCES.....	124
APPENDIX A Operating Instructional Manual.....	138

LIST OF TABLES

Table 1: Difference between negative and positive photoresist.....	21
Table 2: List of p-type and n-type molecular/polymeric organic semiconductors	50
Table 3: Table representing parameters for fabrication process.	69
Table 4: List of different materials and equipments exploited and utilized.....	81

LIST OF FIGURES

Figure 1.1: A pictorial representation of state-of-the-art technique for developing functional multiscale architecture model system towards future integrated circuits.	1
Figure 2.1: Classification of nanoelectronic components.	12
Figure 2.2: Conceptual representation of model-system for fabrication of crossbar junction.	14
Figure 2.3: Schematic representation of lithography process.	18
Figure 2.4: Schematic demonstration of difference between positive and negative photoresist during exposure and development process.	20
Figure 2.5: Figure illustrates the experimental set-up for spin coating photoresist.	23
Figure 2.6: Electromagnetic spectrum showing operating range of frequency for optical lithography.	24
Figure 2.7: Schematic representation of process sequence in micro-transfer molding (μ TM).	30
Figure 2.8: Schematic representation of process sequence in MIMIC.	32
Figure 2.9: Schematic representation of process sequence in micro-replica molding (REM).	34
Figure 2.10: The schematic representation of unit cell of graphene sheet for zigzag and chiral structure.	46
Figure 2.11: Schematic carbon nanotube device structure fabricated using (a) electrostatic and (b) chemical doping.	56
Figure 3.1: Surfactant molecules on the SWCNTs.	63

Figure 3.2: Band diagram of surfactant coated carbon nanotubes.	64
Figure 3.3: SEM characterization of surfactant and CNTs coated with surfactant.....	65
Figure 3.4: EDX characterization of surface functionalized CNTs.	66
Figure 3.5: Schematic representation of process sequence for microfabrication of the base microelectrode array platform.....	68
Figure 3.6: Schematic autocad design of microelectrode array	70
Figure 3.7: Schematic auto cad design. (a) 1 x 2 microelectrode array and (b) 2 x 2 microelectrode array.....	71
Figure 3.8: Microelectrodes are designed such that the smallest feature is greater than or equal to 50 μm in dimensions.....	73
Figure 3.9: Snapshot of mask design.	74
Figure 3.10: Schematic representation of process sequence for microfabrication of PDMS stamp.	76
Figure 3.11: Schematic autocad mask design consists of parallel array for fabrication of PDMS master template.	77
Figure 3.12: Schematic representation of process sequence for patterning nanomaterials via microcontact printing.....	78
Figure 3.13: Snapshot of PDMS stamp.....	79
Figure 3.14: Schematic representation of the experimental set-up used for the electrical characterization of microelectrode array.....	80
Figure 4.1: Optical micrographs of microelectrode array platform at various stages of microfabrication process sequence.....	86

Figure 4.2: Optical micrographs of 1 x 2 and 2 x 2 microelectrode array platform at different stages of lithography process.	87
Figure 4.3: Optical image of microelectrode array after pattern development	88
Figure 4.4: Nanodomain analysis and characterization of microelectrode platform using SEM.	89
Figure 4.5: EDX characterization of microelectrode array	90
Figure 4.6: Optical characterization of PDMS stamp.	91
Figure 4.7: Vertical cross section of PDMS stamps.	92
Figure 4.8: Schematic representation of single p-n junction using nanomaterials.....	93
Figure 4.9: Optical characteristics of assembled junction.	94
Figure 4.10: Optical and SEM image of patterned carbon nanotube.	95
Figure 4.11: SEM characteristics of patterned CNTs using microcontact printing. (a) Parallel array of CNTs and (b) Crossbar junction formation.	96
Figure 4.12: AFM images of patterned CNT onto the micro-electrode array. Repetitive parallel patterns of inked carbon nanotubes are observed.	97
Figure 4.13: I-V characteristics illustrating junction formation.....	101
Figure 4.14: The graph is the I-V characteristic to electrically characterize the effect of passivation of a single device on a chip.	103
Figure 4.15: The data illustrating comparison study of patterned CNTs vs randomly dispersed mixed CTAB-CNTs and SDS-CNTs	107
Figure 4.16: The data illustrates formation of P-N ionic junction when patterned and assembled using CTAB-CNTs and SDS-CNTs.	108

Figure 4.17: The graph illustrates the junction behavior irrespective of P-type or N-type stamped earlier.	109
Figure 4.18: Semi log plot of I–V characteristics of a SWNT ionic junction.....	113
Figure 4.19: I–V characteristics showing polynomial trendline with equation for crossbar junctions, fit curve and ideal diode curves.....	114
Figure 4.20: Schematic representation of P-N junction and band energy diagram. ..	117
Figure.5.1: A pictorial representation of a generic approach for assembling and patterning nanomaterial using microcontact printing.....	120

LIST OF ABBREVIATIONS

AFM – Atomic Force Microscopy

Au – Gold

Ag – Silver

BNC – Bayonet Neill Concelman

Br⁻ – Bromide Ion

CCD – Charge-Coupled Device

CNTs – Carbon Nanotubes

Cr – Chromium

Cu – Copper

CTAB – Cetyl Trimethylammonium Bromide

DI – Deionized Water

EBL – Electron Beam Lithography

EDX – Energy-Dispersive X-ray

Ge – Germanium

GPa – Giga Pascal

GPIB – General Purpose Interface Bus

IPA – Isopropyl Alcohol

I-V – Current - Voltage

FETs – Field Effect Transistors

LB – Langmuir Blodgett

LED – Light Emitting Diode

LOR – Lift- Off Resist

MEA – Microelectrode Array

MEMS – Micro-Electro-Mechanical Systems

MIMIC – Micromolding in Capillaries

MOSFETs – Metal–Oxide–Semiconductor Field-Effect Transistors

MWCNTs – Multiwalled Carbon Nanotubes

N₂ – Nitrogen Gas

Na⁺ – Sodium Ion

OFETs – Organic Field-Effect Transistors

PDMS – Polydimethylsiloxane

REM – Micro-Replica Molding

SAM – Self Assembled Monolayer

SDS – Sodium Dodecyl Sulfate

SEM – Scanning Electron Microscope

Si – Silicon

SNAP – Superlattices Nanowires Pattern Transfer

SWCNTs – Single Walled Carbon Nanotubes

UV – Ultra Violet

μTM – Micro-Transfer Molding

μCP – Microcontact Printing

CHAPTER 1
DISSERTATION OBJECTIVE

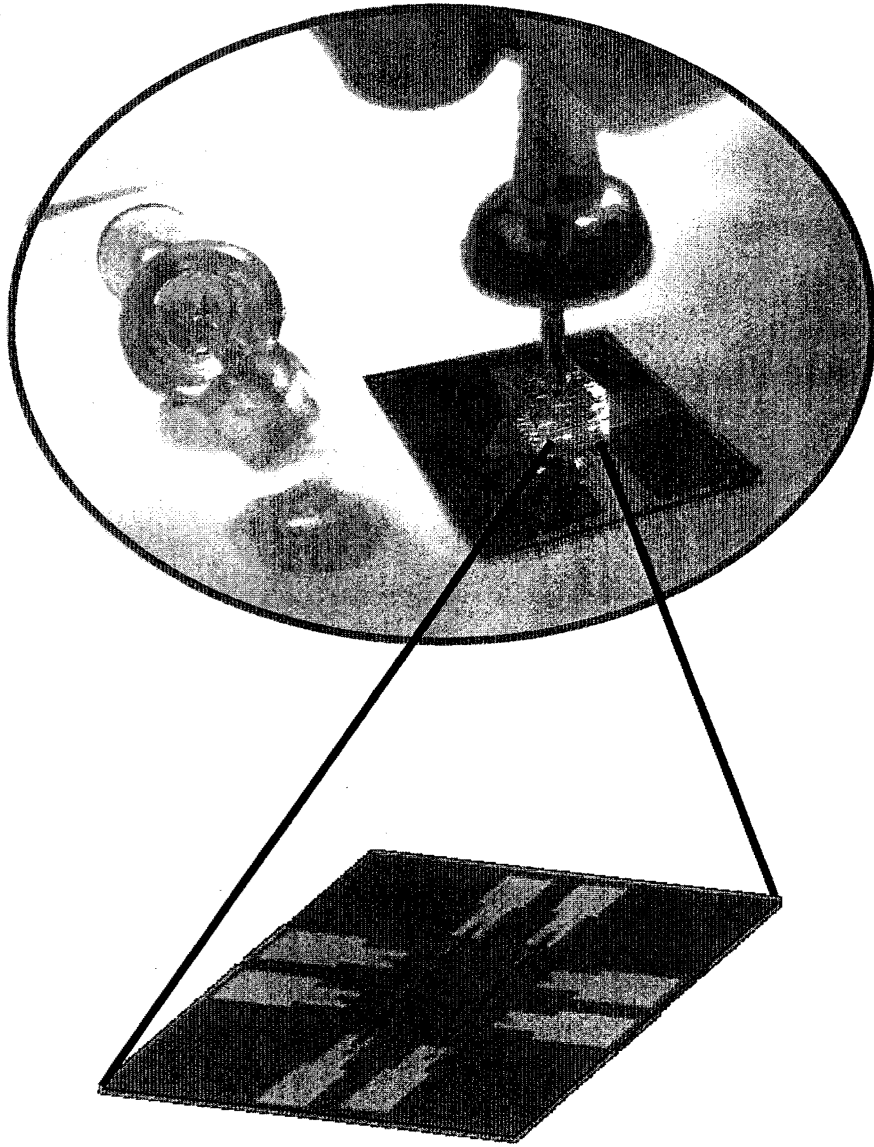


Figure 1.1: A pictorial representation of state-of-the-art technique for developing functional multiscale architecture model system towards future integrated circuits.

The key objective of my dissertation is to fabricate ionically functionalized nanomaterials based multiarray structure crossbar junction that has potential applicability in developing highly dense nanostructured array for miniature and portable biochemical sensors. The functional ionic crossbar nanomaterial junction was achieved by integrating soft and photolithography techniques.

The main focus of the dissertation is to adopt a simple, rapid and cost effective microcontact printing and dispersion method for patterning and doping nanomaterials. Figure 1 shows the state of the art technique for building miniaturized building blocks for electronic devices. In the following sections, key innovations, research contributions, current limitations and potential solutions for overcoming these limitations are described.

1.1 Innovative contributions

- Generation of ionically doped nanomaterials with similar fermi characteristics as standard semiconducting nanomaterial
- A hybrid methodology for building fundamental model systems designed for potential high end applications
- High throughput method to improve productivity for fabricating nanomaterial based future integrated sensor circuits
- Cost effective, rapid, and large scale production technique that opens new field of applications
- Development of nanojunction array towards future biochemical sensor devices.

- Portable and environmental benign green fabrication technique as compared to standard semiconductor processing techniques.
- Integrated various material systems, spanned multiple orders and scaled device architecture to built functional microelectronic structures.
- Instigate this technology for rapid production of multiple lines of nanomaterials for building microelectronic systems.

1.2 Applications

- In contrast to conventional nanomaterial fabrication technique that requires class 1000 clean room this technique can be implemented in a wet chemistry lab
- In contrast to other doping techniques, in dispersion technique control over the dopant concentration is achieved by varying concentration of the medium.
- This proposed technique can be implemented for different nanomaterials such as polymer, molecular semiconductor, nanocomposites and nanorods and nanowires.
- The proposed technique can be implemented on various substrates such as silicon glass and transparent flexible plastic for fabricating transparent flexible device.
- The conceptual model system is built by patterning two types of nanocomposites across each other, namely p-type and n-type onto base microelectrode platform, where at the interface crossbar junction is formed.

1.3 Analytical and experimental contributions

- Soft, flexible elastomeric stamps are fabricated using soft lithography method.
- Simple ink and print concept is executed.
- Double microcontact printing technique is performed for patterning nanomaterials.
- A microelectrode platform is used for electrical characterization of assembled nanojunction device
- To establish exact pattern transfer onto the substrate optical analysis is performed.
- To assets and support optical characterization and confirm seamless flow of current through microelectrode platform and patterned nanomaterials, nanodomain analysis is performed using scanning electron microscope analysis
- Elemental analysis of microelectrode array is performed using Energy-Dispersive X-ray (EDX) characterization
- For creating vacuum, principle of Venturi effect is applied. Simple assembly of aspirator and Buchner funnel is used.
- Master template is fabricated using photolithography for creating replica stamp.

1.4 Material System

- Due to inherent unique electrical, mechanical and thermal properties, quasi one dimensional semiconducting carbon nanotubes are assembled to form nanojunctions. The SWCNTs were purchased from Nanolab.
- For positive pattern transfer and to fabricate the smallest feature size of less than 50 μm , positive tone Shipley 1827 photoresist is used. The photoresist was purchased from Microchem.
- To obtain relief structure greater than 10 μm , SU-8 negative photoresist is used. The negative photoresist was purchased from Microchem.
- The PDMS stamp is fabricated using Sylgard 184. The Sylgard 184 is purchased from Dow Corning.
- For synthesizing extrinsic CNTs, non-hazardous dopants are used. Anionic and cationic organic surfactant, SDS and CTAB respectively, are purchased from Fisher Scientific.

1.5 Motivation

Various CNT based sensors have been developed for detecting chemical, gaseous and biological species. Single carbon nanotube strand is aligned between two metal electrodes to build sensor devices. When specific molecules of interest interact with the CNT, the electrical properties of the nanotubes are altered, enabling detection of the molecules. The measured electrical signal strength through this single strand of CNT is of the order of 10^{-9} A [1, 2]. Due to its low signal strength, the signal to

noise ratio of the devices is very small. Thus, decreasing the sensitivity of the device. Since the electrical characteristics of CNTs are strong function of its atomic structure, mechanical deformation, and chemical doping, the molecules of interaction induce change in conductance. Padigi et. al [3] has demonstrated that in CNT sensors, several orders of magnitude change in conductance and increased signal to noise ratio can be achieved by using a mesh of carbon nanotubes . In the mesh based CNT sensors, the multiple carbon nanotubes are clustered between the positive and negative electrodes. It has been observed that the signal strength is increased to the order of 10^{-6} A. In comparison to single strand CNT based sensors, there is an increase of three orders of magnitude in signal to noise ratio.

However, due to the above resistive configuration, where a single CNT or mesh of CNTs is bridged between the two electrodes and through which current is passed, these CNT devices lack the specificity to detect different molecules. In resistive sensors, it is very difficult to interpret the interaction mechanism between two different types of analysts. Because, due to the binding effect of analyst, the conductance value is increased or decreased depending upon its concentration. To achieve the specificity, CNTs need to align in well-defined reproducible manner and in order to increase sensitivity sensor should consist of non-linear device with gradients exceeding those of linear resistors. Therefore, we proposed to build a crossbar junction nanodevice using n-type and p-type of nanomaterials. The reason for identification of two different analysts is the binding of specific analysts onto two different types of CNT surface that will result in corresponding charge transfer. Due to

the electron-withdrawing molecules or electron-donating molecules, the charge density of the main charge carriers is modulated, in turn modifying the I-V characteristics of the crossbar junction. However, to observe the change in the characteristics curve, the junction need not necessarily have to behave as an ideal semiconducting diode with the exponential electrical characteristics. The observed rectifying polynomial behavior is sufficient for the sensor application since it improves sensitivity. The charge interactions between analyst molecules and charge carrier can be interpreted by studying the drift and in the polynomial curve from the base line curve and analyzing the curve bending in the I-V characteristics, thus, making crossbar junction an ideal candidate for electrically based sensing. However, the crossbar requires slightly more complex ancillary electronics than resistive based biochemical sensors. In my research, I am fabricating a crossbar nanodevice that can be used as a sensor platform. Future crossbar nanosensors, due to its junction configuration, will have improved characteristics in terms sensitivity and specificity.

1.6 Current Limitations and Key Innovations

The current technology requirement in the domain of chemical and biological sensors is geared to increasing the foot print density by miniaturizing the sensor devices. This has been achieved by exploiting one-dimensional nanomaterials. But, the miniaturization trend is getting harder to sustain due to the fundamental physical and technological limitations as well as economical limitations. Fabrication of microdevices and nanosystems for sensor systems using nanomaterials pose

restrictions in terms of parallel processing and process control. Parallel patterning of nanomaterials has issues such as cost, repeatability, precise alignment and high-density assembling. Earlier, attempts have been made to align, pattern and assemble various nanomaterials such as nanowires, nanorods and polymers. 'Logs-on-a-river' for transporting timber and electrical concepts are adopted for aligning nanomaterials. Nanomaterial alignment has been achieved through Langmuir Blodgett (LB) method [4], atomic force microscopy (AFM), superlattices pattern transfer method [5], fluidic alignment, surface patterning and electrophoresis. Despite, all these techniques, capability for aligning nanomaterials in Langmuir Blodgett method, the monolayer area is limited only by the number of the nanomaterials dispersed on the trough surface. While, in the superlattice structure method, nanomaterial arrays of very low density are aligned, the method fell short of achieving large-scale assembly. The AFM technique has limitation in terms of slow process. However, the most common disadvantage with all of the above techniques is cost and patterning a wide range of nanomaterials.

In addition to patterning constraints and limitations, another disadvantage is modulating electrical property of the semiconducting materials for fabrication of cross bar junction for microelectronic sensor device. Two terminal devices such as diodes, transistors, and field effect transistors (FETs) are being built by altering intrinsic properties of various semiconductor materials. Diffusion and ion implantations are the two most common doping techniques in conventional semiconductor industries. Comparative studies have revealed that the diffusion process has lesser control and is

less efficient for large scale doped material production as compared to ion implantation. Few of the other disadvantages with ion implantation are crystallographic damage, amorphization, ion channeling, the use of hazardous materials such as antimony, arsenic, phosphorus, and boron and high voltage safety. Also, thermal annealing of the target is required after each implantation process. However, these above techniques are not feasible for doping nanomaterials, because the nanomaterials will lose their intrinsic electrical properties. Thus, chemical and electrostatic dopings are two techniques for doping nanomaterials. In chemical doping method, chemical dopants are incorporated during material synthesis and can be extrinsically incorporated, as implemented in our case. However, selective doping cannot be achieved during the material synthesis process. While in electrostatic doping, the nanodevice behaves under the influence of the applied electric field. Junction channels are controlled by gate voltage. Although the device shows improved electrical characteristics, the complexity in device fabrication and high gate voltage requirement are few issues associated with electrostatic doping.

Thus, considering the current limitation in the two areas; patterning technique and doping technique, I have incorporated microcontact printing techniques for parallel patterning of high density nanomaterials and dispersion technique for modulating the intrinsic properties of nanomaterials. Carbon nanotube (CNTs) due to its improved electrical properties has been used as material systems in my experiments. Moreover, microcontact printing technique overcomes limitation associated with the above discussed alignment and patterning methods in terms of device fabrication process and

investment. In addition, mass production of high density structures and process control in regularity and repetitiveness is achieved using soft lithography. Also this method is simple, rapid and cost effective. Furthermore, I have used dispersion technique for modification of intrinsic properties of carbon nanotubes. Synthesis of p-type and n-type CNTs using dispersion method overpowers limitations of ion implantation, diffusion, chemical doping and electrostatic process. It uses a simple concept of mixing nanomaterial of interests and dopant substances. Here, I have used organic and non-hazardous surfactants in comparison to semiconductor industries material systems. Looking at the assembly of crossbar junctions using double microcontact printing, alternatively p-type and n-type CNTs are stamped. This technique can stamp CNTs as well as wide range of nanomaterials from nanorods, nanowires, nanofibers, various polymers to nanocomposites.

CHAPTER 2

INTRODUCTION

2.1 Role of nanomaterials

The need for increasing specificity, selectivity and sensitivity of biochemical sensors has lead to the evolution of nanoscale devices and systems. As the size of the devices shrink, the integration of bottom-up and top-down technology provides important techniques in incorporating one-dimensional nanomaterial based structures, which are the key to developing miniaturized devices. Nanodevices created from these nanoscale materials that are of the order of a few tens of nanometers offer novel physical and electrical properties in terms of stiffness, toughness and improved conductivity. These improved properties of nanomaterials are due to the defect-free structure and electron mobility on the circumference of the structure at the nanoscale. Thus, the process of miniaturization with nanomaterials is expected to result in an improvement in efficiency, performance and density of devices. Various nanomaterials ranging from quantum dots [6, 7], nanotubes (NT's) [8, 9], nanofibers [10] and nanowires [5, 11-13] have been synthesized and used as building blocks for devices with nanoscale components. The use of nanomaterials offers the advantage of increased surface area to volume ratio, which in turn has been known to improve nanoelectronic device performance capabilities in terms of current carrying capabilities, break down voltages as well as gating effects [14]. Other types of nanomaterials that are used for building active nanocomponents are conductive organic polymer and molecular semiconductor.

Building nanodevices using nanomaterials requires changes that will necessitate the development of new materials, processing technologies, device structures, and architectures. The following section discusses various trends in fabrication process, different alignment, patterning methods, material synthesis and doping techniques. The section also explains different nanomaterials and its electrical properties for fabrication of diode based junction nanosystems.

2.2 Nanodevice architecture

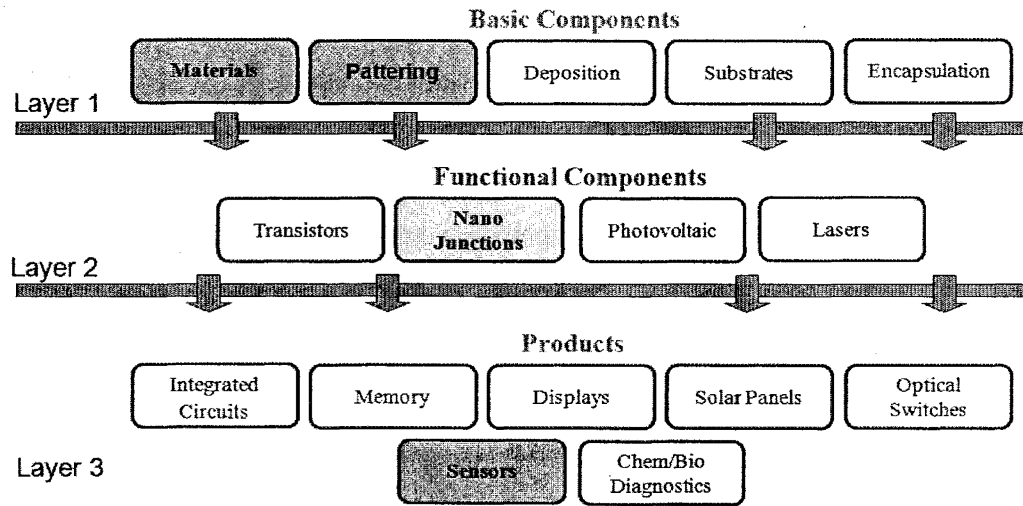


Figure 2.1: Classification of nanoelectronic components.

To understand the structure of nanodevice architecture [15], it is categorized in three distinct layers; basic components, functional components and products, of varying complexity and integration. Looking into details of each layer in figure 2.1, basic components are divided into five different components materials, patterning, deposition, substrates and encapsulation. Each layer relies on many, and in some cases all of the individual components in the layer. For example, to fabricate a series of

transistors or light emitting diodes requires substrates that have been selectively patterned to accept materials that are deposited which are then encapsulated to protect them from the environment. The basic semiconductor components are now accessible, and have reached a performance level that is deemed “good enough” to enable the next phase of technology for development and commercialization of nanotechnologies. However, when it comes to nanomaterials fabrication, assembling and patterning, there are multiple issues and limitations in terms of reliability and repetitiveness. Final layer is assembling of single or more various functional components to form commercialized products such as integrated circuits, memories, displays, solar panels, optical switches, processors and biochemical diagnostics equipment.

2.3 Architectural model system

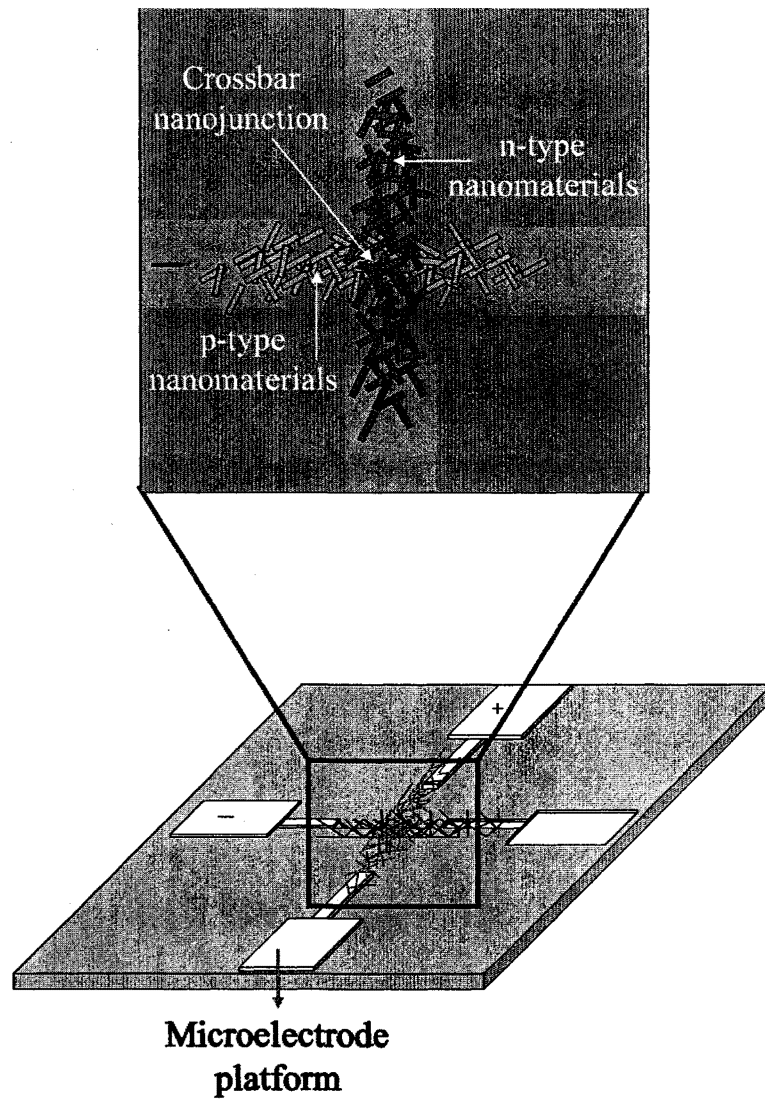


Figure 2.2: Conceptual representation of model-system for fabrication of crossbar junction.

In my architecture model system, the key scientific idea in my research is integration of material systems, spanning multiple orders and scaling of device architecture that

will result in functional nanoelectronic structures. The prototype consists of basic functional crossbar junction. The crossbar in the figure is built by patterning two types of nanocomposites namely p-type and n-type onto base microelectrode platform using microcontact printing, where at the interface crossbar junction is formed. The planar gold microelectrode platform is incorporated for electrical characterization of crossbar nanojunction. The configuration comprises integration of nanoscale nanomaterial to microscale microelectrode array for functional reliable measurements. These simple building blocks can be incorporated for assembling multiarray crossbar junction for a high-end application device. Detail description of fabrication, assembling, and characterization of this nanosystem are discussed in the materials and methods chapter. Figure 3 is a representation of the conceptual device architecture. One of the key aspects in developing the crossbar device architecture is the fabrication of the crossbar itself. The technique that has been utilized to fabricate these structures is a hybrid lithography methodology. The following section discusses in detail various lithography process and their advantages and limitations

2.4 Lithography

2.4.1 Introduction

The word litho means stone and graphein means to write. Original printing surface was stone. Later, Lithography was invented by Johann Alois Senefelder in 1796. He used inked limestone for printing on papers. He chemically treated stones that had affinity to water/oil affected by chemical treatment. It is an art to imprint the text,

pictures, artwork or desired design onto required material. In the electronic world, lithography refers to photolithography and microfabrication used to make integrated circuits and smart devices such as microelectromechanical systems (MEMS) for sensors and actuators. Micro and nanoscale size patterns are structured onto substrate material using microlithography and nanolithography. Typically features smaller than 100 nanometers are considered nanolithographic [16].

In addition to these commercially well-established techniques, a large number of promising microlithographic and nanolithographic technologies exist or are emerging, including nanoimprint lithography, interference lithography, X-ray lithography, extreme ultraviolet lithography, and scanning probe lithography. Some of these emerging techniques have been used successfully in small-scale commercial and research applications. Most common lithography techniques are photolithography, softlithography and Electron beam lithography. This section presents brief description of each of these methods.

2.4.2 Photolithography

Photolithography commonly known as optical lithography has dominated the semiconductor industries for manufacturing chips [17]. Photolithography generally uses a pre-fabricated photomask or reticule as a master from which the final pattern is derived. A typical integrated circuit consists of patterned thin films of metals, dielectrics and semiconductors on various substrates such as silicon, gallium arsenide,

or germanium. In this method, radiation sensitive polymeric materials called resists are used to produce circuit patterns in the substrates.

In photolithography, the process sequence consists of five different steps shown in figure 2.3. The step by step procedure consists of spin coat, exposure, development etch and strip. In spin coat process, a thin layer of photoresist is coated onto base substrate and pre-bake to remove casting solvent. Later, the resist is exposed to an optical light of specific wavelength through a mask. The exposed resist film is then developed typically by immersion in a developer solvent to generate three-dimensional relief images. Exposure may render the resist film more soluble in the developer, thereby producing a positive-tone image of the mask. Conversely, it may become less soluble upon exposure, resulting in the generation of a negative-tone image. When the resist image is transferred into the substrate by etching, the resist film that remains after the development functions as a protective mask. The resist film must "resist" the etchant and protect the underlying substrate while the bare areas get etched. The remaining resist film is finally stripped, leaving an image of the desired circuit in the substrate. The process is repeated many times to fabricate complex semiconductor devices.

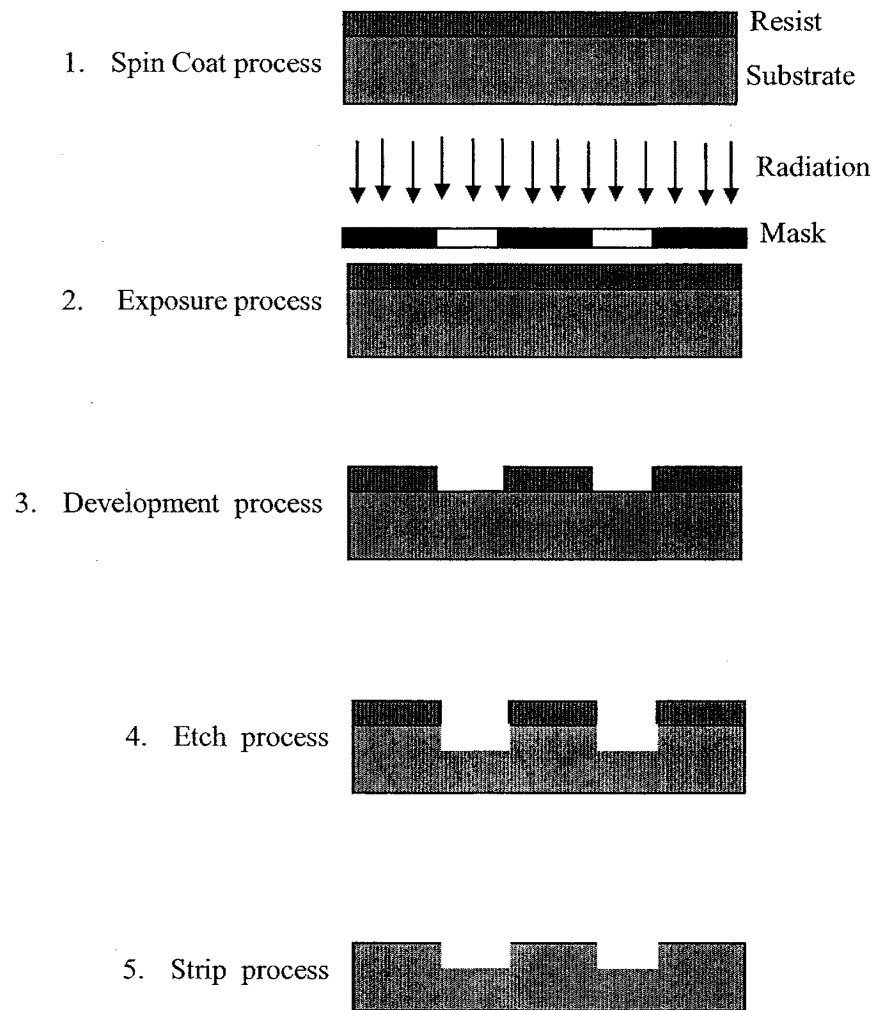


Figure 2.3: Schematic representation of lithography process.

Photoresists

Photoresist is polymer base resin that changes its structure on radiation exposure. The photoresist material should have characteristics and properties as follows:

- (a) Photoresist should be capable of spin-cast into uniform film that adheres to various substrates such as metals, semiconductors, and insulators.
- (b) It should possess high radiation sensitivity

- (c) In addition, it should possess high resolution capability, dictated by solubility/insolubility characteristics.
- (d) Finally, photoresist should withstand extremely harsh environments, for example, high temperature, strong corrosive acids, and plasmas used in subsequent etching, doping and sputtering operations.

Mainly two types of photoresists are used positive and negative tone.

Positive tone

In positive tone resists, a portion of the photoresist that is exposed to light become soluble to the photoresist developer and the portion of the photoresist that is unexposed remains insoluble to the photoresist developer. Photochemical reaction weakens the polymer by rupture of the main/side polymer chain, exposed resist becomes more soluble in developer typically the development rate is 10 times faster as that of unexposed resist. Most commonly used positive photoresist are Shipley series e.g. 1805 and 1827. Originally, Shipley series was manufactured by Shipley but now it is sold by Microchem.

Negative tone

While in negative tone resist, portion of the photoresist that is exposed to light becomes relatively insoluble to the photoresist developer. The unexposed portion of the photoresist is dissolved by the photoresist developer. Polymerization taking place at exposure, cross-linking of polymers adversely affects the solubility. On exposure of negative photoresist, it hardens by random cross linkage. It becomes less soluble due

to increase in molecular weight by UV exposure or photochemical transformation. Negative photoresist is based on epoxy based polymer. Commonly used negative photoresist is SU-8, which was invented by IBM but now it is sold at Microchem. Pictorial and tabular representation of difference between positive and negative photoresists is shown in figure 2.4 and table 1 respectively.

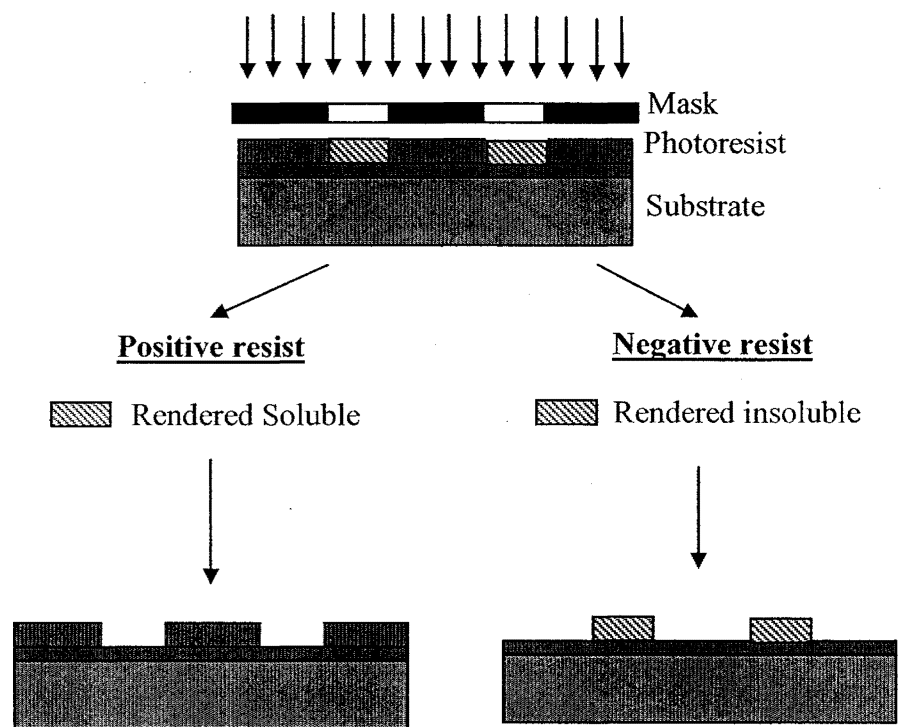


Figure 2.4: Schematic demonstration of difference between positive and negative photoresist during exposure and development process.

Table 1: Difference between negative and positive photoresist.

Characteristics	Positive Photoresist	Negative Photoresist
	Wafer image is opposite of mask image	Wafer image is same as mask image
	Exposed resist hardens and is insoluble	Exposed resist softens and is soluble
	Developer removes unexposed resist	Developer removes exposed resist
Adhesion to Si wafer	Fair	Excellent
Relative cost	More	Less
Developer base	Aqueous	Organic
Minimum feature size	0.5um	2um
Wet chemical resistance	Fair	Excellent
Example	Shipley series	SU-8

Coating process

Coating process involves spin coating and pre-exposure bake. In spin coat process, a thin layer of resist material is applied to a wafer such as Si [18], GaAs [19], InP [20],

glass [21], plastics [22] and metals. The wafer is held on a vacuum chuck as shown in figure 2.5. The vacuum holds the wafer in place during spinning process. Spinning speed is varied from 1500 rpm to 8000 rpm depending on the viscosity of resist and required thickness. The thickness of the photoresist depends on parameters such as resist dispense rate, dispense volume, spin speed, ambient temperature and humidity. Generally photoresists consists of 15% of casting solvent. Casting solvent is added to allow spin application of thin layer onto the base wafer. The residual casting solvent is removed by soft baking at 75 – 100 C for approximately 30-10min followed by cooling process on cold plate. The characteristics of soft-bake consist of stress release, promote resist uniformity on wafer and improve adhesion to the base substrate/wafer. This process is optimized by controlling the temperature profile time/duration. Soft bake also improves etch resistance, line width control and optimizes light absorbance characteristics of the photoresist.

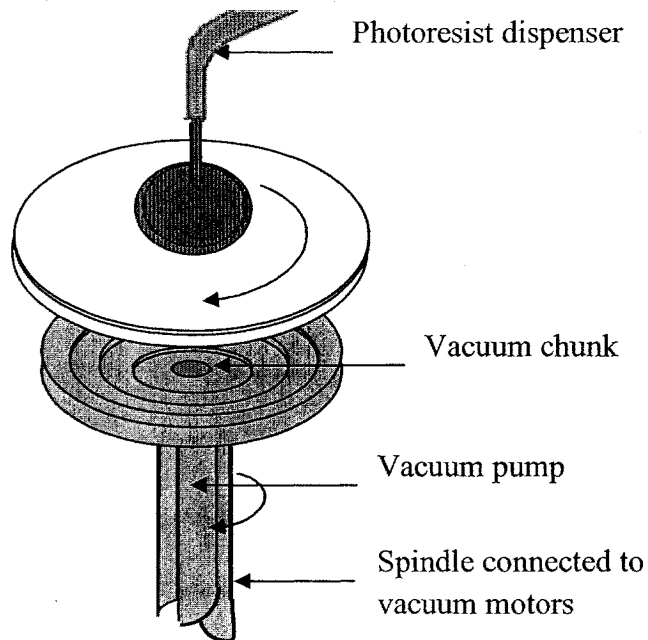


Figure 2.5: Figure illustrates the experimental set-up for spin coating photoresist.

Exposure

After soft baking, the resist coated wafers are transferred to an exposure system. The process involves transfer of mask image onto coated wafer. The perfect alignment, proper intensity, orientation, spectral characteristics and uniformity across the wafer, are few of the controlling parameter studied while exposure. Ultra violet light is used as means of exposure. The extreme UV (EUV) light wavelength ranges from 10-14nm, deep UV (DUV) light wavelength ranges from 150-300nm, while near UV (NUV) wavelength ranges from 350-500nm. Generally, high intensity mercury lamp with illumination of g-line, h-line and i-line having typical wavelength of 436nm, 405nm

and 365nm respectively, is used. The complete range of electromagnetic spectra used for optical lithography is shown in figure 2.6 [23].

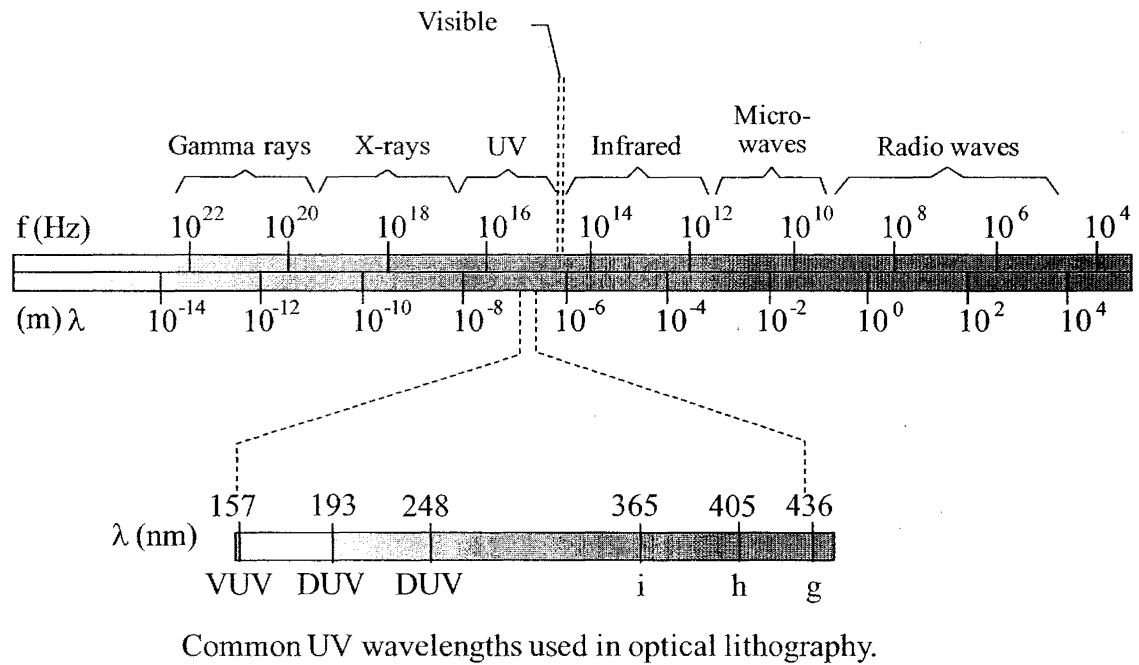


Figure 2.6: Electromagnetic spectrum showing operating range of frequency for optical lithography.

Development

Development process transforms latent resist images joined during exposure into a relief image that will serve as a mask during selective dissolving of resist and etching process. However, the resolution of pattern transfer is affected by diffraction of light. Diffraction of light is observed at the edge of an opaque feature in the mask. Diffraction is also due to non-uniformities in wafer flatness and debris between mask and wafer.

Post-exposure baking

Post exposure baking is generally required for deep UV resist. The process is immediately performed after exposure. The wafer is post-baked to remove residual developer/solvent. Annealing of resist film will further improve the adhesion to the base substrate and improves hardness. Post-baking is also called hard-baking. Typically it is done at 120°C for approximately 20 minutes.

Etching and resist stripping

Etching process is used to etch oxide layer, which is followed by resist stripping. Two type of etching process is used wet etching and dry etching. Etching is a process, where removal of photoresist is performed without damaging the pattern or device fabricated. Most commonly used stripper is organic solvent such as acetone. Acid such as H_2SO_4 are also used as stripper to remove photoresist. Oxidant combination, H_2SO_4 – Cr_2O_3 attacks the resist and not the oxide/ Si. Dry etching involves fewer disposal problems, more controllable stripping, the chemicals used do not disintegrate with time and it doesn't cause undercutting/ broadening of photoresist features. Reactive plasma stripping with oxygen and gaseous chemical reactants (ozone) and radiation (UV) are also few of the dry etching techniques.

2.4.3 Electron beam lithography

Electron beam lithography (EBL) is the practice of scanning a beam of electrons to form a circuit pattern on substrates. The electron beam is scanned across a surface

covered with a positive/negative e-beam photoresist and of selectively removing either exposed or non-exposed regions of the e-beam resist. Depending upon type of resist, the scanned area is dissolved or is rendered insoluble in developer. A typical EBL system consists of the following parts: an electron gun or electron source that supplies the electrons, an electron column that “shapes” and focuses the electron beam, a mechanical fixture that positions the wafer under the electron beam, a wafer handling system that automatically feeds wafers to the system and unloads them after processing and a computer system that controls the equipment.

The primary advantage of electron beam lithography is that it is one of the ways to beat the diffraction limit of light and make features in the nanometer regime. This form of maskless lithography has found wide usage in mask-making, used in photolithography, low-volume production of semiconductor components, and research and development [24]. On the other hand, the key limitation of electron beam lithography is throughput, i.e., the very long time to expose an entire silicon wafer or glass substrate. A long exposure time leaves the user vulnerable to beam drift or instability which may occur during the exposure. Also, the turn-around time for reworking or re-design is lengthened unnecessarily if the pattern is not changed the second time. In addition two types of defects are detected; scanning defects and physical defects. Scanning defects usually occur while deflecting or blanking of electron beam. This is due to electron optical control. Physical defects are more varied, and can include sample charging, backscattering calculation errors, dose errors, fogging, outgassing, contamination, beam drift and particles. Due to back scattering,

the diameter of the incident electron beam is broaden as it penetrates the resist and substrate and it gives the resist unintended extra doses of electron exposure as back-scattered electrons from the substrate bounce back to the resist [25]. However, current limits in terms of resolution in photolithography and soft lithography are approx. 250nm and 1-30nm respectively. Features below 35nm is achieved by EBL, where the smallest structure is sub-10nm [26].

Summarizing, nanostructures can be fabricated using above discussed advanced microlithography and nanolithographic techniques such as e-beam lithography and photolithography respectively. A few more techniques such as X-ray lithography and proximal-probe lithography can also be used for building nanocomponents. Even though all these techniques are capable of providing very small features, however, there is limitation in development and generating large areas of nanostructures rapidly and at low cost. The lack of techniques capable of generating and manufacturing nanostructures rapidly and economically represents a limiting step in the area of nanoscience and nanotechnology. Therefore soft lithography suggests a new conceptual approach in nanomanufacturing. Advanced nanolithographic techniques would be used to make masters, and these structures would then be transferred into organic polymers or other materials using procedures such as printing, molding, embossing, or a combination thereof. The techniques could also be automated. The ability to make both positive and negative replicas and to modify the dimensions and shapes of features present on elastomeric masters by mechanical deformation adds

further flexibility to this methodology. The detailed description of soft lithography is discussed in next section.

2.4.4 Soft lithography

In recent technology, soft lithography refers to a family of techniques for fabricating or replicating structures using "elastomeric stamps, molds, and conformable photomasks". Soft lithography includes techniques such as micro contact printing, micro-transfer molding, micromolding in capillaries, micro-replica molding, solvent-assisted microcontact molding and near-field phase shift lithography. These techniques are called soft lithography because all these techniques use soft flexible, elastomeric polymer material called polydimethylsiloxane (PDMS). PDMS "stamps" with patterned relief are stamped on to the substrate to generate features. The stamps can be prepared by casting PDMS against masters patterned by conventional lithographic techniques, as well as against other masters of interest [26].

The characteristics of PDMS are as follows

- (a) Due to its elastomeric in nature, PDMS can conform to the surface of the substrate over a relatively large area. PDMS is deformable enough such that conformal contact can even be achieved on surfaces that are nonplanar on the micrometer scale. The elastic characteristic of PDMS also allows it to be released easily, even from complex and fragile structures.

- (b) PDMS provides a surface that is low in interfacial free energy (ca. $21.6 \times 10^3 \text{ Jm}^{-2}$) and chemically inert. Polymers being molded do not adhere irreversibly or react with the surface of PDMS.
- (c) PDMS is homogeneous, isotropic, and optically transparent down to about 300 nm. UV cross-linking of prepolymers that are being molded is possible. It has been used to construct elastomeric optical devices for adaptive optics and to fabricate photomasks for use in UV photolithography and contact phase-shift photolithography.
- (d) PDMS is a durable elastomer that can be used up to about 100 times over a period of several months without noticeable degradation in performance.
- (e) The surface properties of PDMS can be readily modified by treatment with plasma followed by the formation of SAMs to give appropriate interfacial interactions with materials that themselves have a wide range of interfacial free energies

Following are the commonly used soft lithography techniques used for soft lithography.

Micro-transfer molding (μ TM)

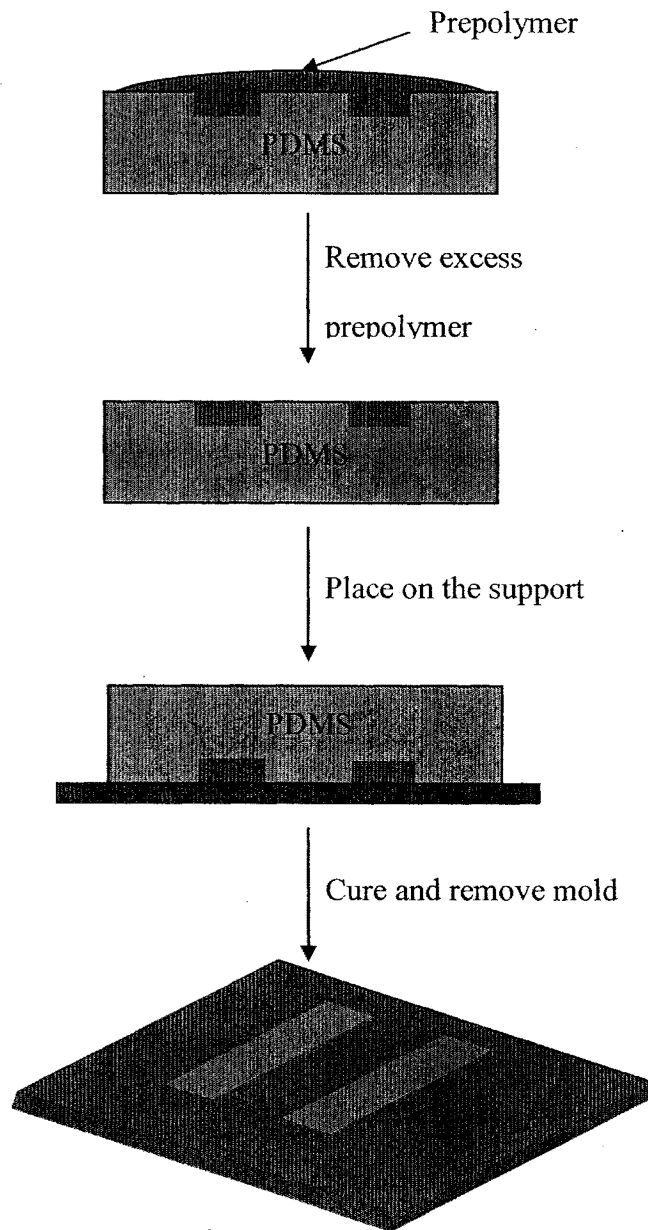


Figure 2.7: Schematic representation of process sequence in micro-transfer molding (μ TM).

A PDMS stamp is filled with a prepolymer or ceramic precursor and placed on a substrate. The material is cured and the stamp is removed. This technique is able to generate multilayer systems. Figure 2.7 demonstrates the procedure for micro-transfer molding (μ TM). In micro-transfer molding (μ TM), thin layer of liquid prepolymer is applied to the patterned surface of PDMS mold and excess liquid is removed by scraping with a flat PDMS block or with a stream of nitrogen or air. The mold gets filled with PDMS and is then placed in contact with the surface of the substrate. The prepolymer is cured by illuminating with UV light or by heating it. Later, on peeling of the mold, patterned microstructures are left on the surface of the substrate. This technique can produce patterned microstructures of a wide variety of structures. μ TM is capable of generating waveguides, interconnects and isolated microstructures [27, 28].

Micromolding in capillaries (MIMIC)

In MIMIC, continuous channels are formed when a PDMS stamp is brought into conformal contact with a solid substrate. A low viscosity polymer is then placed at the open end of the channels. The capillary action spontaneously fills the channels with a polymer precursor. After curing the prepolymer into a solid, the PDMS is peeled and removed from the substrate. When the solvent evaporates, the materials in the solution or suspensions solidify in the confined channel and form microstructures. On removal of PDMS stamp, microstructures are revealed. The resulting structures are usually thinner than the height of the channels in PDMS stamps [29].

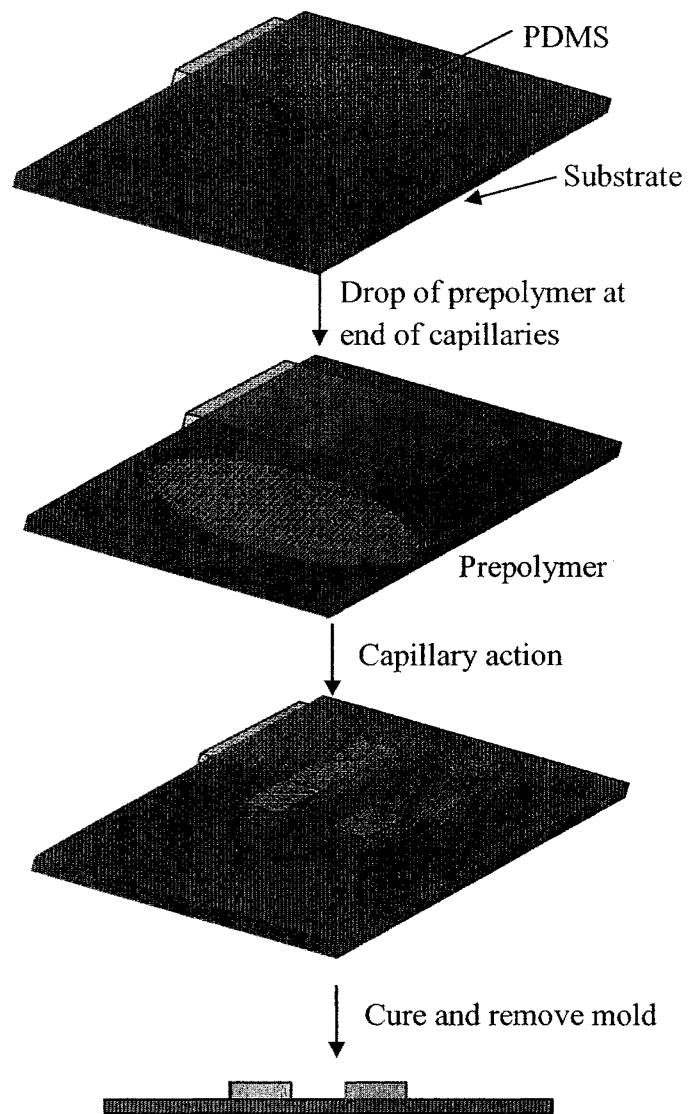


Figure 2.8: Schematic representation of process sequence in MIMIC.

With the advantage of patterning microstructures, there are other several limitations to this technique. MIMIC requires hydraulic connected network of capillaries. Also there should not be any isolation of structures. In this technique, capillaries are rapidly filled and can flow approx. 1cm. However, over the larger distance, the rate of filling

decreases significantly owing to the viscous drag in the capillary. The rate of filling also decreases as the cross section of the capillary decreases [26]. Figure 2.8 illustrates the procedure for MIMIC. In addition, the shapes and size of features present on the PDMS can be manipulated in a controlled way by deforming the mold using mechanical compression, expansion, stretching and a combination of all. In this approach the relief features in the surfaces of a PDMS are mechanically deformed and transferred onto the substrate [30].

Micro-replica molding (REM)

Replica molding is an efficient method for the duplication of shape, morphology and structure, present on the surface of the mold. A PDMS stamp is cast against a conventionally patterned master. UV- or thermally curable prepolymers are then molded against the secondary PDMS master. In this way, multiple copies can be made without damaging the original master. The cured polymers possess almost the same dimensions and topologies as the pattern on PDMS. The fidelity of this process is largely determined by the weak van der Waals interactions. This technique offers duplication of three dimensional topologies in a single step process and faithful duplication of complex structures, and micro nanostructure resolution in simple, reliable and inexpensive way [31].

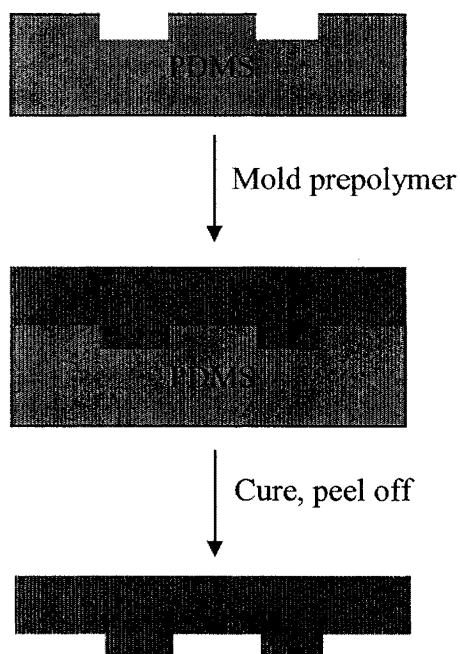


Figure 2.9: Schematic representation of process sequence in micro-replica molding (REM).

Figure 2.9 explains the procedure for micro-replica molding. The relief structure on the PDMS mold can, in turn, be faithfully replicated by using this structure as a mold for forming structures. In few seconds prepolymer is UV- or thermally cured. The relief structures on the replica are complementary to those of the mold and very similar to those of the original masters [32, 33].

Microcontact printing μ CP)

Microcontact printing uses a PDMS stamp to pattern or deposit molecules on the base surfaces. The stamp is first 'inked' with a solution of desired materials; often nanomaterials, material composites, proteins or thiols [34]. The relief pattern on the

surface of a PDMS stamp is later pressed onto the surface to form pattern microstructures. The soft PDMS stamp makes conformal contact with the surface and molecules are transferred directly from the stamp to the surface in the span of a few seconds.

Advantages of microcontact printing compared to the other alignment techniques are as follows [26, 35].

- (a) The technique is a low cost and require very little investment than traditional photolithography in mass production,
- (b) This technique is a non clean room technique and can be carried out in ambient temperature.
- (c) As compared to conventional lithography process this technique can generate features on both curved and reflective substrates and rapidly pattern large areas. The technique is well-suited for applications involving large or nonplanar (nonflat) surfaces.
- (d) Using these technique variety of materials have been patterned including metals and polymers.
- (e) The method complements and extends existing nanolithographic techniques and provide new route to high-quality patterns and structures with feature sizes as small as 30nm. This technique develops patterns with smaller details than photolithography in laboratory settings (~30nm vs ~100nm). The resolution depends on the mask used and can reach 6 nm.
- (f) It is well-suited for applications in biotechnology, plastic electronics.

(g) This technique does not need a photo-reactive surface to create a nanostructure,

Therefore, in my research I have in-cooperated both soft lithography and photolithography for fabrication of microelectrode array and alignment of nanomaterial respectively, for building crossbar junction. The following section discusses about different types of alignment techniques.

2.5 Patterning and alignment techniques

In order to fully achieve the potential of nanomaterials, it is essential to assemble them into well-ordered structures. Another key concept in bottom-up technology is to assemble building blocks to form ordered functional systems. Numerous methods have been demonstrated for constructing crossed nanomaterial junctions. An atomic force microscope (AFM) has been used in positioning the nanomaterials. In addition, recently, a wide variety of alignment techniques, such as Langmuir Blodgett method and superlattice nanowire pattern transfer methods as well as fluidic alignment have been used. Surface patterning of nanomaterials based on their inherent or modified hydrophilicity are used to form arrays of nanodevices.

2.5.1 Langmuir Blodgett method

The Langmuir-Blodgett technique has been used to assemble one-dimensional nanoscale building blocks. “Logs on water” concept is applied for alignment and patterning of nanomaterials [36]. In the nineteenth century, during timbering season,

logs piled through winter season are rolled down due to flooding of river. Thus, Whang et al. used this concept to align and pattern semiconductors and metal nanowires on a wafer surface [4]. The common feature between log and nanowires is that they are one dimensional, the length is comparatively larger than diameter. Scientifically, the process to align these 1-D nanomaterials is now called as the Langmuir Blodgett method [37]. From nanocrystals, nanorods to nanowires are patterned by the Langmuir–Blodgett technique. In this technique, nanomaterials are capped or mixed with surfactants and are dispersed onto water surface of a Langmuir–Blodgett trough. The interaction between the surfactants and the nanowires causes the nanomaterials to float on the water surface. Then the floating nanomaterials are compressed to higher density on the surface, with computer-controlled trough barriers mimicking the banks of the logging river. Finally, nanomaterials reorient themselves and align parallel to the trough barrier, forming a closely packed monolayer. This monolayer can then be transferred onto any substrate, such as silicon wafers or other plastic substances. The disadvantage of the LB technique is that a formation of monolayer is limited by the number of the nanomaterials dispersed on the trough surface. However, this technique did not demonstrate control of spacing and other properties critical to integrated and interconnected arrays

2.5.2 Superlattices nanowires pattern transfer (SNAP)

Superlattice nanowires pattern transfer (SNAP) technique is used for fabricating arrays of aligned, high aspect ratio silicon NWs with the goal of developing a reliable

nanofabrication approach for creating ultrahigh density arrays with bulk like controllable conductivity characteristics [5]. However, in the SNAP method, only nanowires can be patterned during the fabrication process, which is the biggest disadvantage with this method [38]. It can produce large NW arrays from virtually any thin-film material, including metals, insulators, and semiconductors. The dimensions of the NWs can be controlled with near-atomic precision, and NW widths and spacing can be as small as a few nanometers. In the SNAP process, a piece of a GaAs/Al_xGa_{1-x}As superlattice serves as the master and is differentially etched leaving a comb-like structure. Material of interest is then evaporated onto the master. Later, the master is dropped onto a substrate precoated with a thin epoxy layer. The interface between the evaporated metal and the superlattice is etched, leaving nanowires on the surface. Dry etching translates the metal nanowire array into the supporting substrate. The assembly of nanowires into arrays patterned is critical to the realization of integrated electronic and photonic nanotechnologies.

2.5.3 Atomic force microscopy

The AFM, though primarily used as an imaging tool with atomic resolution, is also evolving into a precision manipulation tool. In this technique, generally, a piezoelectric XYZ positioning stage is equipped with few nanometers precision control that enables two dimensional precise assemblies of microparticles [39]. Using the real-time visual feedback, the behavior of the particles manipulated by an AFM probe, is investigated. While in some cases, using AFM, substrate is first patterned and

later, used as a template for immobilization of nanomaterials. H. Iwasaki used indirect method, where oxide patterns are drawn onto the surface by applying a dc voltage between a conductive AFM tip and the Si substrate [40]. The oxide patterns are then used as the templates for immobilization of biomolecules with the help of linker molecules. Atomic force microscopy is one of the best tools for alignment, assembly of micro and nanomaterials, but its usage is low because of its slow process. Despite attempts that have been made to align nanomaterials using electrical methods, this technique fell short of achieving large scale assembly and patterning wide range of nanomaterials.

2.5.4 Electrophoresis

Electrophoresis is the most common technique used in fluidic alignment. Nanomaterials from nanoparticles to nanotubes have been aligned across the metal electrodes using a dc electric field. Effects of electric field strength, nanomaterials concentration in the suspension, and the solvents used for dispersion are few of the variables taken into account while aligning nanomaterials. E. -K. Suh et, al [41] has demonstrated improved dispersion of CNTs in dimethylformamide solution compared to ethanol. CNTs mostly moved towards anode for the applied electric field indicating the negative charge of the nanotubes. Experimental results exhibit the possibilities of precise positioning of nanotubes on pre-patterned electrodes by controlling the magnitude of electric field as well as the concentration of CNT suspension. However,

large scale patterning and high density assembly of the nanomaterials is unattainable with this technique.

2.5.5 Fluidic alignment

Hierarchical assembly of 1-dimensional structures into well ordered network has been demonstrated by combining both surface patterning and fluidic alignment technique. Yu. Hang et.al [42] has demonstrated patterning of nanowires in fluidic flow. In general, arrays of nanowires are suspended in fluidic channel structures formed between a PDMS mold. Nanowires get aligned along the direction of fluidic flow. Controlling the flow rate, varied degree of alignment can be achieved. High flow rate produces larger shear force near the substrates and hence leads to better alignment. The spacing between the nanowires is further reduced to 100nm or less by chemically functionalizing substrate with NH_2 -terminated monolayer which will be partially positive charged than bare silicon substrate. Various nanowires such as gallium phosphide (GaP), Indium phosphide (InP), silicon (Si) are patterned using these techniques.

The ability to precisely position nanomaterials will enable the construction of novel micro/nanoscale electronic, optical, and quantum devices as well as novel materials, sensors, mechanisms, and machines. However, the above methods have disadvantages of limited control over spacing between two nanostructures. Furthermore, these methods, despite producing arrayed nanostructures, are highly complex and difficult to

implement. All these techniques either require vacuum conditions or have low probabilities of success due to their highly selective manner of nanomaterial deposition, greatly limiting their mass production for practical applications. In contrast, we have developed a high-density crossbar array junction prototype using a simple, rapid, and low-cost microcontact printing technique that has the capability of being automated. Integrating this soft lithography technique for relief imprinting and the standard photolithography technique for fabrication of the microelectrode platform, multiple crossbar junction device prototypes were developed.

2.6 Nanomaterials

2.6.1 Carbon nanotube

Carbon nanotube presents new class of materials for investigating fundamental one dimensional (1D) physics and for exploring nanoelectronics and molecular electronics. The CNTs improved unique electrical, mechanical and thermal properties are arguably the most significant characteristic of this new material. Because of the symmetry and unique electronic structure of graphene, the structure of a nanotube strongly affects its properties. The numerical values are listed below.

Properties of CNTs

- (a) Due to their nanoscale dimensions, electron transport in carbon nanotubes will take place through quantum effects and will only propagate along the axis of

the tube. Because of this special transport property, carbon nanotubes are frequently referred to as “one-dimensional” in scientific articles.

- (b) Size - The size of nanotube is approximately 0.6 to 1.8nm in diameter [43]. In comparison to electron beam lithography that creates line as wide as 50nm [44].
- (c) Density – Density of CNTs is noted to be 1.33 to 1.4 gms/cm³ [45] .
- (d) Tensile strength – CNTs are the strongest and stiffest materials on earth. CNTs are stronger than steel. Steel breaks at 2 billion pascals while the strength of CNTs is 25 times greater and is 45 billion pascals [46].
- (e) Resilience – CNTs can be bend at larger angles and can be straightened without causing any fracture or damage, where as metal fracture at the grain boundaries [47].
- (f) Current carrying capacity - Current carrying capacity of CNTs is estimated to be 1 billion A/cm² while the super conducting metal burns at 1 million A/cm² [48].
- (g) Field transmission - CNTs has also showed field emission and can emit phosphors at 1 to 3 volts if electrodes are spaced 1 micron apart [49].
- (h) Heat transmission – CNTs are expected to be very good thermal conductors along the tube and are good cooling agents; its thermal conductivity is as high as 6000 W/m.K, whereas diamond of only 3320 W/mK [50].
- (i) Temperature stability – CNT is stable at 2800 °C as compared to metal wires in microchip that melts at 600 to 1000 °C [51].

Due to the above improved properties researchers and scientists are using CNTs in various applications. A single CNT can be either metallic or semiconducting, depending only on diameter and chirality, while the local carbon-carbon bonding remains constant. The ability to yield both metallic and semiconducting SWNTs without doping is unique among solid-state materials and has led to speculation that SWNTs might thus serve as a key building block for carbon-based electronics. Some common use of CNTs and limitations in each the applications are listed below.

Uses of carbon nanotubes

- (a) Several groups have successfully built functional microelectronic carbon nanotube devices. Single semiconducting carbon nanotubes are placed in between two electrodes to demonstrate FETs, diodes [9, 52-54]. Electron flow through the channel is controlled by applying voltage near the third electrode. While in diode configuration, the current is permitted to flow in one direction only.
- (b) DNA trace and chemical markers can be found using nanotube tipped atomic force microscopy [55]. Several variants of a gene are identified in the strands. This technique is the only one technique yet invented for imaging the chemistry of a surface. So far it is only used on short strands of DNA.
- (c) Non-Volatile Random Access Memory developed by Nantero Inc., are commercially available NRAM [56]. A screen of CNTs are laid on a support and is forced to make contacts by applying voltages; ON state and separate;

OFF state. But, the limitation with this device is its switching speed is around 1 megahertz which is much slower than conventional memory chips.

- (d) Tweezers are fabricated from nanotubes by attaching two nanotubes to the glass rod [57]. Particles bigger than the width of nanotubes can be picked up but the difficulty lies in the releasing of the nanoparticles [58].
- (e) Various chemical and gas sensors [59] have been demonstrated using CNTs [60]. When carbon nanotubes are exposed to alkalis, halogens and other gasses at room temperature, the adsorbed molecule changes the resistive properties of the CNTs. However, selectivity is an issue, as CNTs adsorbs wide range of molecules and distinguishing different molecules is a key limitation in fabrication of a sensor.
- (f) As CNTs store hydrogen and lithium ion in their hollow cylinder, CNTs are used as efficient fuel cells [61]. However, the fabrication process is complex and expensive.
- (g) Resolution of scanning electron microscopy has been improved by using CNT at the tip of a scanning probe [62]. Lateral resolution of approx. 10 times greater has been achieved. Due to use of CNTs at the tip, imaging of deep pits is possible in nanostructures but vertical resolution is still an issue. The tips are made individually and therefore are costly.

Classification of CNTs

Several types of nanotubes exist, and they can be divided into two main categories. In the carbon nanotube family, depending upon graphene sheet rolled around them, carbon nanotubes can be categorized either as single walled carbon nanotube (SWCNTs) or multiwalled carbon nanotube (MWCNTs) [63].

Single walled carbon nanotubes (SWCNTs)

These one dimensional nanomaterials are allotropes of carbon. Most single-walled nanotubes (SWNT) have a diameter of close to 1 nanometer, with a tube length that can be many thousands of times longer. The structure of a SWNT can be conceptualized by wrapping a one-atom-thick layer of graphite called graphene into a seamless cylinder. The way the graphene sheet is wrapped is represented by a pair of indices (n,m) called the chiral vector [64]. The integer's n and m denote the number of unit vectors along two directions in the honeycomb crystal lattice of graphene. As shown in figure 2.10, if $m=0$, the nanotubes are called “zigzag”. If $n=m$, the nanotubes are called “armchair”. Otherwise, they are called “chiral” [65].

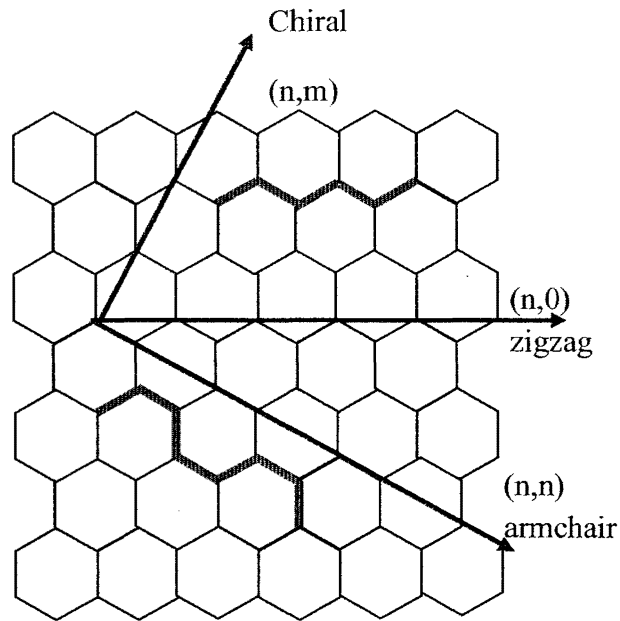


Figure 2.10: The schematic representation of unit cell of graphene sheet for zigzag and chiral structure.

Multiwalled carbon nanotubes (MWCNTs)

Multi-walled nanotubes (MWNT) consist of multiple layers of graphite rolled in on themselves to form a tube shape. There are two models which can be used to describe the structures of multi-walled nanotubes. In the Russian Doll model, sheets of graphite are arranged in concentric cylinders [66], e.g. a (0, 8) single-walled nanotube (SWNT) within a larger (0, 10) single-walled nanotube. In the Parchment model, a single sheet of graphite is rolled in, around itself, resembling a scroll of parchment or a rolled up newspaper [67]. The interlayer distance in multi-walled nanotubes is close to the distance between graphene layers in graphite, approximately 3.3 Å [68].

2.6.2 Nanowires

A nanowire is a wire of diameter of the order of a nanometer. Alternatively, nanowires can be defined as structures that have a lateral size constrained to tens of nanometers or less, and an unconstrained longitudinal size. At these scales, quantum mechanical effects are important, thus, nanowires are also called as “quantum wires”. Many different types of nanowires exist; metallic, semiconducting, and insulating (e.g., SiO_2 , TiO_2). Moreover, metal and semiconductor nanowires cover a wide range of material systems, from noble metals (e.g., Au, Ag, Cu), single element semiconductors (e.g., Si and Ge), compound semiconductors (e.g., InP, CdS and GaAs as well as heterostructures), nitrides (e.g., GaN and Si_3N_4) to carbides (e.g., SiC) [69]. Nanowires of functional material covers a wide range of material systems, from functional oxides (e.g., ZnO, SnO_2 , and In_2O_3), structural ceramics (e.g., MgO, SiO_2 and Al_2O_3), composite materials (e.g., Si-Ge, SiC- SiO_2), to polymers. Semiconductor nanowires are potential effective building blocks for nanoscale devices. Unique properties of these nanowires drive from their versatility in geometry and composition [70]. Many room-temperature applications have already been demonstrated, such as single-nanowire field-effect transistors (FETs), diodes, and logic gates combining both n-type and p-type nanowires.

Similar to CNTs, nanowires are 1-dimensional nanomaterials. They have many interesting properties that are not seen in bulk materials. The electrical properties of these nanowires are studied using STM. Every material has definite conductivity; the

conductance of a wire is inversely proportional to the length of the wire. On the other hand, as the length of the wire is reduced, the mean free path of electrons and the electron transport mechanism changes from diffusive to ballistics. It has been found that in certain nanowires due to quantum confinements, nanowires has discrete quantized conductance values in multiples of $2e^2/h$, which is approx. 12.9 KOhm [71]. Moreover, the conductance is no longer dependent on the length of the wire. Due to its discrete conductance in nature, there are many applications where nanowires may become important in electronic, opto-electronic and nanoelectromechanical devices, as additives in advanced composites, as metallic interconnects in nanoscale quantum devices, as field-emitters and as leads for biomolecular nanosensors.

2.6.3 Molecular semiconductors

Organic molecules/polymers with a π -conjugated (hetero) aromatic backbone are capable of transporting charge and interact efficiently with light. Therefore, these systems can act as semiconductors in opto-electronic devices similar to inorganic materials. However, organic chemistry offers tools for tailoring materials' functional properties via modifications of the molecular/monomeric units, opening new possibilities for inexpensive device manufacturing. These structures comprising molecular and polymeric units exhibit the common feature of ' π -conjugated bonds' giving rise to delocalized filled and empty π -orbitals that greatly impact the optical and electrical properties. In contrast to inorganic semiconductors, the solid-state

structure of these materials is based on weak interactions, principally van der Waals and dipole in chains imparting properties from conductors to insulators [72].

Promising applications are inexpensive light emitting diode (LED) [73] and thin film transistors [74]. The main advantage of such applications includes low operating voltage and simplicity of device fabrications. But important issues of concern in such applications are the device stability and the operational lifetime of organic LED. Also, the control of metal/polymer interface is of great importance. The metal-oxide-semiconductor field-effect transistor (MOSFET) based on inorganic materials is the crucial building block in the electronics industry. These devices have proven to be reliable, highly efficient, and with performance increasing regularly, according to Moore's law. Instead of competing with conventional Si/GaAs technologies, OFETs may find niche applications in low-performance radio-frequency technologies, sensors, and light emission, as well as in integrated optoelectronic devices, such as pixel drives and switching elements in displays. The advantages of organic systems include vapor/solution phase fabrication and good compatibility with different substrates, including flexible plastics, and opportunities for structural tailoring. This trend is driven by the demand for inexpensive, large area, flexible devices processed at far lower substrate temperatures than Si chips.

A number of organic semiconductor classes have been discovered, which are based on the principal of π -conjugated small molecules and polymers. A complete list of organic semiconductors is listed in table 2 below.

Table 2: List of p-type and n-type molecular/polymeric organic semiconductors [72].

Molecular p-type semiconductors	Rubrene (air, PMMA), P5, P5 (PVP-CP), P5 (Al ₂ O ₃), P5 (SiN _x), P5 (Ta ₂ O ₅), P5 (Gd ₂ O ₃), P5 TiO ₂ +PαMS, P5 (BZT or BST), P5-precursor, P5-precursor, Me ₄ -P5, P5-TIPSA, 6T, 8T, DH-6T, DH-4T, Me ₂ -6T, Et-6T, Bis-BDT, Bis-TDT, DPh-BDX, DH-PTTP, DH-PPTPP, Dec-(TPhT)2-Dec, DH-FITTFI, ADT, PcCu, DT-TTF, PcCu, Ta ₂ O ₅ , Bis-BDX
Polymeric p-type semiconductor	P3HT, PQT-12, PTTT-14, F8T2, TS6T, BS8T2, PCB-R, PTAA, CTFB
Organic n-type semiconductor	T3CN, DFH-6T, DFH-4T, FTTTTF, DFHCO-4TCO, DFHCO-4T, DFPCO-4T, CF-PTZ, Cl4-Ph2NTTF, NTCDI(8-18), PDI8, PDI13, PDIF-CN2, F-P5, FPcCu, C60, C60 (on P5), C84, BBL

Despite numerous advantages in using nanomaterial, there are multiple shortcomings associated with their use of any type of nanomaterials. Due to the size of the nanomaterials, there are difficulties in the symmetrical alignment and array patterning for integrated nanosystems. In addition, there are issues associated with the repetitive, symmetric patterning and alignment in terms of positioning, fabricating and assembling them into nanodevices.

2.7 Method for synthesis of extrinsic nanomaterials

Doping has played important role in semiconductor device fabrication. Rectifying p-n junction, transistors are few electronic components based on bulk semiconductor. An introduction of small quantities of dopant atoms modulates the chemical and physical properties of semiconductor materials by improving device performance capabilities, conductivity of the semiconductor materials and thereby forms active device structure. In conventional semiconductor industries, semiconducting materials mainly Si are modulated by material engineering process, e.g. diffusion and ion implantation methods. Chemical dopants on the other hand are added during the material synthesis process or can be extrinsically incorporated, as has been implemented in this case. Doping of nanomaterials such as carbon nanotubes cannot be achieved by conventional process. CNT based nanodevices are fabricated electrostatically or they are chemically doped. The following section describes techniques for introducing dopant atoms in semiconducting materials as well as methods for modulating electrical properties of nanomaterials.

2.7.1 Ion Implantation

Ion implantation process [75] works by ionizing desired atoms. Ionization includes steps of creating ions of the desired impurity atom, using electric fields to accelerate the ions to the required energy, transporting the ions down a beamline to the silicon wafer and finally scanning the beam, or moving the silicon wafer, or both, such that uniform doping of the silicon wafer is accomplished. The experimental set-up consists

of accelerator, where the ions are electrostatically accelerated to a high energy, and a target chamber, where the ions impinge on a target, which is the material to be implanted. Each ion is typically a single atom, and thus the actual amount of material implanted in the target is the integral over time of the ion current. The dose determines conductivity or conductance of the target on completion of the process.

Typical ion energies are in the range of 10 to 500 keV. Energies in the range 1 to 10 keV can be used, but result in a penetration of only a few nanometers or less. Energies lower than this result in very little damage to the target, and fall under the designation ion beam deposition. Higher energies can also be used: accelerators capable of 5 MeV are common. However, there is often great structural damage to the target, and because the depth distribution is broad, the net composition change at any point in the target will be small. The energy of the ions, as well as the ion species and the composition of the target determine the depth of penetration of the ions in the solid: A monoenergetic ion beam will generally have a broad depth distribution. The average penetration depth is called the range of the ions. Under typical circumstances, ion ranges will be between 10 nanometers and 1 micrometer. Thus, ion implantation is especially useful in cases, where the chemical or structural change is desired to be near the surface of the target. Ions gradually lose their energy as they travel through the solid, both from occasional collisions with target atoms and from a mild drag from overlap of electron orbitals, which is a continuous process. The loss of ion energy in the target is called stopping.

Disadvantage of ion implantation

The following are the limitations and disadvantages associated with ion implantation process [76],

(a) Each individual ion produces many point defects in the target crystal on impact such as vacancies and interstitials called as crystallographic damage [77]. Vacancies are crystal lattice points unoccupied by an atom: in this case the ion collides with a target atom, resulting in transfer of a significant amount of energy to the target atom such that it leaves its crystal site. This target atom then itself becomes a projectile in the solid, and can cause successive collision events. Interstitials results when such atoms come to rest in the solid, but find no vacant space in the lattice to reside. These point defects can migrate and cluster with each other, resulting in dislocation loops and other defects.

(b) Ion implantation causes damage to the crystal structure of the target, which is often unwanted; ion implantation processing is often followed by a thermal annealing. This can be referred to as damage recovery [78].

(c) The amount of crystallographic damage can be enough to completely amorphize the surface of the target: i.e. it can become an amorphous solid in some cases. Complete amorphization of a target is preferable to a highly defective crystal: An amorphized film can be regrown at a lower temperature [79].

(d) Some of the collision events result in atoms being ejected (sputtered) from the surface, and thus ion implantation will slowly etch away the surface. The effect is only appreciable for very large doses.

(e) A diamond cubic crystal viewed from the $\langle 110 \rangle$ direction, showing hexagonal ion channels. If there is a crystallographic structure to the target and especially in semiconductor substrates where the crystal structure is more open, particular crystallographic directions offer much lower stopping than other directions. The result is that the range of an ion can be much longer if the ion travels exactly along a particular direction, for example the $\langle 110 \rangle$ direction in silicon and other diamond cubic materials. This effect is called ion channeling [80], and, like all the channeling effects, is highly nonlinear, with small variations from perfect orientation resulting in extreme differences in implantation depth. For this reason, most implantation is carried out a few degrees off-axis, where tiny alignment errors will have more predictable effects. There is no relation between this effect and ion channel of a cell membrane.

(f) In the ion implantation semiconductor fabrication process of wafers, it is important for the workers to minimize their exposure to the toxic materials used in the ion implanter process, where hazardous elements, solid source and gasses are used, such as Arsine and Phosphine. For this reason, the semiconductor fabrication facilities are highly automated, and may feature negative pressure gas bottles safe delivery system (SDS). Other elements may include Antimony, Arsenic, Phosphorus, and Boron. Residue of these elements show up when the machine is opened to atmosphere, and can also be accumulated and found concentrated in the vacuum pumps hardware. It is important not to expose yourself to these carcinogenic, corrosive, flammable, and

toxic elements. Many overlapping safety protocols must be used when handling these deadly compounds.

(g) High voltage power supplies in ion implantation equipment can pose a risk of electrocution. In addition, high-energy atomic collisions can, in some cases, generate radionuclides. Operators and Maintenance personnel should learn and follow the safety advice of the manufacturer and/or the institution responsible for the equipment. Prior to entry to a high voltage area, terminal components must be grounded using a grounding stick. Next, power supplies should be locked in the off state and tagged to prevent unauthorized energizing.

2.7.2 Surface diffusion

Diffusion in silicon is directly associated with native point-defects and impurity-related defects [81]. Impurity related defects arise from the introduction of group-III elements or group-V elements into the silicon lattice, due to its nature of highly soluble in silicon, it dissolve almost and completely on substitutional lattice sites and are easily ionized. In addition, native point-defects exist in the pure silicon lattice. Every material transport in silicon like self- and dopant diffusion is influenced by point-defects. Point-defects are generated due to the reactions occurring at the surface during oxidation, nitridation, and silicidation [82]. When the silicon crystal is heated, point defects flow from the surface into the bulk and the opposite type is transported to the surface. If impurities are introduced into the silicon lattice, the gradient of the local concentration causes a diffusion process. The diffusion process shows high

temperature dependence and, hence, for significant matter transport through diffusion the temperature must be above 800 °C for almost all dopants.

2.7.3 Electrostatic and chemical doping

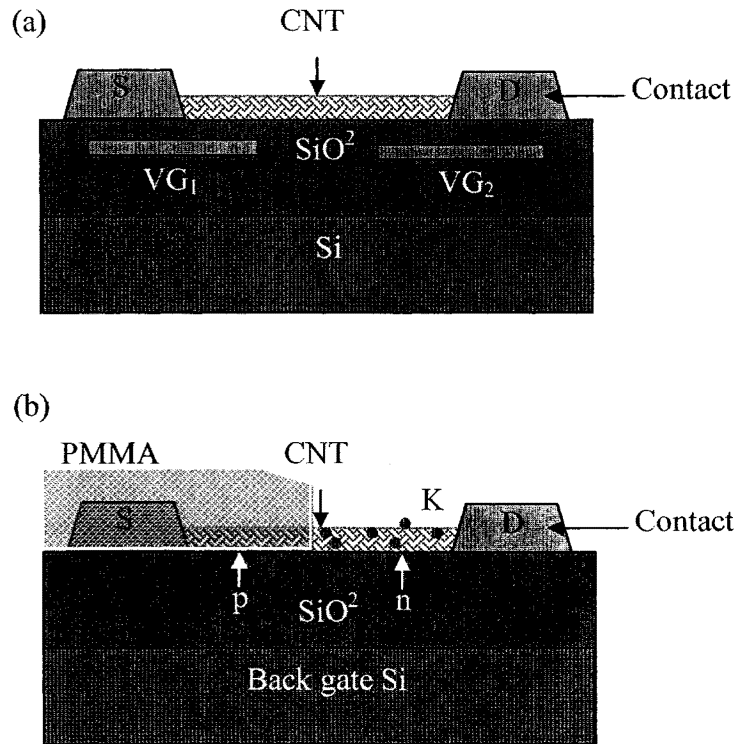


Figure 2.11: Schematic carbon nanotube device structure fabricated using (a) electrostatic and (b) chemical doping.

It has been observed, when carbon nanotube is doped using conventional semiconductors techniques, it loses electrical properties. The electrostatic [83] and chemical doping method [84, 85] are used for doping CNTs. Figure 2.11(a) illustrates electrostatic doping technique using CNT by split gate configuration [86]. The gates were oxide embedded using CVD technique. To establish both p (hole) and n

(electron) doping onto a single tube, a SWNT needs to exhibit ambipolar behavior. An ambipolar device is hole conducting (p channel) when the gate bias is sufficiently negative and electron conducting (n channel) when the gate bias is sufficiently positive, with $V_{G1} < 0$ and $V_{G2} > 0$, an electrostatically doped p-n junction (p-n with respect to S contact) should be realized. By reversing the bias, $V_{G1} > 0$ and $V_{G2} < 0$, a p-n junction of the opposite polarity (n-p with respect to S contact) is achieved.

A p-n junction diode is fabricated using chemical doping [87] as demonstrated in figure 2.11(b). A p-type CNT is employed between two contacts; source and drain. Polymethylmethacrylate (PMMA) layer covers the half part of nanotube, leaving behind the left half uncovered. Potassium (K) doping [88] is adsorbed onto the uncovered half nanotube. The PMMA covered half part remains as p-type [89]. The potassium donates electron and converts CNT from p-type to n-type. Thus, forming a p-n junction at the interface. Though the technique is simple, it has limitation in terms of high density structure formation. Thus, surface functionalization doping technique has been proposed for modulating intrinsic property of CNTs.

CHAPTER 3

MATERIALS AND METHODS

The fabrication and assembly of the crossbar ionic junction nanodevice consists of the following five steps:

- (i) synthesis of extrinsic nanomaterials by surface functionalization method,
- (ii) fabrication of microelectrode array using photolithography technique,
- (iii) fabrication of a polymer PDMS stamp using a rapid soft lithography technique,
- (iv) patterning of p-type and n-type nanomaterial using a PDMS stamp in crossbar fashion and
- (v) electrical characterization of crossbar nanojunction.

To validate the methodology, two experiments were conducted using two different nanomaterials:

- (i) Extrinsic multiwalled carbon nanotubes for fabricating a crossbar semiconductor nanojunction
- (ii) Synthesized extrinsic single walled carbon nanotubes for fabricating a crossbar ionic junction. Assembling both types of nanojunction incorporates the basic four steps described earlier.

3.1 Synthesis of extrinsic nanomaterials

Nanomaterials ranging from quantum dots to organic molecular semiconductors have been synthesized and used as building blocks for devices with nanoscale components. Due to its 1-dimensional characteristics, the use of nanomaterials offers the advantage of increased surface area to volume ratio for a device. Despite these numerous advantages explained in chapter 1, there are multiple shortcomings associated with the use of nanomaterials. First, due to the size of the nanomaterials, there are difficulties in the symmetrical alignment and array patterning for integrated nanosystems. In addition, there are issues associated with the repetitive, symmetric patterning and alignment in terms of positioning, fabricating and assembling them into nanodevices. Second, discontinuity, synthesis defects and cracks in certain nanomaterials, such as nanowires and nanorods, result in poor electrical conductivity. Defects in MWCNTs on the other hand have been used advantageously. They have provided improved conductivity due to electron mobility at the defect sites within inner walls of CNTs. Seamless structure; covalent bonding and extensive p-overlap and van-der-Waals interaction of shells in the MWCNTs provide improved physical properties such as stiffness, conductivity and toughness. This has made the use of MWCNTs as building blocks for nanoscale devices, the major research focus in a nanodevice-based technology. In the last ten years, fabrication of single as well as multiple junction-based devices using a wide range of nanomaterials with performance characteristics comparable to the silicon-based devices has been demonstrated [11, 90, 91]. This has

been adopted in developing improved interconnects, increasing the device dynamic performance characteristics, and finally, serving as efficient conductors of heat.

In the CNT family, MWCNTs (Chemical Inc through Fisher Scientific, Hampton, NH) defects in the outer shells causes electron tunneling between inner shells that increases charge conductivity. Despite the inability to distinguish and sort semi-metallic and metallic MWCNTs during synthesis, both types of MWCNTs show unique properties such as stiffness in terms of tensile strength in the order of 200 GPa [92]; improved elastic modulus, young's module equal to 1 Tpa [93] and results in stretching beyond 20 percent of their original length and improved toughness. This makes MWCNTs approximately two orders of magnitude times stronger than steel. Hence, with these physical, mechanical and electrical properties MWCNTs are suitable for building nanodevices. In addition, due to composition and geometry, fullerenized MWCNTs exhibit electrical conduction property, this is similar to regular conductors. Also, during the synthesis of MWCNTs it has been determined that approximately 80 percent of the CNTs are semiconducting , hence by assembling nanodevices from a mixture of MWCNTs, the devices are functioning as an aggregate of MWCNTs, integrated together to form the devices. This fact has been utilized to create functional device elements in the current application.

Through single walled carbon nanotubes (SWCNTs) have electron transport only on the outer shells, trading SWCNTs with MWCNTs for fabricating nanodevices has been identified as the method to be adopted in developing nanoscale devices. This is because, due to its multiple tubes embedded into each other, tuning the electrical

properties of MWCNTs is complex. In addition, formation of surfactant micelle layer around SWCNTs has been demonstrated and alteration of the SWCNTs intrinsic properties can be achieved. Also, an electron transport in SWCNTs is efficient around single tube. Thus, in my experiments, I have assembled an ionic nanojunction using surface functionized SWCNTs. Similar to the fabrication of p-n semiconductor junctions that involves the interfacing of extrinsic (p-type and n-type) semiconducting material, the formation of P-N ionic junctions also involves integrating extrinsic (cationic and anionic) nanomaterials, where charge transport and modulation is achieved through the ion molecules. For the synthesis of extrinsic SWCNTs, two types of surfactants were used; sodium dodecyl sulfate (SDS) and cetyl trimethylammonium bromide (CTAB), having Na^+ positive ionic charge (anions) and Br^- negative ionic charge (cations) on its hydrophilic ends respectively. Doping SWCNTs with SDS and CTAB produces anionic SWCNTs and cationic SWCNTs respectively. This is achieved by chemically modulating an intrinsic Fermi energy level of the SWCNTs (E_{fi}).

A 1-ml aqueous solution of SDS (Sigma-Aldrich co-operation, St. Louis, MO, USA) (1% by weight, concentration greater than the critical micelle concentration (CMC)) was sonicated with 1 mg of SWCNTs (Cheap Tubes, Brattleboro, VT, USA) of diameter 1-2 nm and length 5 to 30 μm . SWCNTs surfactant solution was sonicated for 30 minutes for a homogenous dispersion and to form a micelle layer around SWCNTs. As both SDS and CTAB surfactant easily dissolve in DI water, there is no change in protocol for functionalization of SDS-SWCNTs and CTAB-SWCNT's to

synthesize P-type and N-type extrinsic SWCNTs respectively. To indicate the functionalization of SWCNTs, the two probe resistance is measured across microelectrode and change in the resistivity is observed. The resistance of extrinsic SWCNTs decreases on functionalization. Further detailed discussion is provided in results chapter.

The surfactant concentration (1% by volume) greater than critical micellar concentration (CMC) is considered to achieve a uniform micelle formation around the nanotube [94]. Due to weak electrostatic van der Waals interaction, molecules are aligned and oriented perpendicular and parallel on to the carbon nanotube. The direction of orientation corresponds to energy minima for the nanomaterial complex [95]. Due to a weak electrostatic van der Waals interaction, the molecules are aligned and oriented perpendicular and parallel onto the carbon nanotubes. The hydrophobic group of surfactant is electrostatically adsorbed onto the surface of carbon nanotube and the hydrophilic group is oriented towards an aqueous phase covering the entire surface. Figure 3.1 shows a half cylinder of SWCNTs with SDS and CTAB surfactant molecule perpendicular oriented onto its surface. In figure 3.2 the band diagram study shows that the Fermi level of undoped SWCNTs is at the center of the band gap. Whereas, the adsorption of SDS molecules onto SWCNTs adds anionic dopant thereby shifting the Fermi level towards the valence energy band (E_v) below the intrinsic Fermi energy level. Conversely, adsorption of CTAB molecule onto SWCNTs adds cationic dopant thereby shifting the Fermi level towards the conduction energy band (E_c) above the intrinsic Fermi energy level. As a result, SWCNTs behave

as P-type (anionic) and N-type (cationic) nanomaterials. Using these extrinsically doped SWCNTs (anionic-type and cationic-type), the crossbar ionic nanojunction device is fabricated. Figure 3.3 and 3.4 shows SEM and EDX characterization of CNTs coated with surfactants.

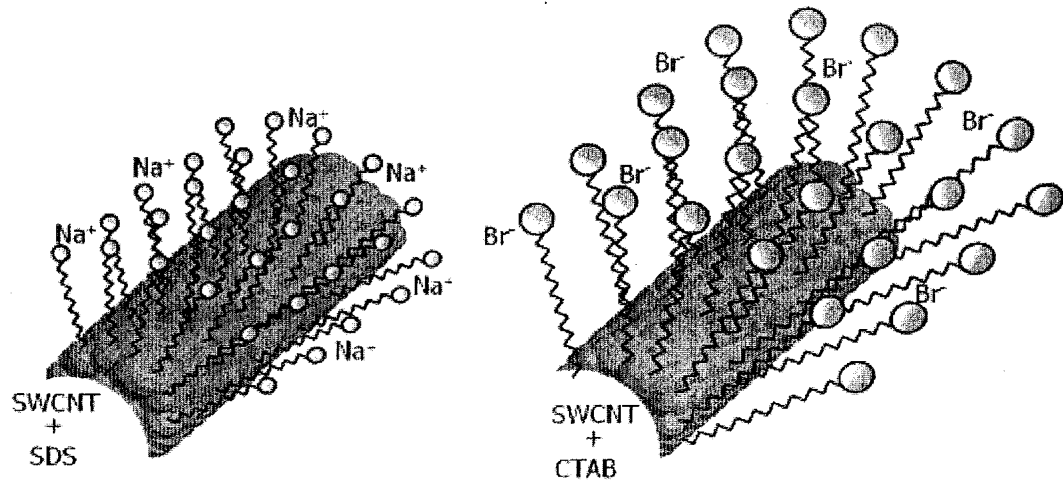


Figure 3.1: Surfactant molecules on the SWCNTs. (a) and (b) SDS and CTAB form a uniform layer or a micelle around nanotubes with hydrophobic group adsorbed onto SWCNTs surface and hydrophilic heads having Na^+ and Br^- ions towards the aqueous phase respectively. The surfactant molecules are perpendicularly oriented to SWCNTs due to a weak van der Waals electrostatic force.

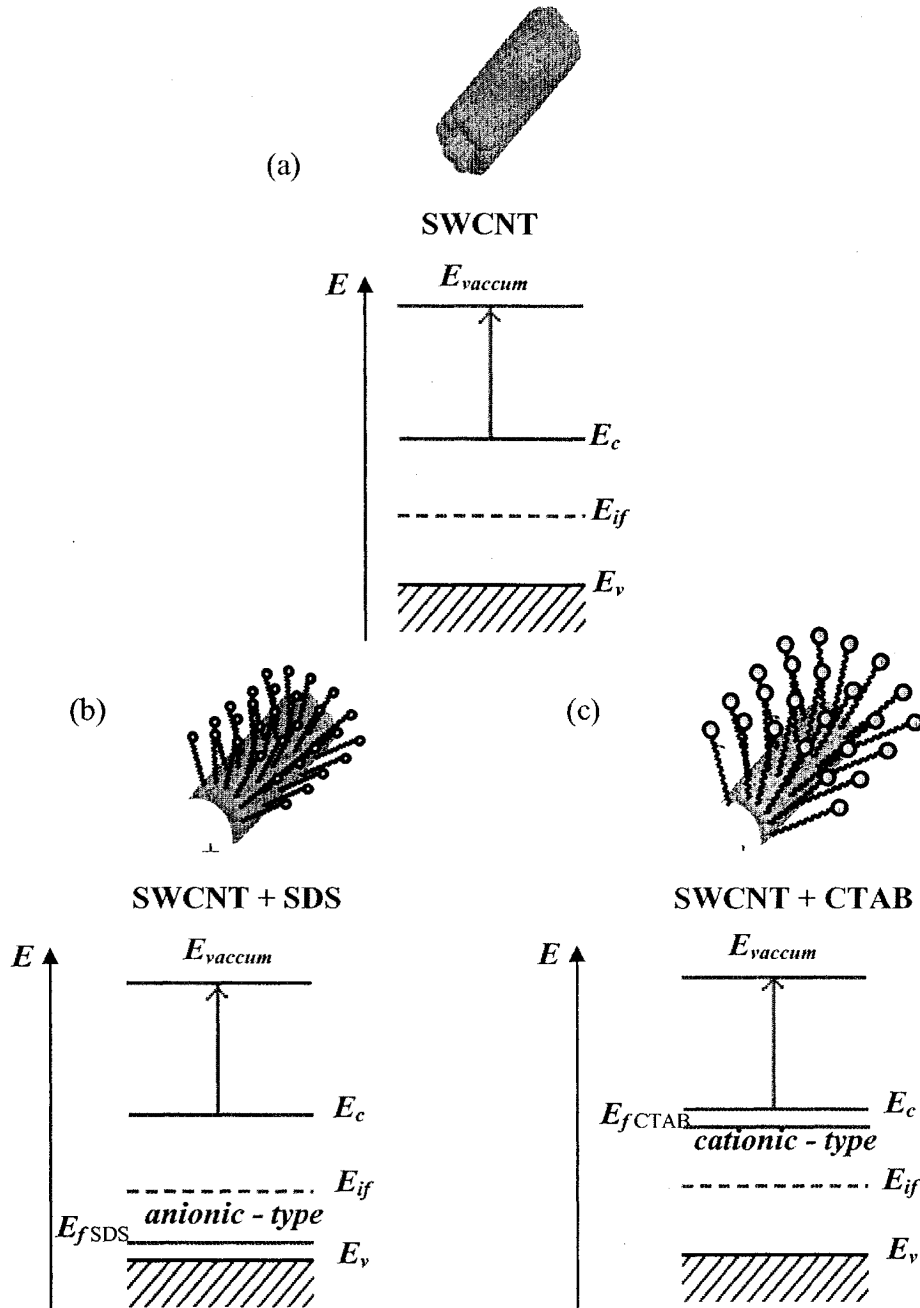


Figure 3.2: Band diagram of surfactant coated carbon nanotubes. (a) Undoped SWCNTs has Fermi energy level at the center of the band gap, (b) SWCNTs treated with SDS where the Fermi level was modulated and has shifted below the intrinsic Fermi energy level of SWCNTs towards the valence band, (c) SWCNTs treated with

CTAB; resulted in the Fermi level shift above intrinsic energy level of SWCNTs towards the conduction band.

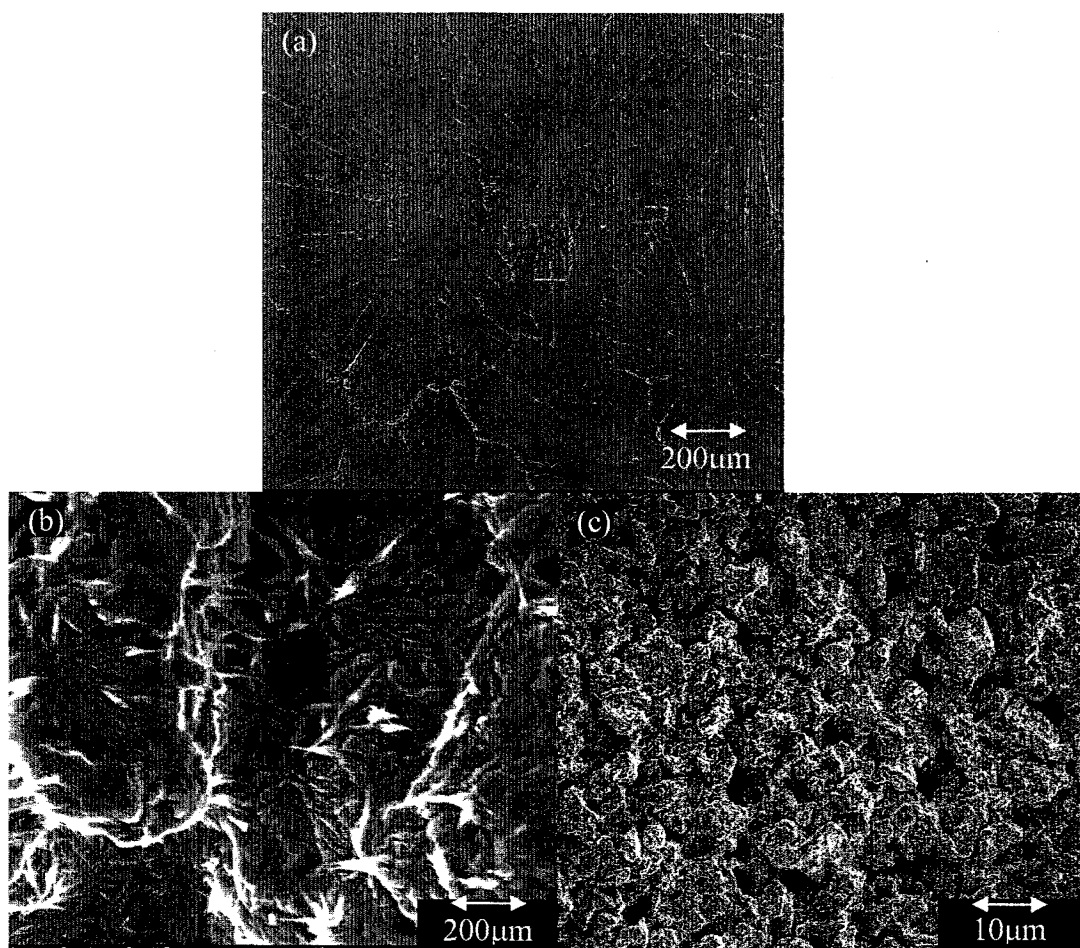


Figure 3.3: SEM characterization of surfactant and CNTs coated with surfactant. (a) Surfactant dispersed on to a base substrate. The flower like radial lines illustrates surfactant tendency to form micellation. (b) and (c) demonstrate clusters of CNTs coated with surfactant at two different magnifications.

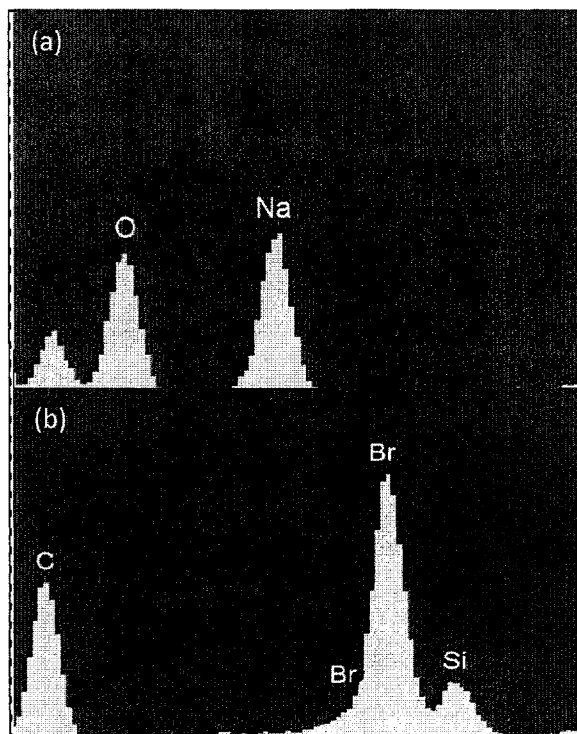


Figure 3.4: EDX characterization of surface functionalized CNTs. (a) Elemental analysis shows presence of sodium ions in CNTs coated with SDS and (b) CNTs coated with CTAB show the presence of negative bromide ions.

3.2 Microelectrode array

Simple and standard photolithography techniques have been used for microfabricating planar base microelectrode platforms. The microfabrication technique uses the fundamental principle of optical lithography. It consists of a four-step process sequence: substrate preparation, photoresist application, exposure, and developing and finally metal sputtering and lift off. Figure 3.5 shows a schematic representation of a process sequence for microelectrode array platform assembly. The preparation process involves cutting of a 4-inch diameter Si wafer into a small silicon chip of size of

approx. 1x 1 inch. The silicon chip is then cleaned by rinsing in acetone, isopropyl alcohol (IPA), and finally in de-ionized (DI) water to remove dirt. Later, prior to photoresist application the rinsed silicon chip is dried using inert N₂ gas, and later heated to a temperature sufficient to dry out the moisture present onto the surface that will interface adhesion of the photoresist polymer. In the photoresist application process, Shipley 1827 (MicroChem, Newton, MA, USA) photosensitive positive photoresist is spin coated to approximately a thickness of 3000 Å by spinning at 3000 rpm for 60 sec. This is followed by the exposure and developing process. This process consists of a soft bake step for 5s at 113°C to remove the excess solvent from the photoresist. Substrate exposure occurred at 35mW/sec powered at 365 nm ultra violet (UV) light for 4s using the contact masking method, and the pattern was developed by immersing the exposed substrate into a bath of “Micro Dev” solvent developer. The developed substrate was again cleaned with DI water to remove excess developer and blow dried by N₂ gas to remove DI water residue. The patterned microelectrode was sputtered with a uniform gold film of approximately 50 nm. The sputtering process was followed by an acetone lift off and blow-dried using N₂ to remove acetone. These photolithographically fabricated MEAs are used for I-V characterization of crossbar junction device. Table 3 shows the experimental parameter for fabrication of MEA using different photoresists.

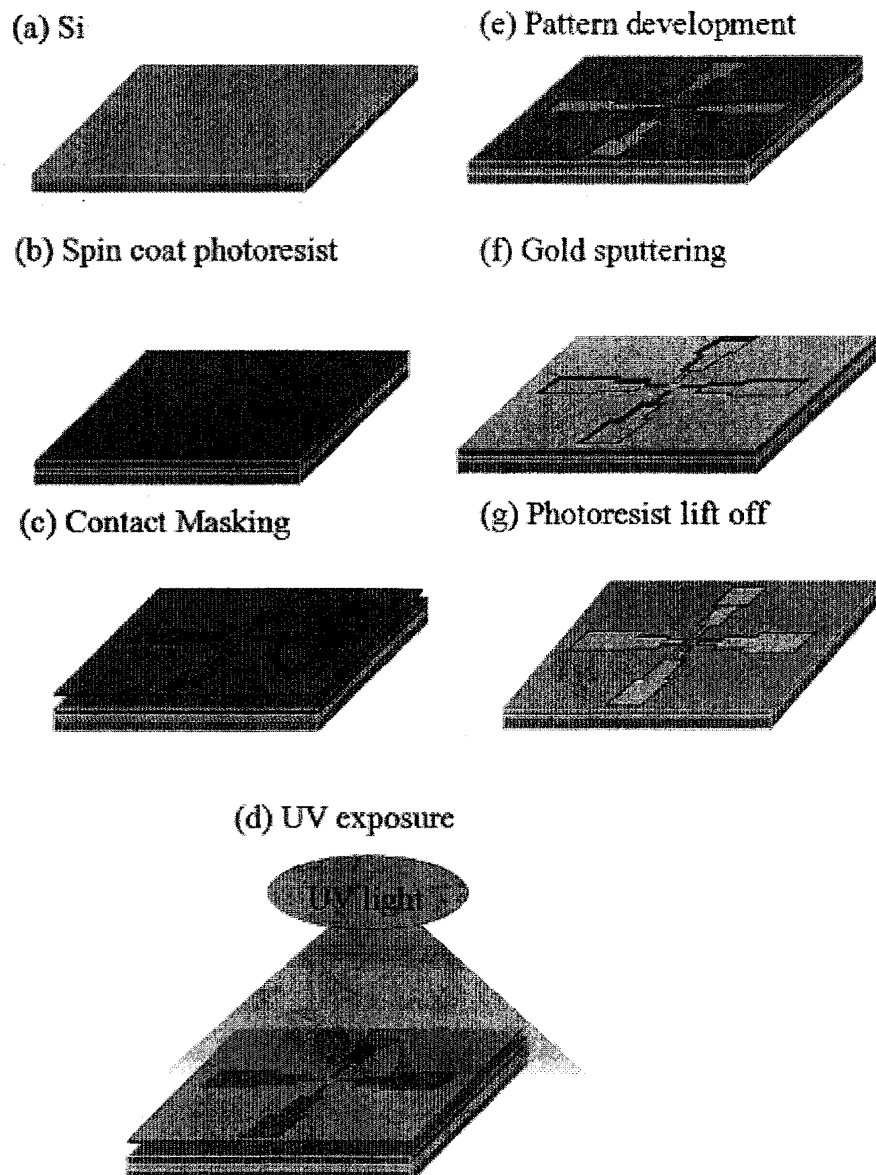


Figure 3.5: Schematic representation of process sequence for microfabrication of the base microelectrode array platform. (a) Clean Si wafer, (b) Spin coated photosensitive positive Shipley 1827 photoresist at 3300 rpm for 60 s, (c) Contact masking for pattern transfer, (d) 365nm UV-Exposure for 4 sec, (e) Pattern development in a developer for approx. 1min, (f) Sputtering thin film of gold of 50nm, (g) Photoresist lift off using acetone.

Table 3: Table representing parameters for fabrication process.

	Type of Photoresist		
	1827	1805 + LOR	SU-8
Company	Shipley	Shipley	Microchem
Resist tone	Positive	Positive	Negative
Spin coat	~3000 rpm/60 s	~3000 rpm/60 s	~3000 rpm/60 s
Film Thickness	3 μm	~0.5 μm	100 μm
Prebake	113 °C/5sec	113°C/10sec	65°C/5 min 95°C/15 min
UV-light	365 nm	365 nm	365 nm
Exposure	~ 4 sec	~6sec	~ 7 sec
Developer	1:1 developer and DI	Remover 1165 Microposit CD- 26 developer	SU-8 developer, 1:1 developer and IPA
Development time	~90sec	~90sec	~90sec
Lift off	Acetone lift off	Acetone lift off and LOR remover	NA

3.3 Mask design for microelectrode array fabrication

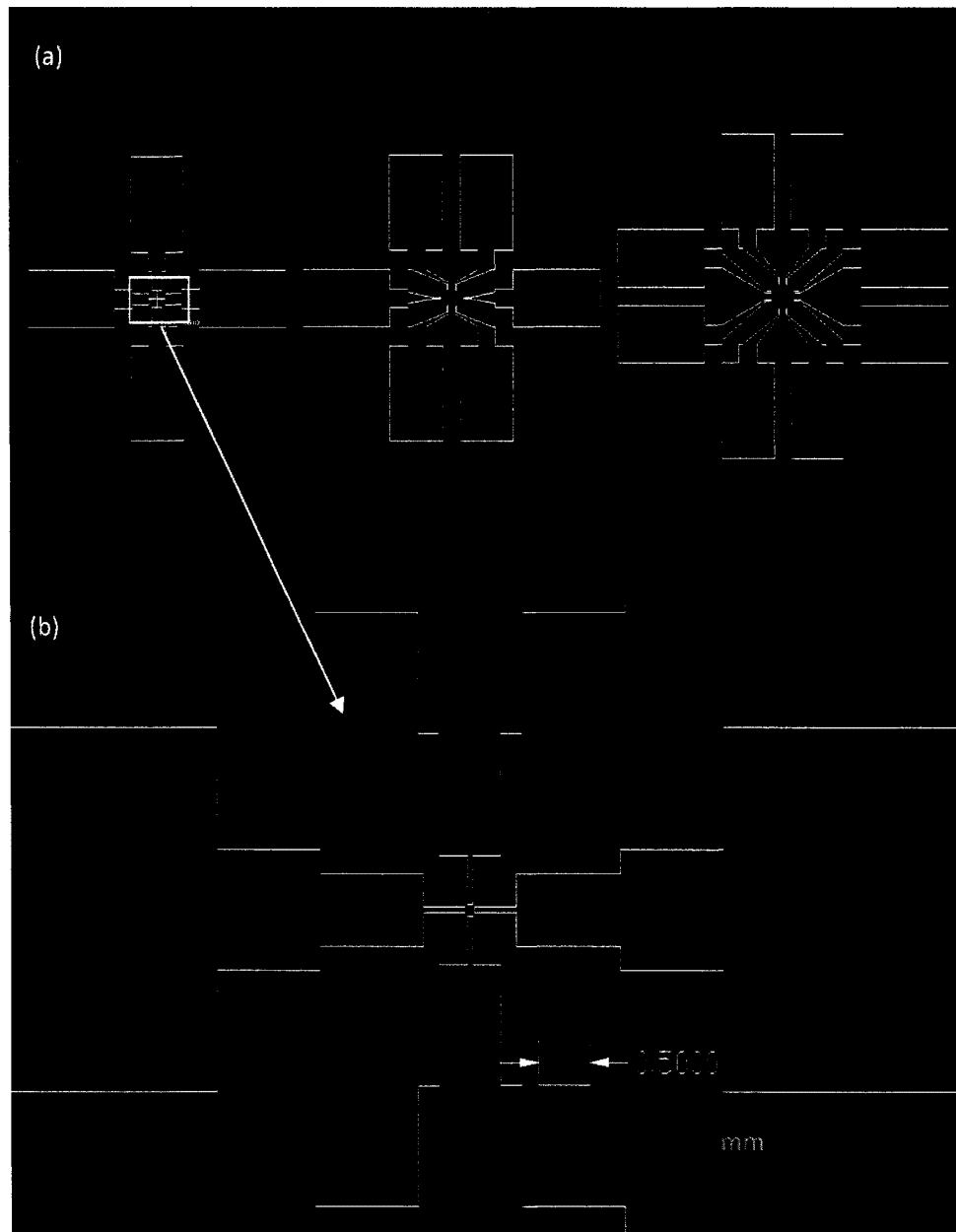


Figure 3.6: Schematic autocad design of microelectrode array. (a) 1 x 1, 1 x 2 and 2 x 2 microelectrode array, (b) 1 x 1 microelectrode, where one set of two microfingers aligned across each other and second set perpendicular aligned to first set of microelectrode fingers.

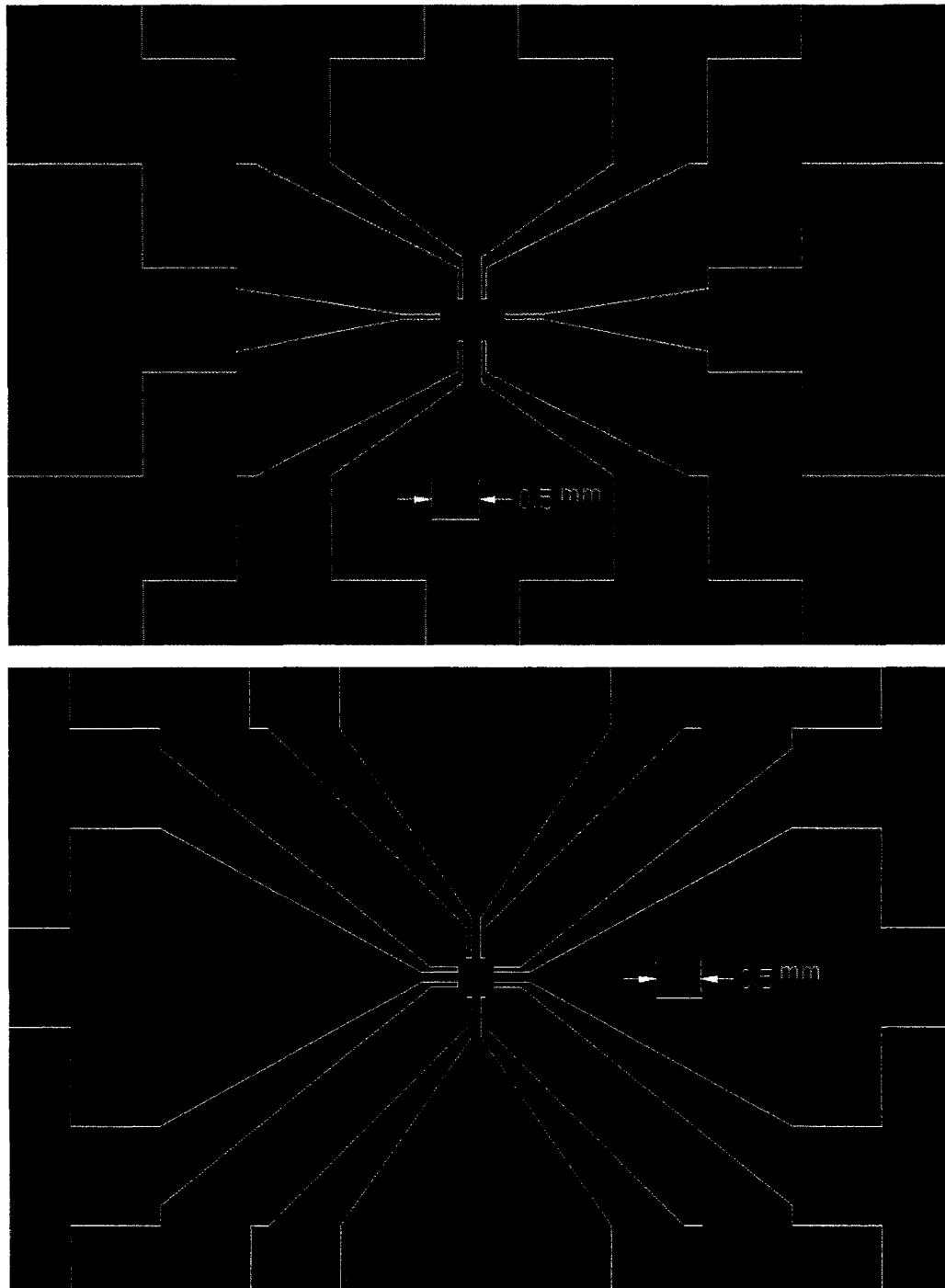


Figure 3.7: Schematic auto cad design. (a) 1 x 2 microelectrode array and (b) 2 x 2 microelectrode array.

For mask fabrication, design of microelectrodes array and master templates for stamp fabrication is drawn using AutoCad software. Figure 3.6 and 3.7 represents 1 x 1, 2 x 1 and 2 x 2 microelectrode array. A 1 x 1 microelectrode array consists of four microfingers. The metallic gold electrode fingers are 100 μm apart with fingertips facing each other in a cross-junction fashion. The geometric design of each set of micro fingers was designed in a graded step pattern with width varying from 50 μm to 5mm. This was done to target seamless current flow to and from the micro to the nanodomain and vice versa and integrate the microscale contacts to the external measurement circuitry. The electrode pads are of 3 mm x 5 mm in dimension. While in 2 x 1 microelectrode array, pair of microfingers is aligned adjacent to each other with a separation of 0.1 mm. In 2 x 1 and 2 x 2 microelectrode array, the tips are placed 1.3 mm and 0.85 mm apart across each other. The design ensures exact pattern transfer of nanomaterials onto fingertips for electrical characterization.

The smallest critical dimensions achieved using photolithography in our laboratory using contact mask is 50 μm . The edges of fingers tip are of different length to ensure features size greater than 50 μm . Figure 3.8 illustrates the design constraints for fabrication of microelectrode array. Contact lithography is use to achieve highest optimal resolution. Thus, mask dimensions are drawn considering 1:1 pattern transfer. In addition, negative mask is design for MEA because following gold deposition; positive developed photoresist can be lift-off using simple acetone wash method, whereas a complex technique such as plasma etching is required for negative photoresist. The MEA design patterned is transparent on negative mask. While, for

stamp fabrication, SU-8 is used because relief structure greater than $1\text{ }\mu\text{m}$ can be achieved and also photoresist lift-off is not required. However, positive mask is fabricated for negative SU-8 photoresist. The difference between the positive and negative mask is shown in figure.

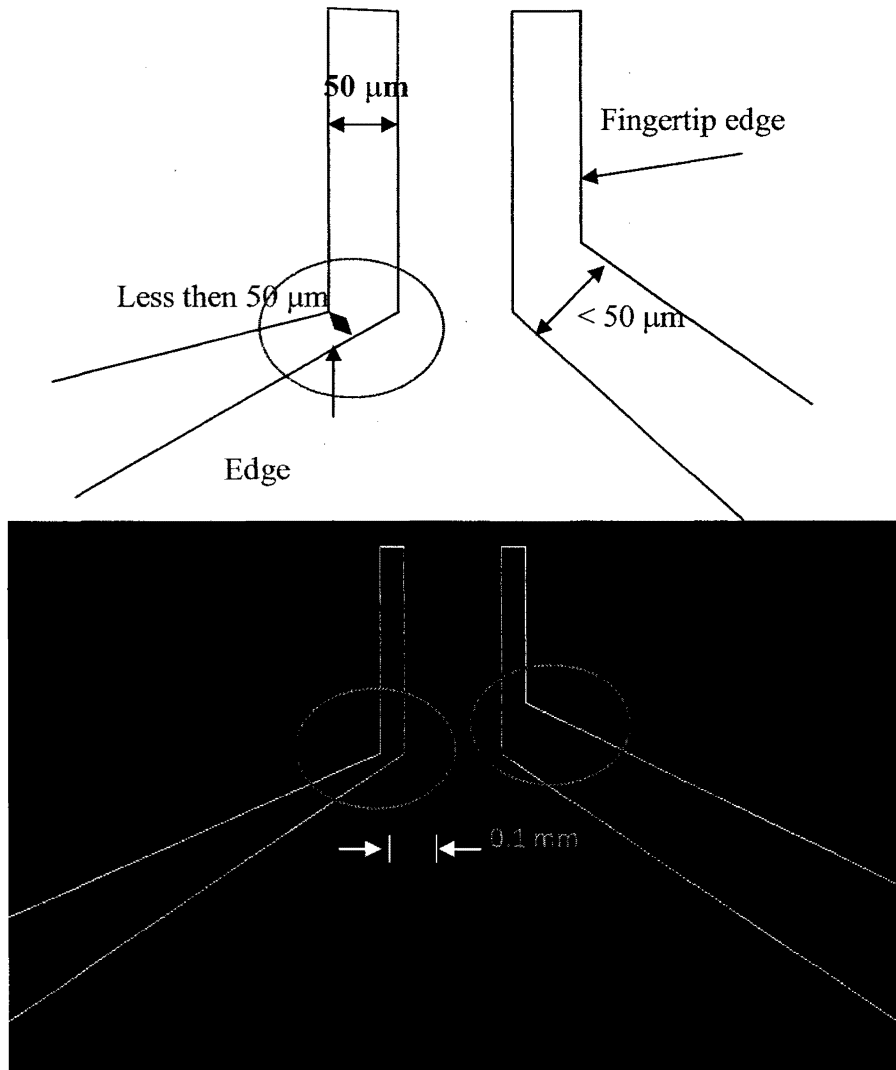


Figure 3.8: Microelectrodes are designed such that the smallest feature is greater than or equal to $50\text{ }\mu\text{m}$ in dimensions.

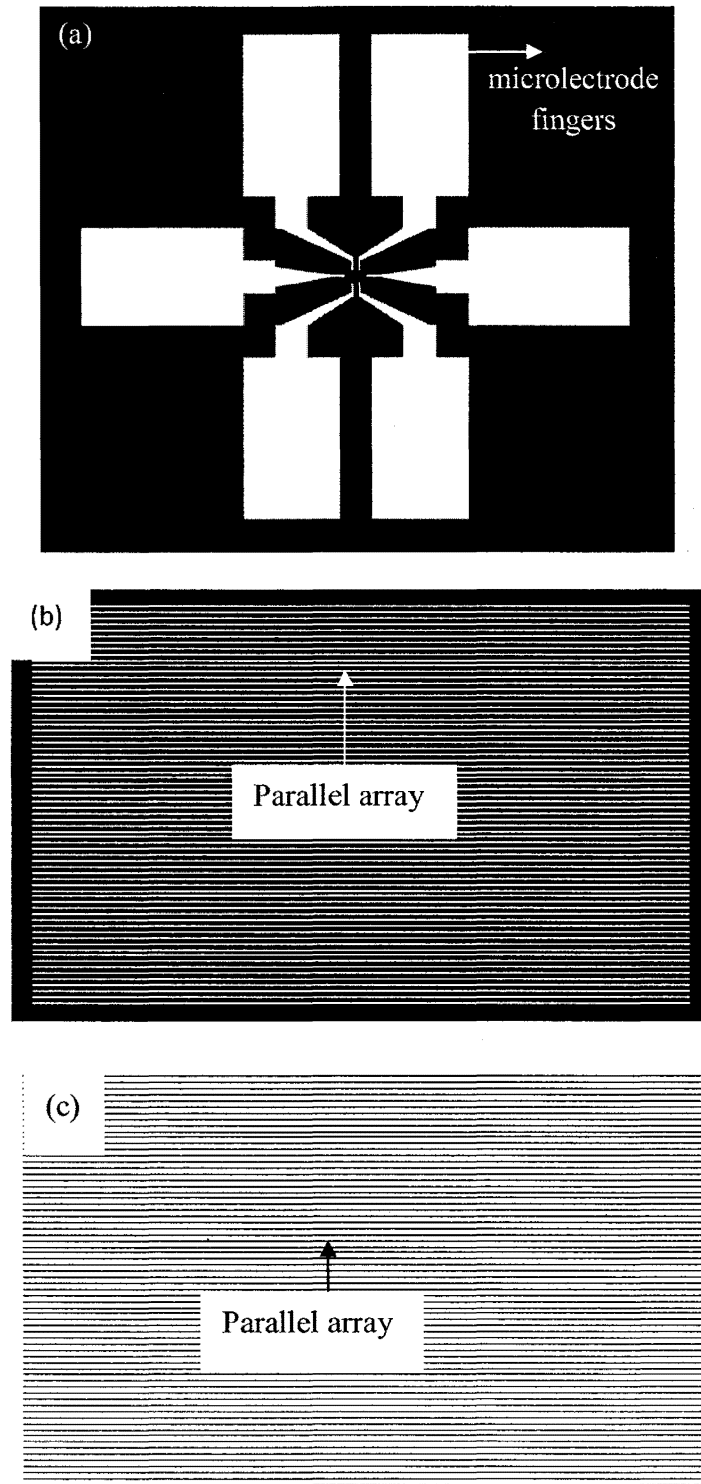


Figure 3.9: Snapshot of mask design. (a), (b) positive mask for MEA and (c) negative mask for PDMS master template for positive and negative tone resist respectively.

3.4 Stamp fabrication

For crossbar patterning of nanomaterial in parallel symmetric array, a PDMS stamp with a parallel relief structure was fabricated using soft lithography techniques. Prior to the PDMS stamp fabrication; a master mold with a negative pattern having a microchannel structure was fabricated using the previously described photolithography techniques. A positive mask with the parallel array shown in figure 3.9. The softlithography technique is comprised of a two-step process of mixing and curing. During the mixing process, Sylgard 148 (Dow Corning, Midland, MI, USA) was used, which consisted of two liquid components- the curing agent and the elastomer. The curing agent and the elastomer were mixed in a ratio of 1:10 and stirred for approximately 2-3 minutes in a glass container. While stirring air bubbles were formed into the liquid mixture. Degassing of air molecules was done by placing the liquid mixture into a large plastic container and creating a vacuum. Venturi effect; an aspirator and a Buchner funnel assembly were used for the creation of a vacuum of about approx. 10 torr. After 2 hours of degassing, the viscous mixture was poured onto the master mold template in a Petri dish and heated to a temperature of approximately 75°C for 2 – 3 hours depending upon the thickness of the stamp. After solidification, the solid polymeric stamp was peeled-off. Due to cross-linking, soft and flexible PDMS stamp is fabricated. Figure 3.8 shows a schematic representation of the process flow for fabricating the PDMS stamp. The autocad design for fabrication of PDMS stamp is shown in figure 3.10.

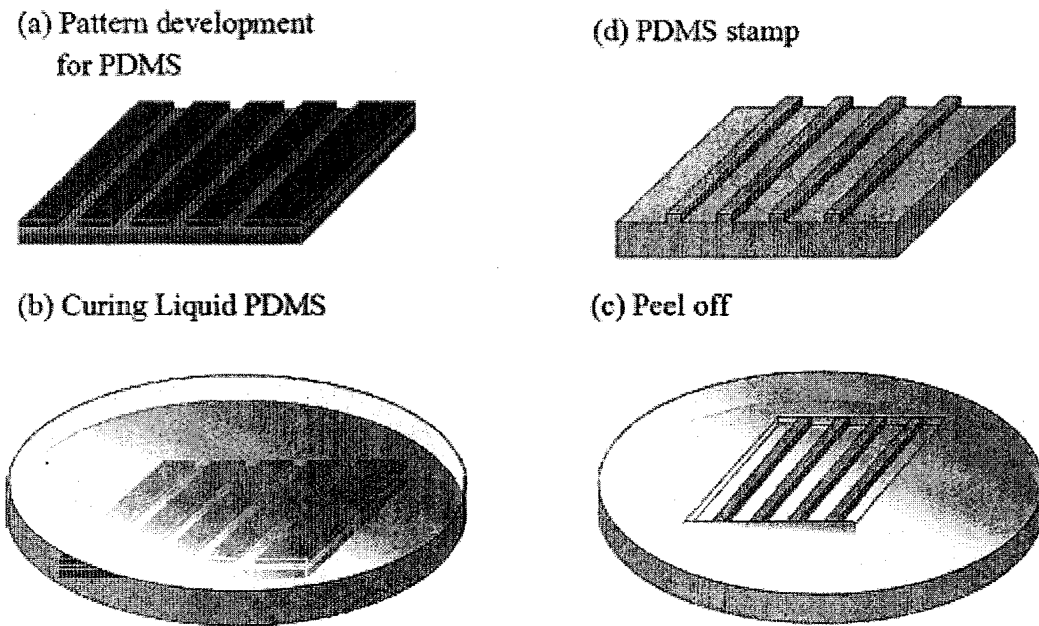


Figure 3.10: Schematic representation of process sequence for microfabrication of PDMS stamp. (a) Fabricated master template/mold using standard photolithography processes, (b) Transfer of the viscous liquid elastomer onto master template and (c) PDMS stamp peel-off post hardening, (d) PDMS stamp with microrelief structure for microcontact imprinting.

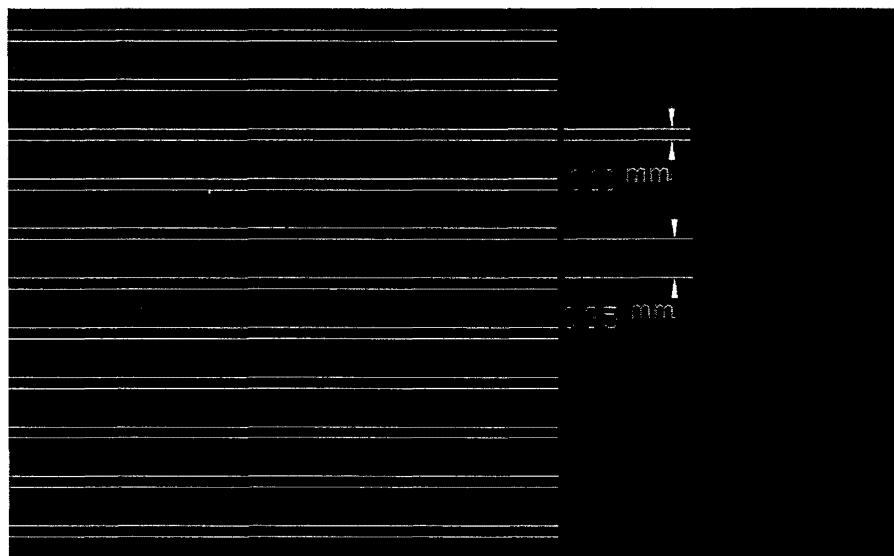


Figure 3.11: Schematic autocad mask design consists of parallel array for fabrication of PDMS master template. The line width is 100 μm and spacing between two parallel lines is 35 μm .

3.5 Patterning nanomaterials

The double microcontact imprint patterning was performed to form the crossbar junction. The PDMS stamp in figure was inked alternatively with p-type and n-type CNTs and was transferred in a grid like manner onto the base platform. The n-type CNTs were cross patterned by a phase shift of 90° to the p-type CNTs to form an array of junctions onto base microelectrode array. Due to the parallel relief structure on the PDMS stamps, repetitive parallel patterning of the CNTs bundles was achieved. The microelectrode platform was patterned with CNTs and later thoroughly dried for approximately 1 hr in an ambient atmosphere to remove excess solvent from the surface. Finally, the assembled crossbar junction was electrically characterized to

demonstrate the formation of the junction. Figure 3.12 shows the schematic diagram demonstrating the process sequence for fabricating the junction nanodevices using CNTs. The snapshot of PDMS stamp is shown in figure 3.13.

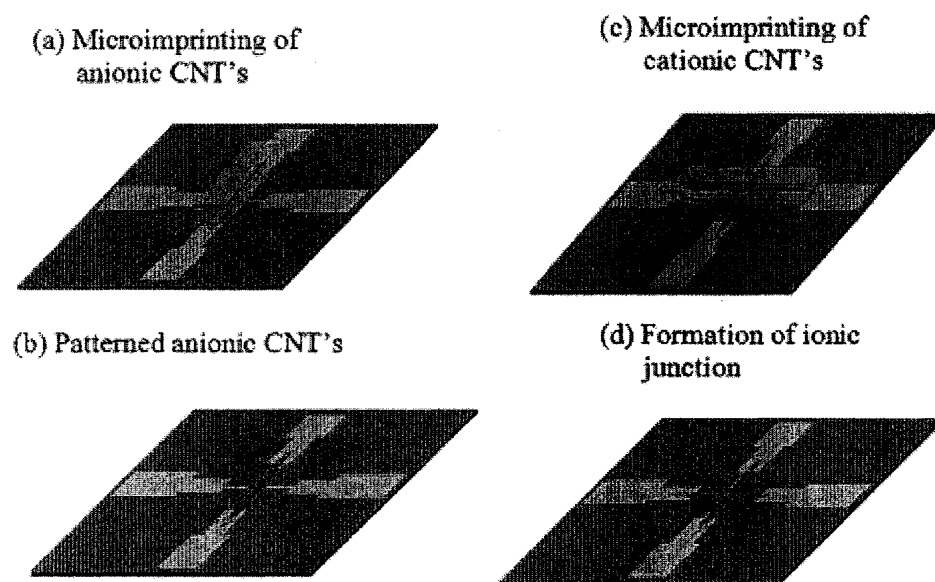


Figure 3.12: Schematic representation of process sequence for patterning nanomaterials via microcontact printing. (a) Microimprinting of anionic CNTs using PDMS stamp, (b) Patterned CNTs across two microcontacts, (c) PDMS stamp is phase shifted by 90° to imprint cationic CNTs across other set of microcontacts, (d) Formation of ionic nanojunction using the softlithography techniques.

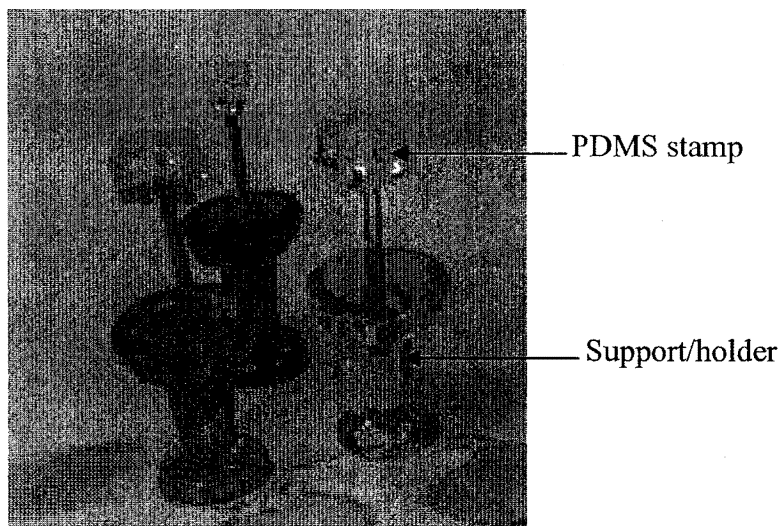


Figure 3.13: Snapshot of PDMS stamp. Stamps were cut in small size of area approx. 0.5 cm^2 and push pins were embedded for support and means for holding for patterning, aligning and assembling nanomaterials.

3.6 Instrumentation

The experimental setup consisted of a micro manipulator system comprising of two 3-axis mechanical micro-positioners (KRN-09S, J.Micro Technology) with a compound microscope (LMS-2709) for visualization (J. Micro Technology, Portland, OR). A Femto-Ammeter, Keithley 640 (Keithley, Ohio, USA) was used to acquire the signal and controlled by LABVIEW V.7.1. The schematic of the measurement system is illustrated in Figure 3.14. The micro-positioners equipped with micro needles, were placed and aligned using the appropriate alignment screws, under a microscope in order to make contact with gold contact pads on the chip.

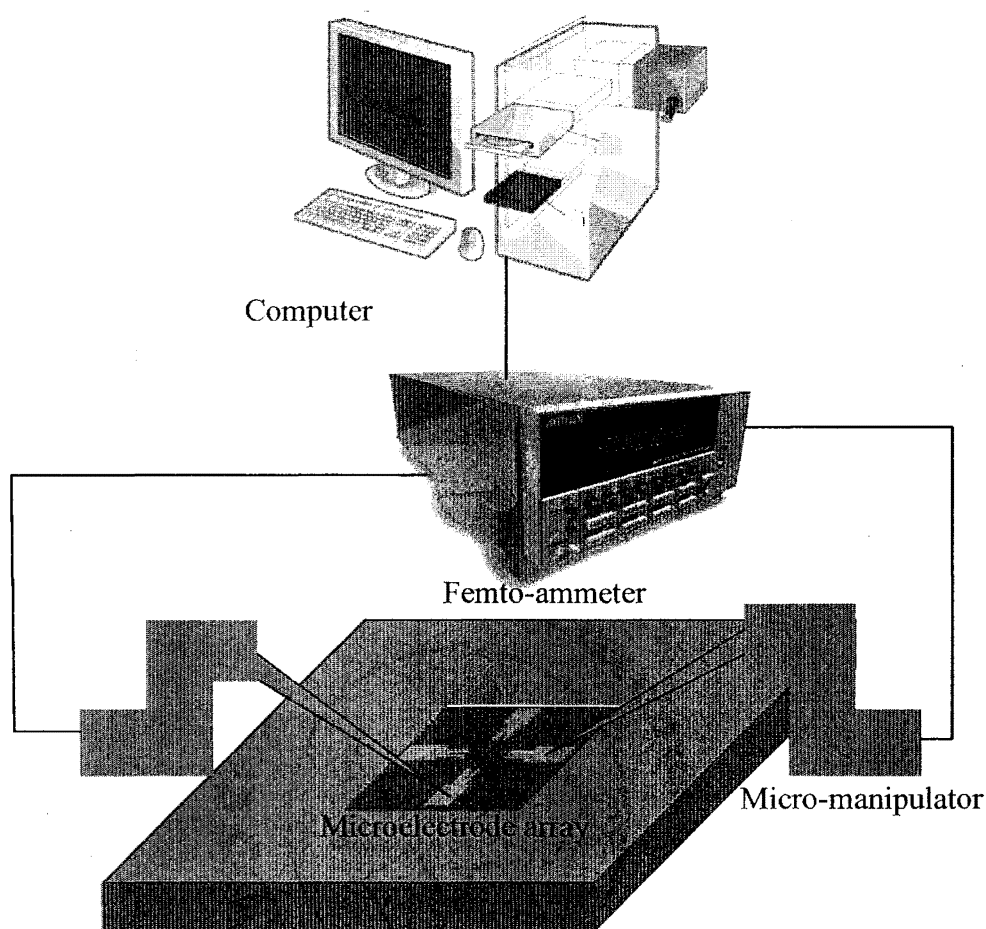


Figure 3.14: Schematic representation of the experimental set-up used for the electrical characterization of microelectrode array.

The micron-sized electrodes are probed to Keithley femto-ammeter through micro-manipulators. The femto-ammeter is interfaced with a computer for recording and storing measurements through LAB VIEW. The pictures of the nanotube-micro-electrode array system are captured using a CCD Camera. The micro-positioners were connected to the femto-ammeter through BNC connectors. The femto-ammeter was in turn connected to the computer through the IEEE-488 general purpose interface bus

(GPIB) to acquire and record the data values. This was followed by the measurement of characteristic electrical behavior associated with CNTs junction formation. Data was collected for each of the junction and stored in MS Excel file format separately. Appropriate steps were adopted to reduce the effect of noise and electromagnetic interference by placing the complete set-up in faradays cage.

Table 4: List of different materials and equipments exploited and utilized.

Materials/Equipments	Company Name
Sylgard 148	Dow Corning, Midland, MI, USA
Carbon nanotubes	
Multiwalled carbon nanotubes	Strem chemical Inc through Fisher Scientific, Hampton, NH, USA
Single walled carbon nanotubes	Cheap Tubes Inc., Brattleboro, VT, USA
Surfactants	
CTAB	Fishers Scientific, Scientific, Hampton, NH, USA
SDS	Fishers Scientific, Scientific, Hampton, NH, USA
Photoresists	
SU-8	Microchem Corporation, Newton, MA, USA
Shipley 1827	Shipley – Microchem, Newton, MA, USA

Developer	
Developer concentrate	Rohm and Haas Corporate, Philadelphia, PA, USA
SU-8 developer	Microchem Corporation, Newton, MA, USA
Equipments	
Mask aligner	Hydralign Series 200 IR, Optical Associates Inc (OAI) San Jose, CA, USA
UV- power meter	306 UV- Powermeter mW/cm ² , OAI, Jose, CA, USA
Hot plate	Systems and Technology International Inc. (STI), Tolland, CT, USA
Spin coater	P6700 Series, Specialty Coating System Inc., Indianapolis, IN, USA
Mask fabrication	Outputcity, CAD/Art Services, OR, USA
Sputter coater	208HR, Cressington Scientific Instruments Ltd, Watford WD19 4BX, England (UK)
Femto-ammeter	Keithley 6430, Keithley, OH, USA
Microscope	
Optical Microscopy	32-0108A-238, Micropublisher 3.3, QImaging Corporation, Burnaby, Canada
Software	
Multiphysics modeling –	COMSOL Inc, Burlington, MA, USA

COMSOL	
Lab view	National Instruments, Austin, TX, USA
16 bit data acquisition board	CB-68LPR, National Instruments, Austin, TX, USA
Autocad	Autodesk Inc., San Rafael, CA, USA
Image capture	QCapture Pro5.1, QImaging Corporation, Burnaby, Canada.

CHAPTER 4

RESULTS AND DISCUSSION

Integration and assembling of crossbar junction consists of fabrication of MEA, fabrication of PDMS stamp and, finally assembling and patterning of extrinsic carbon nanotubes. At each stage, the device is characterized and optimized, to get a desired result and to evaluate its perfection on fabrication. The following chapter presents results and discusses them in detail

4.1 Microelectrode array characterization

A microelectrode array (MEA) is an arrangement of several electrodes for electrical measurement of an assembled device. In order to characterize multiple junctions and measure I-V curves, three types of microelectrode designs were fabricated; 1 x 1, 1 x 2 and 2 x 2. All these devices were fabricated using standard photolithography. In MEA, electrodes fingers are fabricated using gold metal. Figures 4.1 and 4.2 show optical micrographs of 1 x 1, 1 x 2 and 2 x 2 MEA platform at various stages of lithography process respectively. Figure 4.1(a) shows perfect pattern transfer of microelectrode mask design onto a photoresist; detail description of mask design is explained in chapter 3. Later, onto pattern development, a photoresist relief structure is examined. The vertical cross-section of the microelectrode pattern substrate is analyzed for lift off process. In vertical cross section in figure 4.3, the undercut identified during lithography process reveals that perfect lift off can be realized during lift off process.

Thus on evaluation of developed pattern, the substrate is then sent to next stage which is gold sputtering. During gold coating stage, lustrous uniform thin gold film surface is observed on sputtering. The edges of the microelectrode array are seen and are also examined. The gold film needs to be of optimal thickness for continuous flow of electrical signal through the microelectrode array. If the film is too thin, gold clusters are created. Nucleations of gold islands form an irregular film. In addition, if the gold deposit film is thick, acetone lift off cannot be accomplished. Acetone cannot flow into the under-cut, for photoresist to react and get dissolved to expose microelectrode fingers. Figure 4.1(c) shows microelectrode array platform for electrical characterization of assembled crossbar nanojunction device.

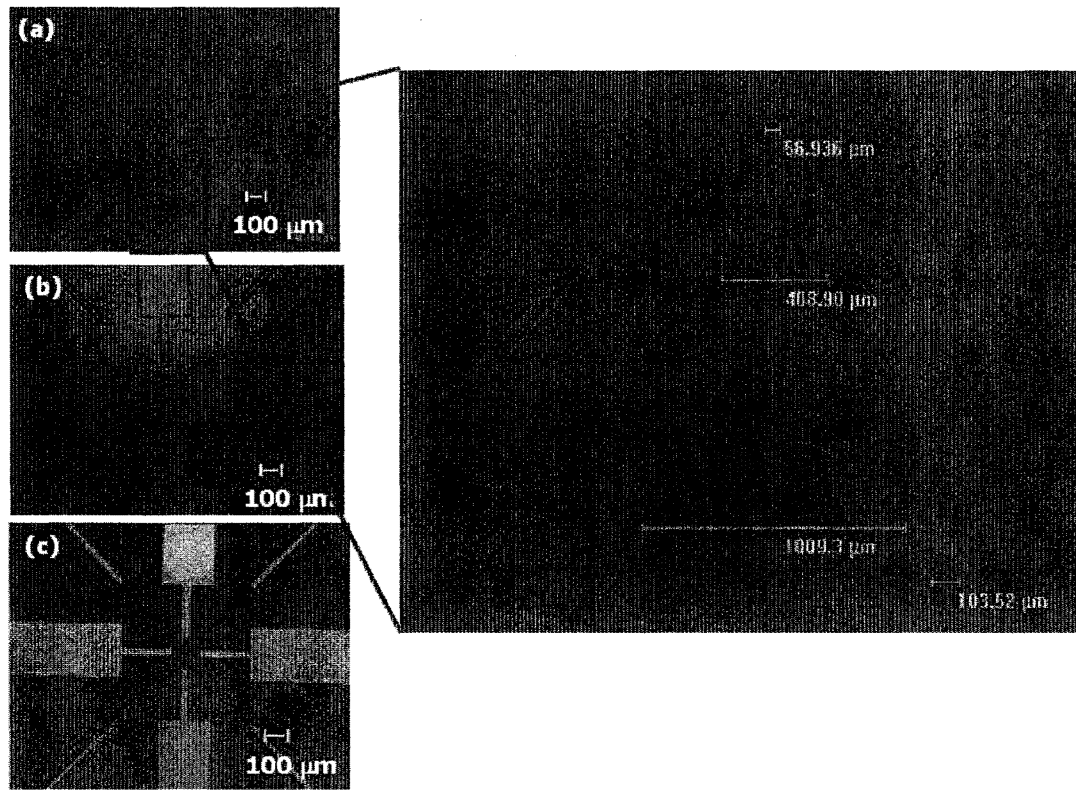


Figure 4.1: Optical micrographs of microelectrode array platform at various stages of microfabrication process sequence. (a) Developed pattern after pattern development process, (b) Uniform thin film of gold sputtered after the sputtering process, (c) Microelectrode array platform for electrical characterization of assembled crossbar nanojunction device.

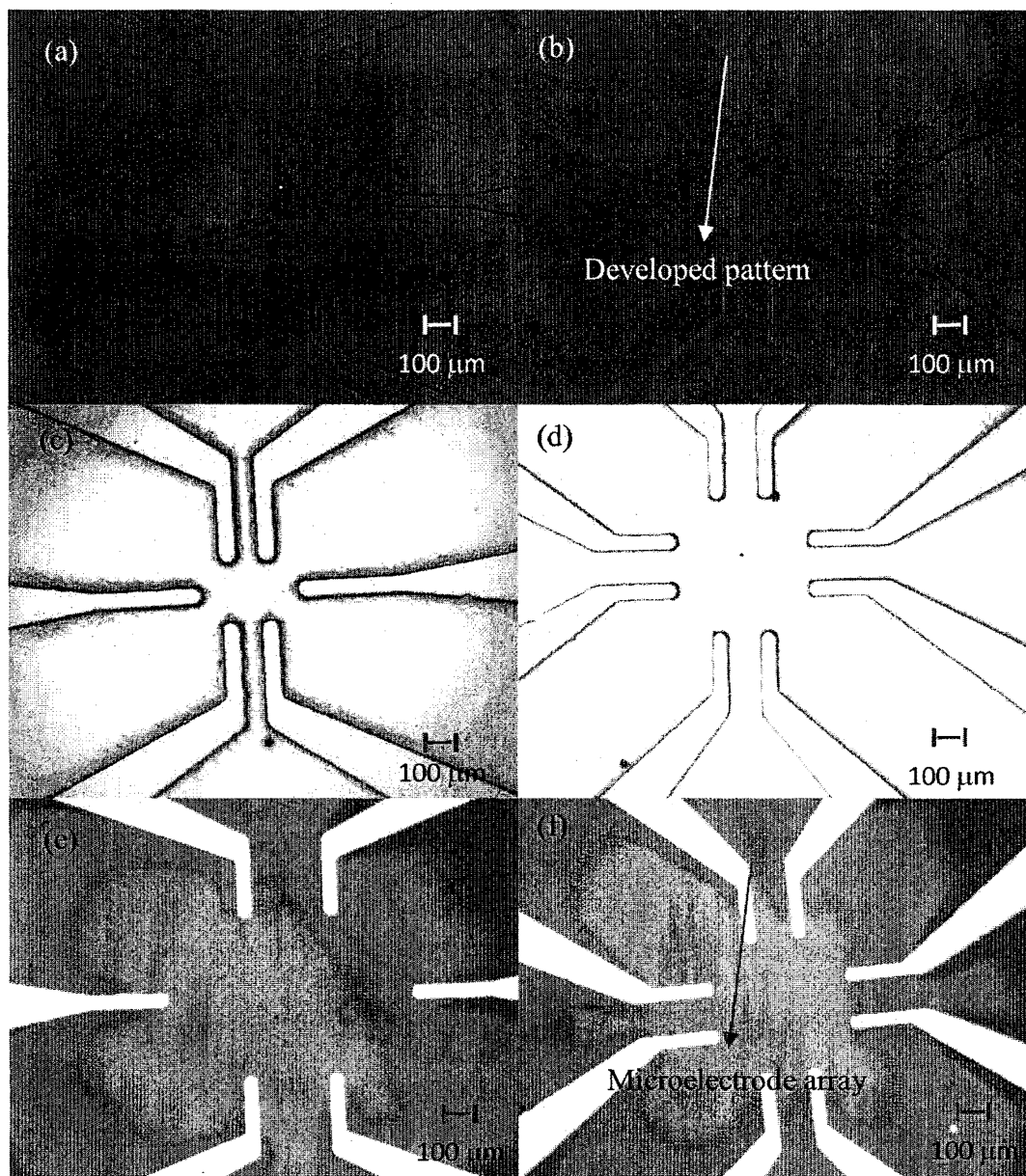


Figure 4.2: Optical micrographs of 1 x 2 and 2 x 2 microelectrode array platform at different stages of lithography process. (a) Perfect pattern transfer after pattern development process, (b) After gold sputtering, microelectrode edges are observed due to underlining photoresist relief structure, (c) Microelectrode array platform for electrical characterization of assembled crossbar nanojunction device.

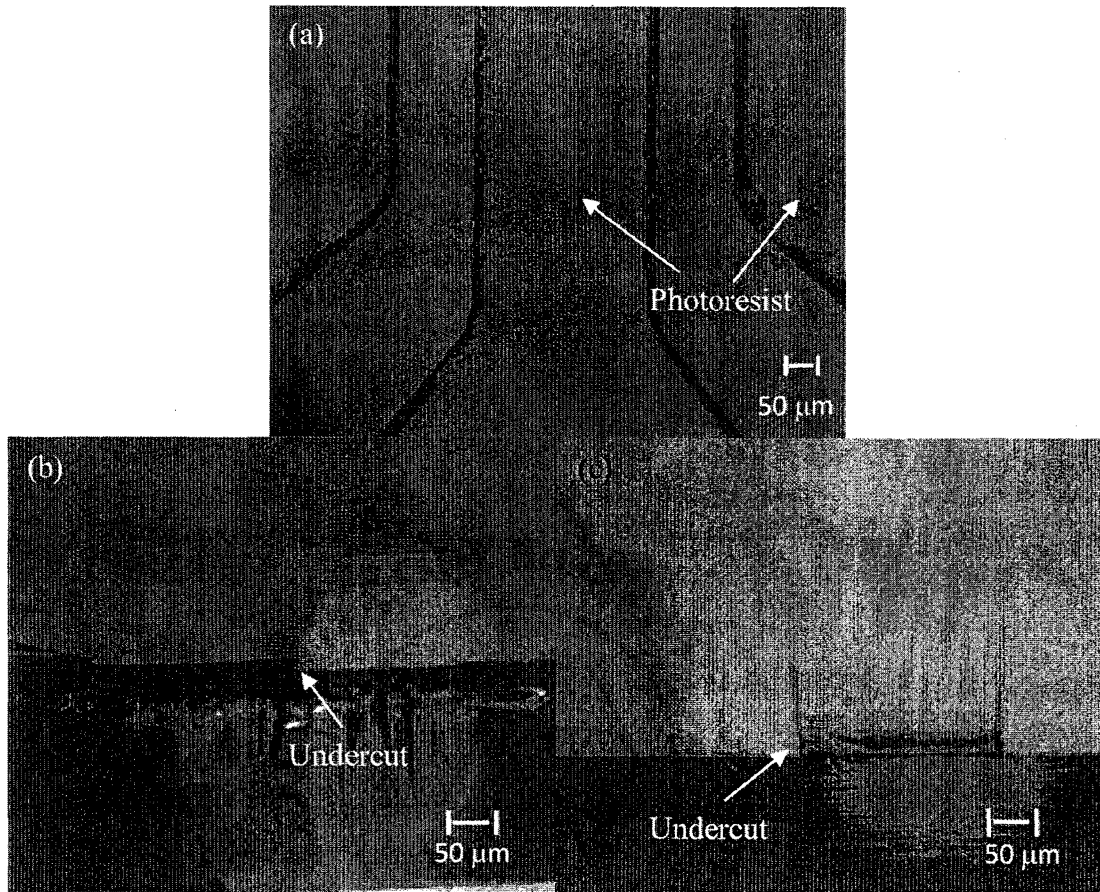


Figure .4.3: Optical image of microelectrode array after pattern development; (a) The relief structure is undeveloped photoresist. (b) and (c) shows vertical cross section of figure (a). The arrow mark shows undercut at the edge of photoresist on development process.

The SEM characterization performs nanoscale analysis. Figure 4.4 asserts and supports the optical characterization. The observation establishes that gold film is uniformly deposited and there is no nucleation while sputtering. In addition, to validation optical characterization of MEA, EDX was also performed onto single

microelectrode fingers. It provides elemental analysis which confirms absence of other elements except Si, Au and Cr. Silicon being the base substrate and Au and Cr is deposited during sputter coating. Figure 4.5 illustrates EDX analysis of MEA.

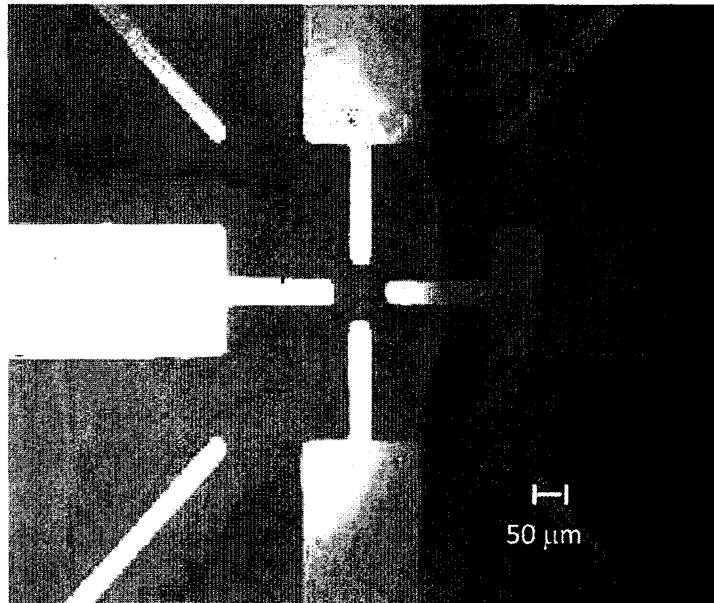


Figure 4.4: Nanodomain analysis and characterization of microelectrode platform using SEM.

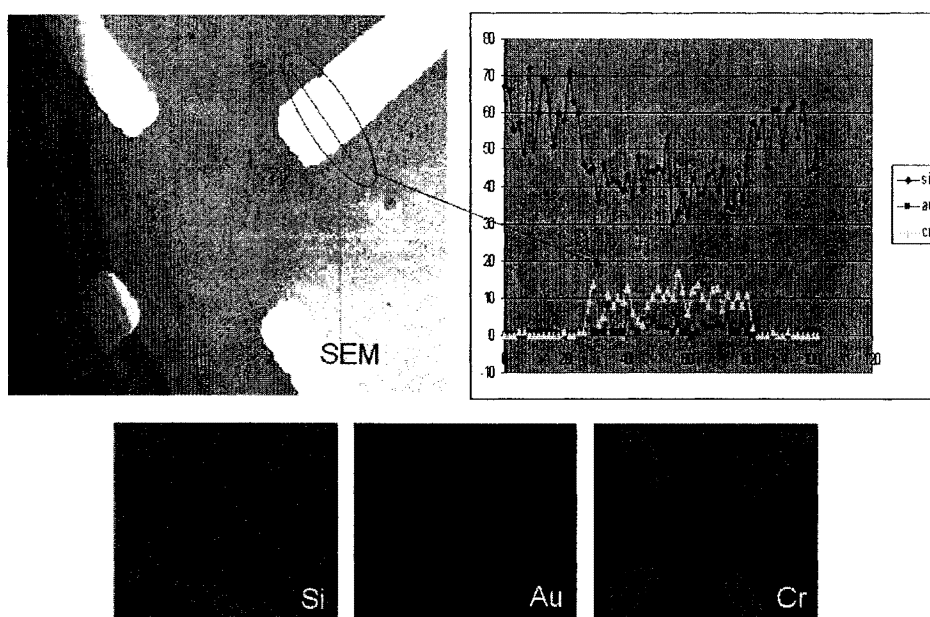


Figure 4.5: EDX characterization of microelectrode array. (a) Scanning electron microscopy characterization of metallic gold micro-electrode array. (b) Energy-dispersive X-ray (EDX) analysis of the microelectrode platform showing three different elements: silicon (Si), Chromium (Cr) and Gold (Au).

4.2 PDMS stamp characterization

Second stage of assembling process is fabrication of PDMS stamps. The stamps consist of parallel arrays of relief structures, which assist patterning of CNTs. The master template is fabricated using standard photolithography as explained in chapter 3, which is then used as a mold for fabricating flexible polymeric PDMS stamps. Multiple replicates can be made from a single master template. The top view and vertical cross section of PDMS stamp is shown in figures 4.6 and 4.7 respectively.

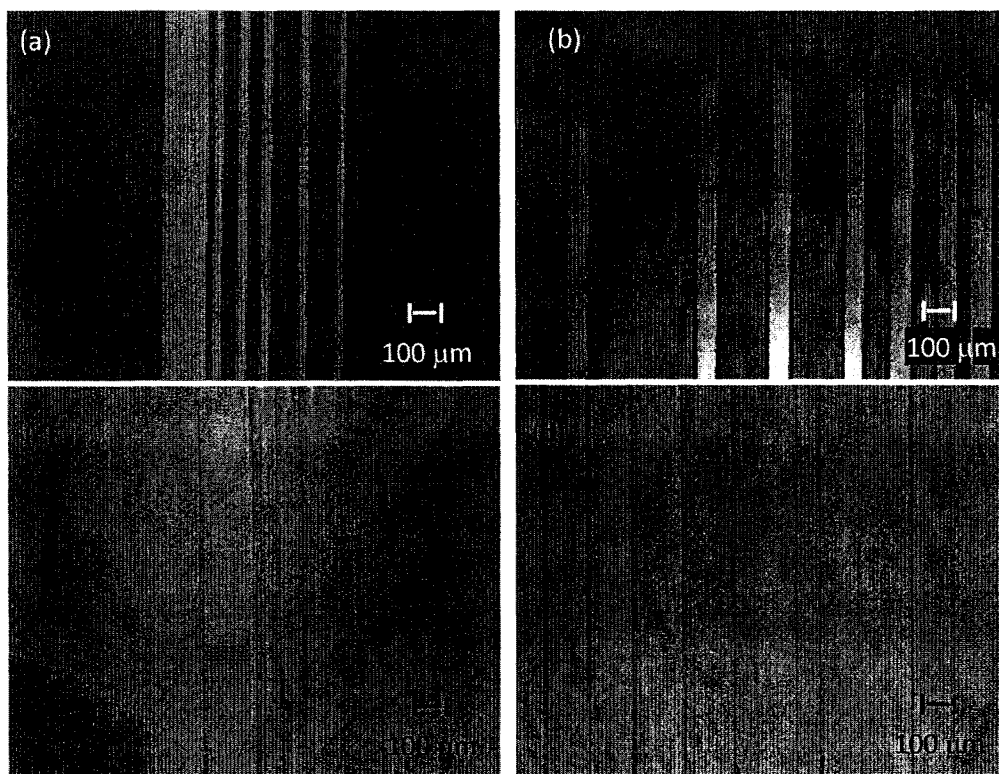


Figure 4.6: Optical characterization of PDMS stamp. (a) and (b) Master template with graded microchannel array of size varying from 50 μm to 150 μm , (c) and (d) PDMS stamp with negative replica of master template (a) and (b) respectively show microrelief structure.

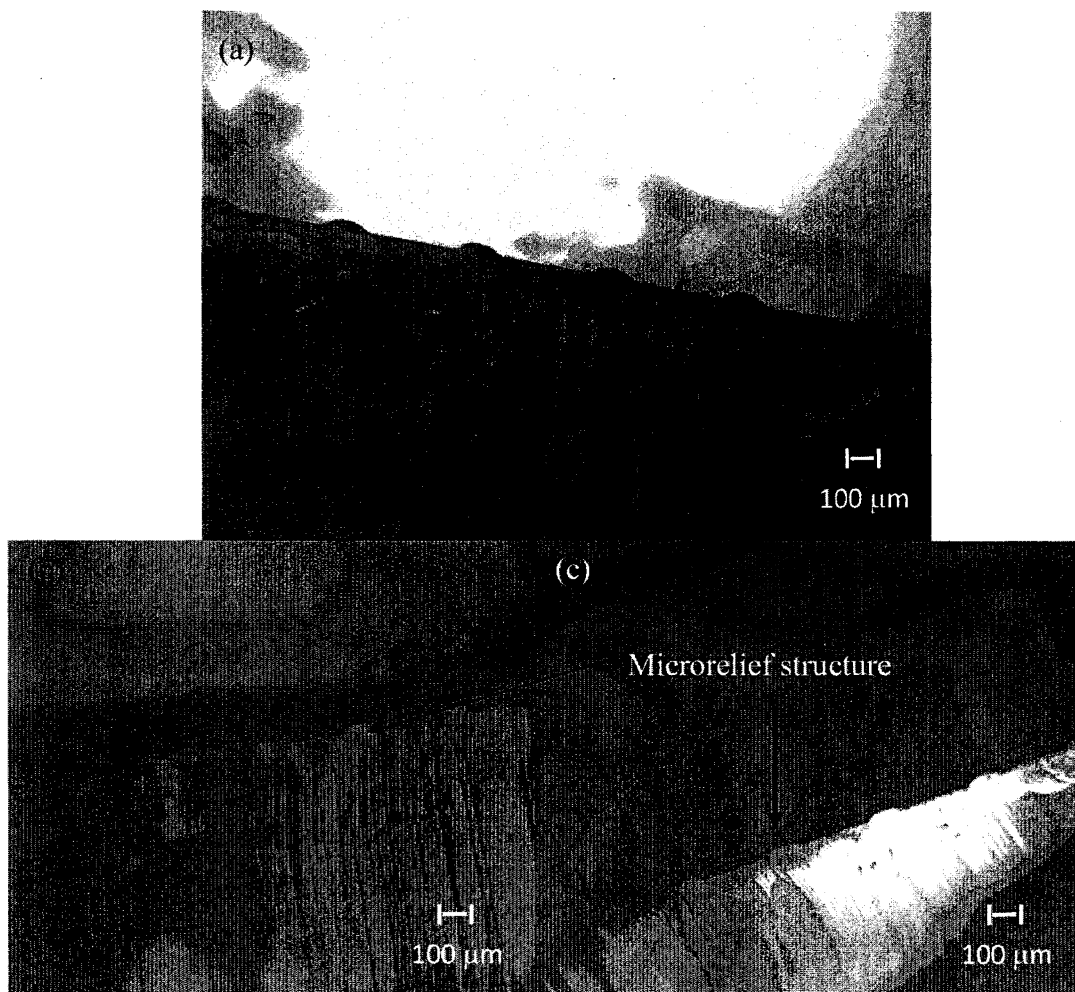


Figure 4.7: Vertical cross section of PDMS stamps. Optical micrograph of vertical cross section of PDMS stamp having parallel relief structures of line width 100 μm and height approx. 1 μm. The spacing between two relief structures is 400 μm.

4.3 Patterned CNT characterization

Microcontact printing technique is used for assembling and patterning CNTs. The schematic diagram representing the crossbar junction formation using p-type and n-type CNTs is shown in figure 4.8.

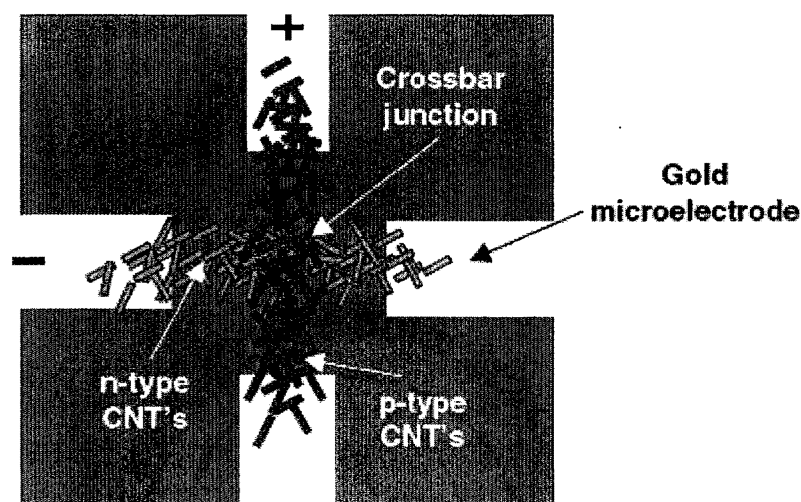


Figure 4.8: Schematic representation of single p-n junction using nanomaterials

PDMS mold was inked with the CNTs and was stamped on the Si substrate. Due to parallel relief wall-like structure the MWCNTs were aligned in parallel fashion. Before impressing second type of CNTs, the first type of CNTs were dried and later, second type CNTs were aligned. Figure 4.9 shows optical characteristics of patterned CNTs respectively. In SEM image 4.11, the dark band shows the presence of CNTs while the light grey area is absence of CNTs. The crossbar p-n junction formation is demonstrated in figure 4.11(b). Another type characterization using atomic force microscopy is shown in figure 4.12. Repetitive parallel impression of CNTs is inked onto base substrate. The island shows clusters of MWCNTs and the dark region

indicates the silicon base substrate in the absence of CNTs. The regular patterns of the dark regions were observed due to the trenches on the PDMS stamp.

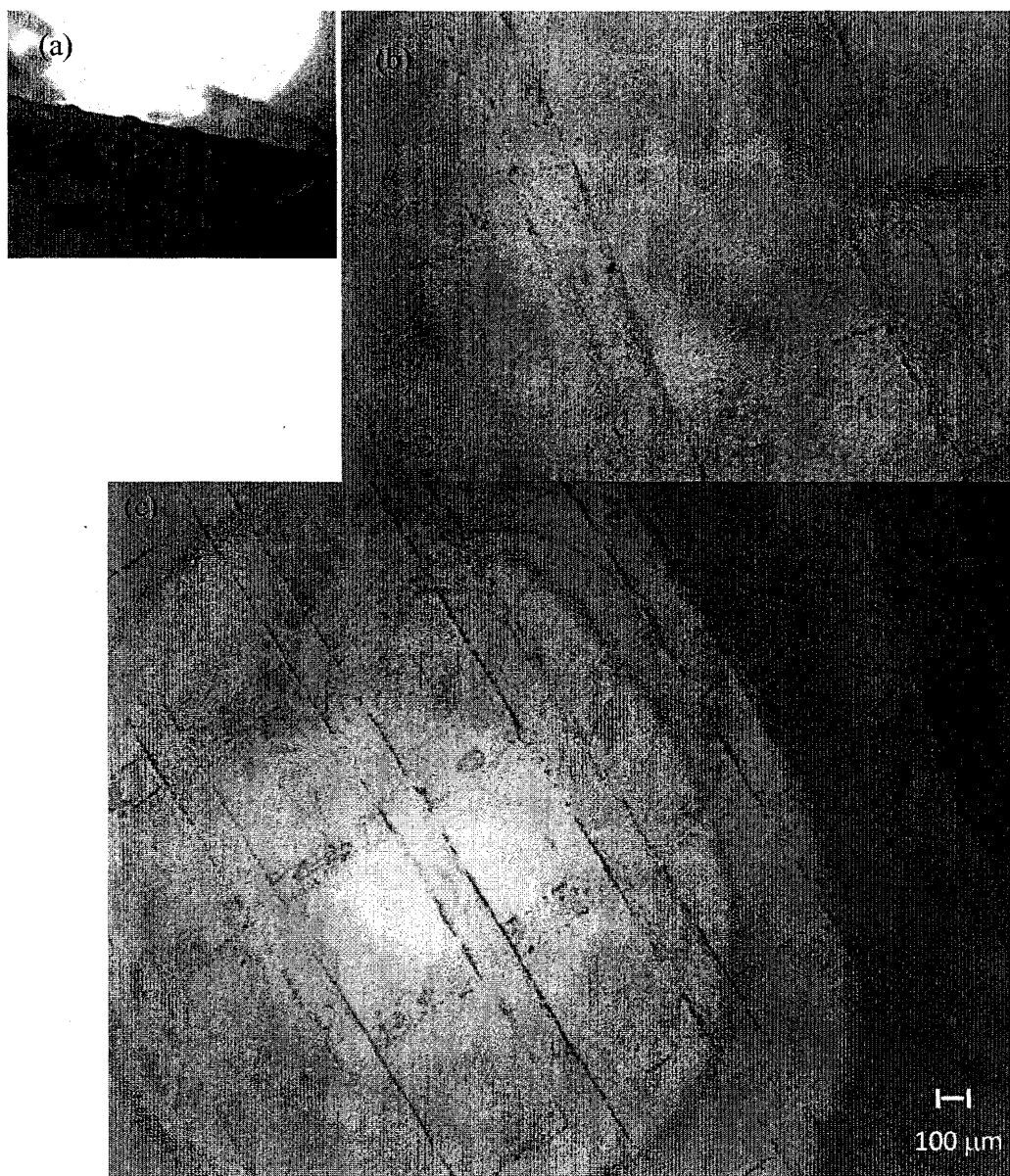


Figure.4.9: Optical characteristics of assembled junction. (a) PDMS stamp used for patterning CNTs, (b) and (c) Optical image demonstrating junction formation at the intersection of two perpendicular aligned surfactant coated CNTs on Si substrate

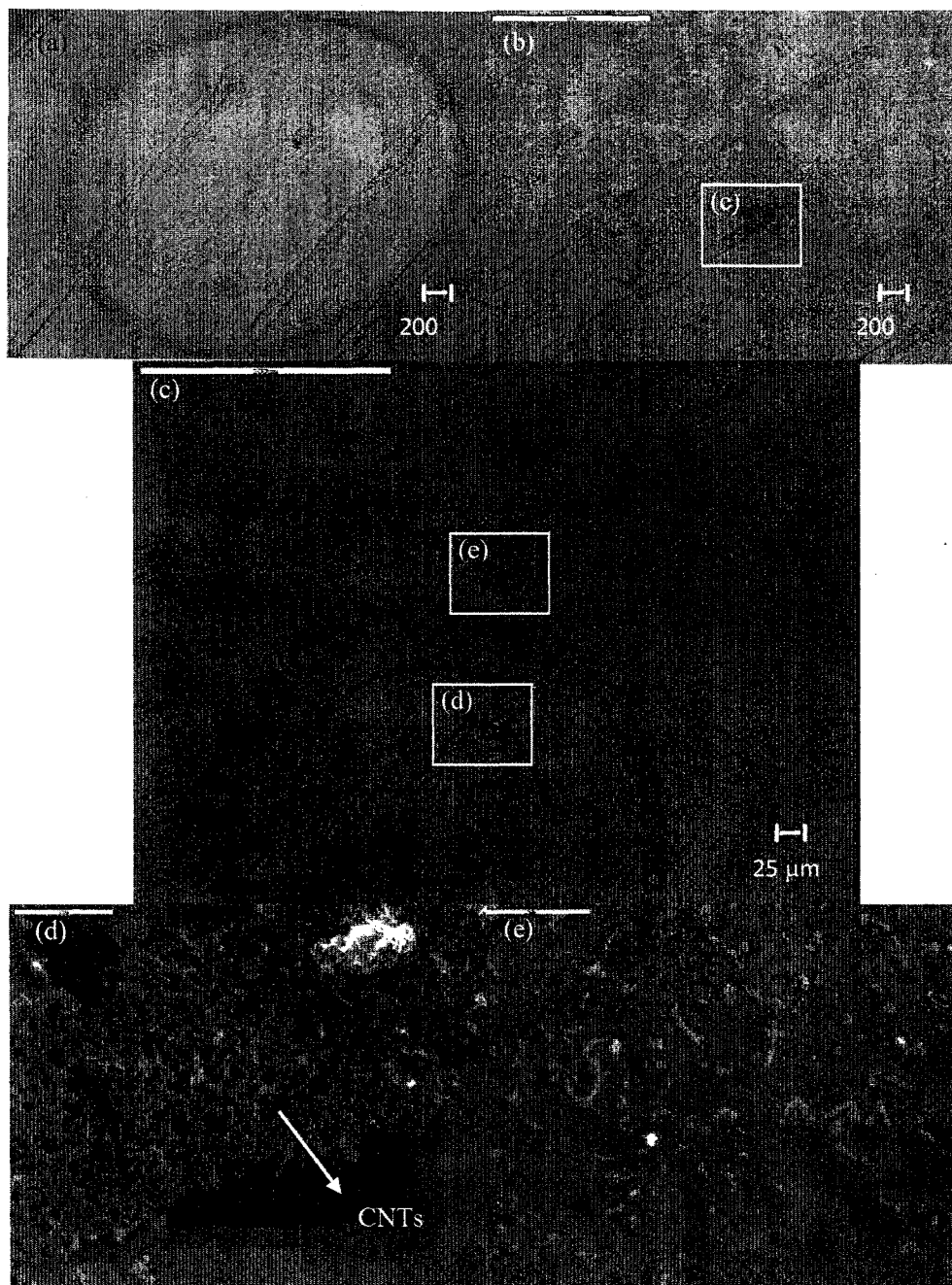


Figure 4.10: Optical and SEM image of patterned carbon nanotube. (a) Optical micrograph of parallel array of pattern CNTs. (b), (c), (d) and (e) are SEM image confirming connection between multiple adjacent CNTs.

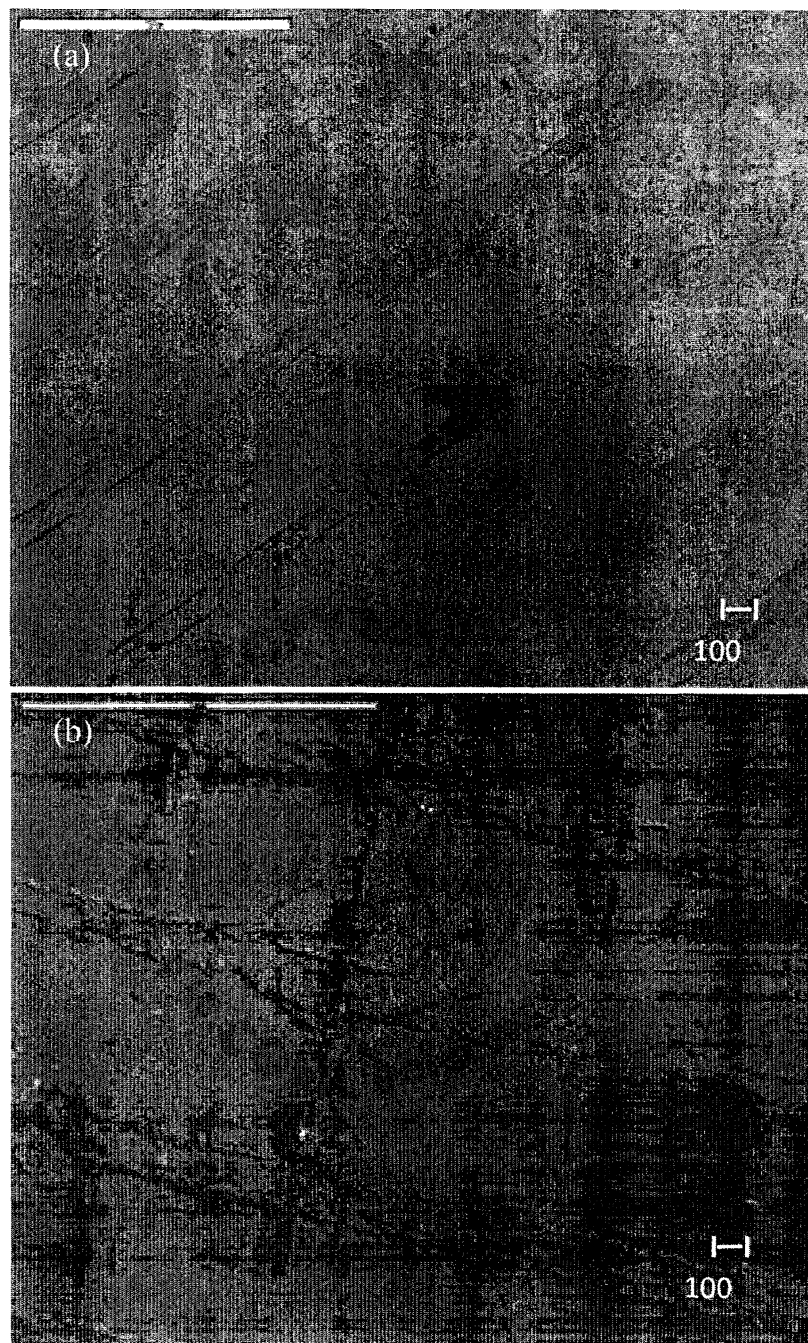


Figure 4.11: SEM characteristics of patterned CNTs using microcontact printing. (a) Parallel array of CNTs and (b) Crossbar junction formation.

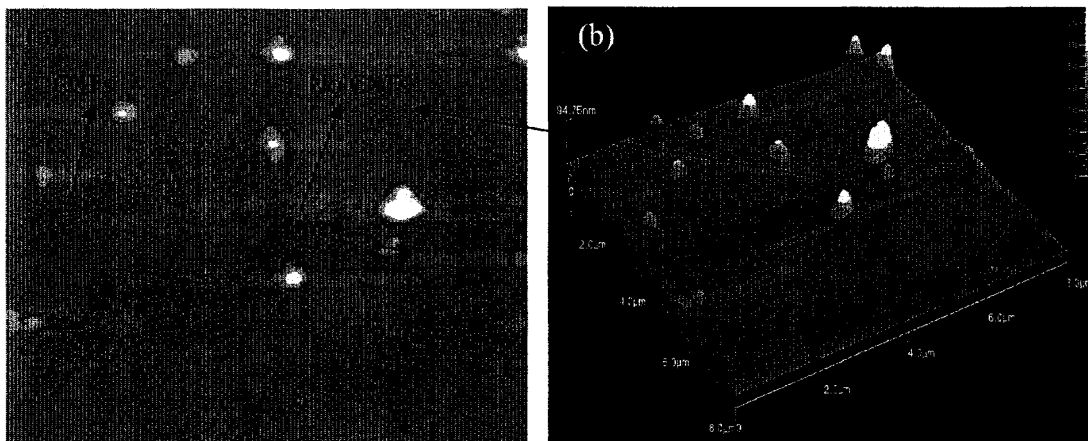


Figure 4.12: AFM images of patterned CNT onto the micro-electrode array. Repetitive parallel patterns of inked carbon nanotubes are observed.

4.4 CNT device characterization

As explained in chapter 3 two types of nanomaterials were exploited; extrinsic MWCNTs and chemically functionalized SWCNTs. The detail description of each microdevice formed, its experimental process and I-V characteristics is explained in the section below. Randomly dispersed CNTs have resistive lumped element characteristics and show ohmic behavior. These randomly dispersed CNTs have been patterned to form different device configurations such as transmission lines and transistors by physically assembling the CNTs into well-ordered patterns. The nanostructures so formed demonstrated specific device characteristics. The p-type and n-type CNTs in this application were stamped in a crossbar manner to form a nanojunction. The crossbar junction I-V characteristics were tested for two cases: unpatterned/patterned and with/without passivation.

4.4.1 Multiwalled carbon nanotube device

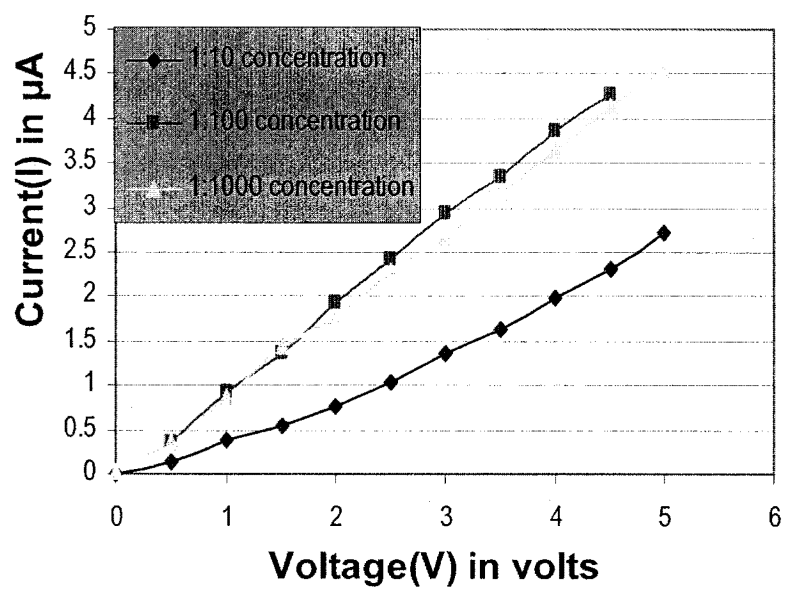
For preparation of p-type and n-type (length: 50 nm) MWCNTs of specific density, the stock solution of each type of aqueous suspension of MWCNTs (Fisher Scientific, Hampton, NH, USA) comprising of approximately 10^{12} nanotubes/ml was centrifuged at 4000 rpm for 3 min. Due to centrifugation, the MWCNTs were concentrated at the bottom of the centrifuge tube. 10 μ l of the concentrated MWCNTs sample in each case was separately suspended in 90 μ l of DI water and vortexed for 3 min. 25 μ l of this suspension of MWCNTs was diluted in ethanol in the ratio of 1:10, 1:100, and 1:1000. Ethanol dilution was performed due to ethanol's volatile nature; MWCNTs dried at a faster rate compared to DI water dispersed MWCNTs. Different concentrations of MWCNTs dilution were used to determine the optical electrical conductivity in the patterned format. Finally, the PDMS mold was inked with the MWCNTs at the optimal concentration and was stamped on metallic gold electrode substrate

The I-V characteristics of a crossbar junction MWCNTs were plotted by applying 0-5 V DC voltage with step size of 0.1 V across the junction and measuring output current using a subfemto-ammeter remote (Keithley 6430, Keithley, Ohio, USA). The junction current variations in response to the changes in the applied voltage were recorded for varying concentrations of MWCNTs in the crossbar junction arrays. Figure 4.13(a) demonstrates that for a specific concentration of cross patterned

MWCNTs between two microelectrodes there was a rectifying crossbar junction behavior. It was observed that the typical junction behavior was seen only for 1:10 concentration. Figure 4.13(b) is the I-V plot that maps the variation of the measured current for the range of applied voltage from 0-5V. It was observed that there was an increase in the current with unpatterned MWCNTs as compared to the current measured from a control substrate in the absence of MWCNTs, thus showing resistive lumped element characteristics. It was also observed that the current through p-type unpatterned MWCNTs was higher than in n-type unpatterned MWCNTs which contradict the theoretical and practical conclusion that current through p-type MWCNTs should be lesser than n-type MWCNTs. This was due to the fact that the stock concentration of p-type MWCNTs in solution was higher, as compared to n-type MWCNTs in solution. Figure 4.13(c) shows effect of base substrate resistance and contact resistance. The increase in resistance value was observed as the distance between electrodes was increased. The value of resistance varies approximately between $150\ \Omega$ to $5\ \text{M}\Omega$ showing the effect of base substrate resistance.

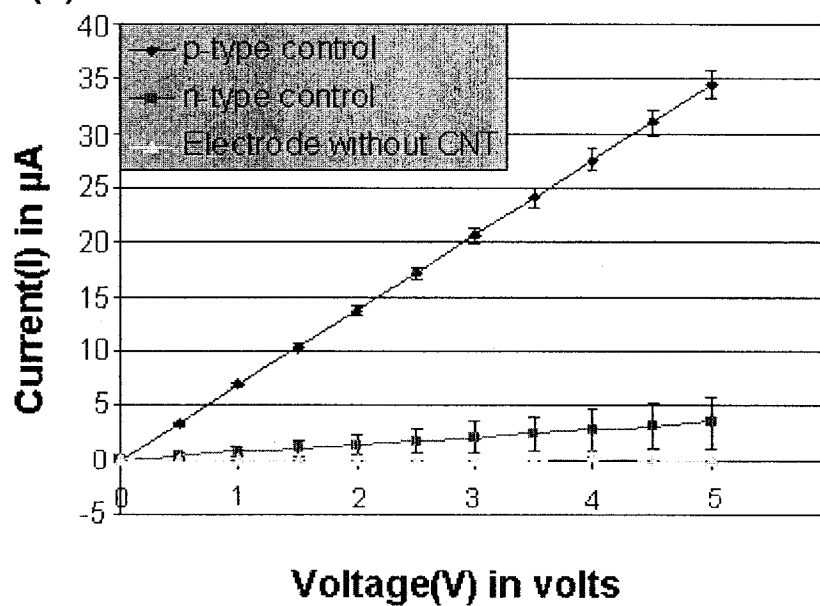
(a)

I-V Characteristics



(b)

I-V Characteristics



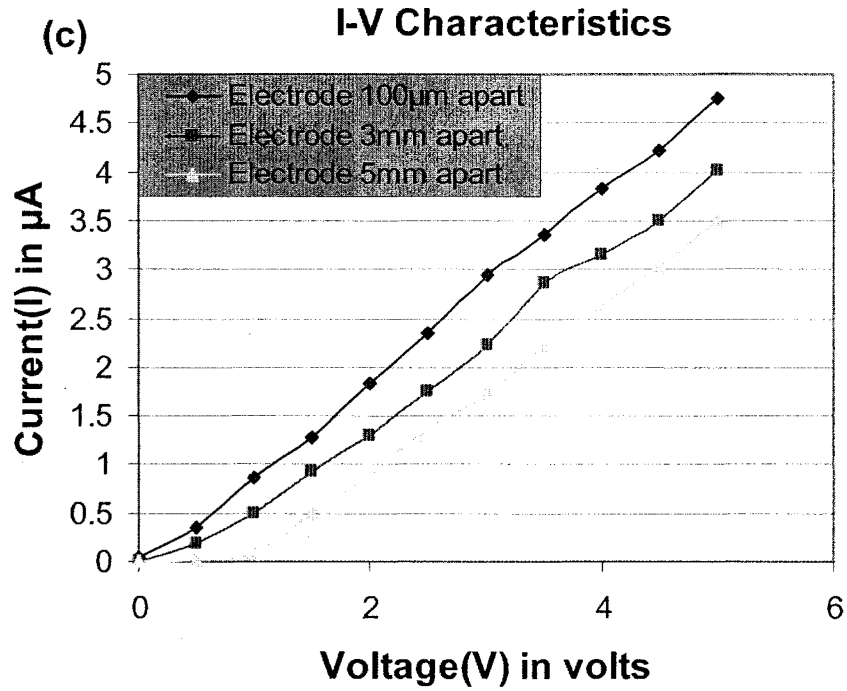


Figure 4.13: I-V characteristics illustrating junction formation. (a) p-type and n-type MWCNTs were ethanol diluted in the ratio of 1:10, 1: 100, and 1:1000 to determine the optimal electrical conductivity at varying concentrations. The data reading shows the junction I-V characteristics of the patterned MWCNTs forming crossbar nanojunction at different concentrations. (b) The I-V plot shows the resistive nature of silicon substrate and unpatterned MWCNTs. Increase in current is observed due to unpatterned MWCNTs. The conductive nature of MWCNTs decreases resistance and thereby increases current. Disordered MWCNTs, having resistive lumped element characteristics, shows ohmic behavior. (c) The graph shows the effect of contact resistance and the base substrate resistance. The current is measured at the base microelectrode for varying distance of separation between them.

The surface of semiconducting MWCNTs often contains electronically active states because of unsaturated surface bonds or dangling bond states. Surface passivation aims to re-bond these dangling bonds with a passivation agent. The surface passivation on the patterned MWCNTs was created by adding a small quantity of the elastomer polymer (PDMS) on the patterned MWCNTs. This passivation technique using an elastomer was simple and easy to implement. Reduction of fluctuation in the current in the I–V characteristics of the device due to effect of ambient atmosphere was observed as compared with the unpassivated surface. In addition, fluctuation in current due to atmospheric ambient condition was observed and measured. The maximum-minimum (max-min) value at each voltage was calculated without/with passivation and the difference of max-min deviation was plotted in figure 4.14. Patterned crossbar junction passivated using PDMS has less variation in current than junction formed without passivation. The difference of max-min without/with passivation was 0.00073- 0.031 μA and 0.0013 – 0.0046 μA respectively.

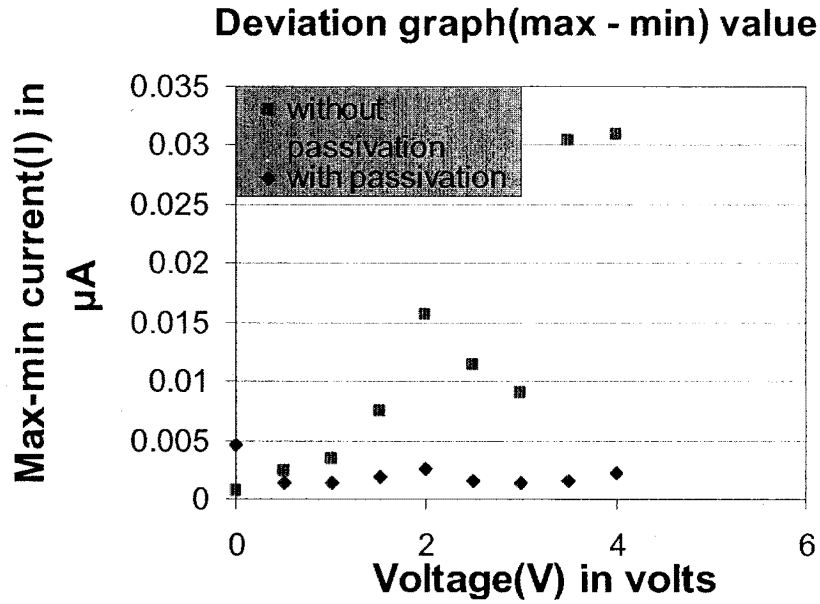


Figure 4.14: The graph is the I-V characteristic to electrically characterize the effect of passivation of a single device on a chip. The deviation of current between max to min is plotted at different voltage readings. The applied voltage is varied from 0 V to 5 V and the current ranges from 0.00073 μA to 4.3046 μA .

The I-V characteristics obtained from such devices obey the rectifying crossbar junction behavior. When the MWCNTs are patterned across the base electrodes, the electron transfer between the two electrodes is due to transport of electrons through the multiple shells of the MWCNT grid, as well as electron tunneling and charge transfer between two adjacent MWCNTs. This, in turn is expected to decrease the resistance between two electrodes. The I-V characteristics were measured from two configurations of MWCNTs, namely unpatterned and patterned MWCNTs. The unpatterned tubes are comprised of random dispersion of the tubes between electrodes

and, in the case of patterned MWCNTs; they were stamped between the Microelectrodes. The comparative studies of the I-V curve of unpatterned and patterned MWCNTs shows lumped resistive and diode-like behavior respectively. For fabrication of the microelectronic devices, microscale printing of the nanoscale materials results in the grouping of the nanomaterials. To analyze the electrical behavior of these devices, the electrical properties of the whole grouped nanomaterials need to be studied. In our experimental research, a key fundamental issue with the MWCNTs nanomaterial for device formation is to distinguish between semiconducting and metallic MWCNTs. This has a direct effect on the junction properties. Secondly, the concentration of MWCNTs solution plays an important role in the device formation. The sparse and densely packed MWCNTs show two different characteristic behaviors; ohmic linear resistive curve and rectifying junction behavior respectively. When the low concentration of MWCNTs solution (1:100, 1:1000) is patterned, it was observed that the MWCNTs did not form an interconnection between the microelectrodes, resulting in resistance I-V characteristic curve. This linear I-V curve is due to the contact and the base substrate resistance. When the concentration is increased (1:10), the MWCNTs are closely packed. This results in the formation of an electrical conducting path between two microelectrodes, showing the rectifying crossbar junction behavior.

4.4.2 Single walled carbon nanotube device

In the doping process it has been well established that the conductivity of an intrinsic semiconductor can be increased by adding small, controlled amounts of “impurities” with more or fewer valence electrons than the intrinsic semiconductor. Also, it has been noted that while the resistance of undoped SWCNTs is 10-20 k Ω at room temperature, an increase in electrical conductance at low temperatures is also observed, which reaches to $4e^2/h=2G_0$ quantum conductance (6.45 k Ω in resistance) and is limited at ~ 1.5 K Ω . However, as explained in chapter 3, doped SWCNTs with surfactant molecules, intercalates Na⁺ and Br⁻ molecules between the individual tubes, which increases the conductance due to positive and negative ions [96]. This results in a decrease of resistance of approximately 720 Ω and 186 Ω for SDS-SWCNTs and CTAB-SWCNTs respectively.

The I-V characteristics of a crossbar P-N junction SWCNTs were plotted by sweeping an input voltage from -5 to 5 V DC voltage with the step size of 0.1 V. Using a subfemto-ammeter (Keithley 6430, Keithley, Ohio, USA), the input voltage was applied and simultaneously ionic junction current variation was recorded at varying voltages. Figure 4.15 demonstrates comparative I-V characteristics of patterned and randomly dispersed CNTs. The figure 4.16 and 4.17 demonstrates the forward and reverse bias junction characteristics. Due to ion transport the turn-on voltage is in between 2 to 3 V depending upon the amount of SWCNTs patterned. The current values are approx. -0.514 μ A - 6.09 μ A and 0.0113 μ A - 6.81 μ A at voltage range 0-1 V and 1-2 V respectively. Polynomial increase in current to 0.105 mA is observed at 5

V. Similarly, a trend in rectification has been noted with the current variation in microampere, where single strands of p-type and n-type CNTs are aligned to form a p-n junction [1]. In addition, I-V junction characteristic is also measured, where P-type SWCNTs stamped first and N-type later and vice-versa. The I-V exponential/polynomial curve is identical whether P-type SWCNTs or N-type SWCNTs is stamped first. In figure 4.17, each data reading is an average of two single junctions noted from two different devices. The turn-on voltage is different for all the devices due to the amount of carbon nanotube aligned across the junction. The larger the amount of SWCNTs patterned at the junction, the larger is the junction barrier and so is the turn-on voltage.

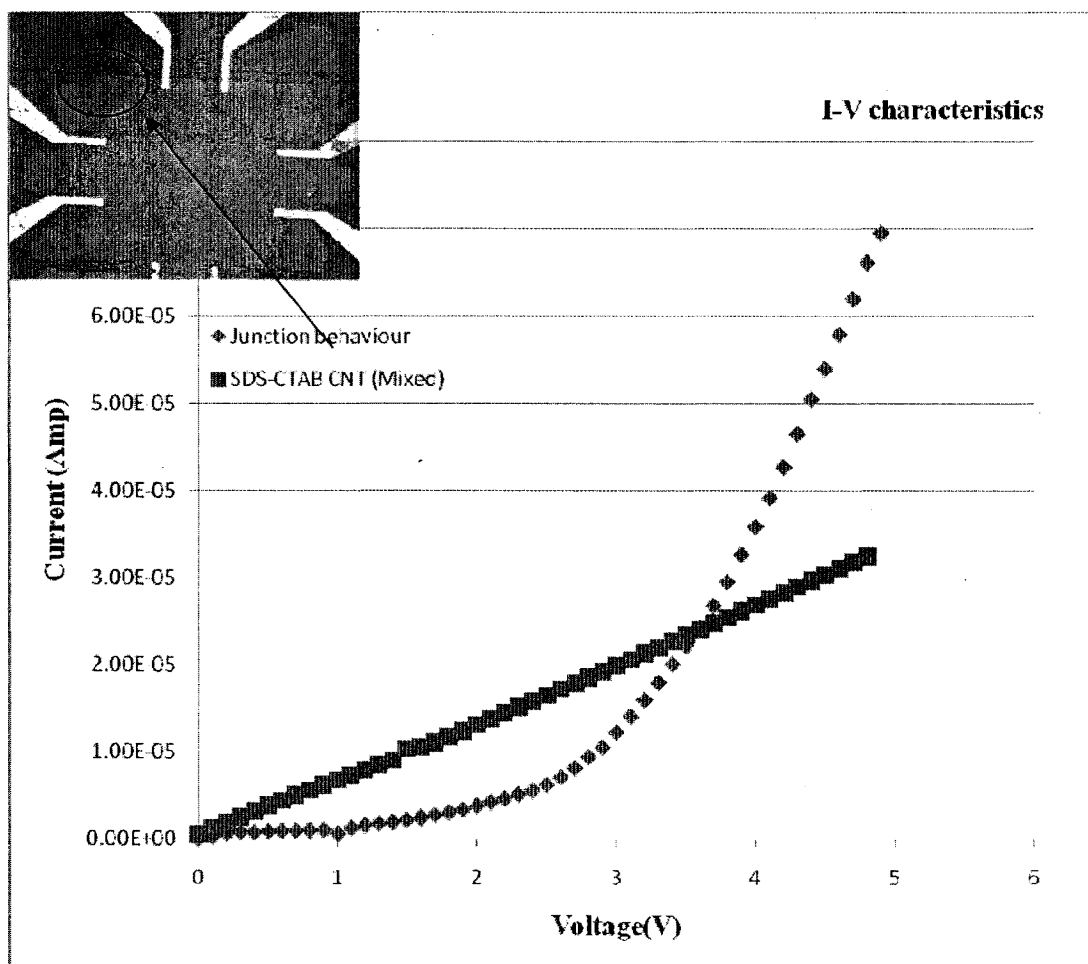


Figure 4.15: The data illustrating comparison study of patterned CNTs vs randomly dispersed mixed CTAB-CNTs and SDS-CNTs. The P-N junction formed by patterning P-type and N-type CNTs shows rectification behavior versus linear behavior observed by randomly dispersed mixed P-type and N-type CNTs across a microelectrode array.

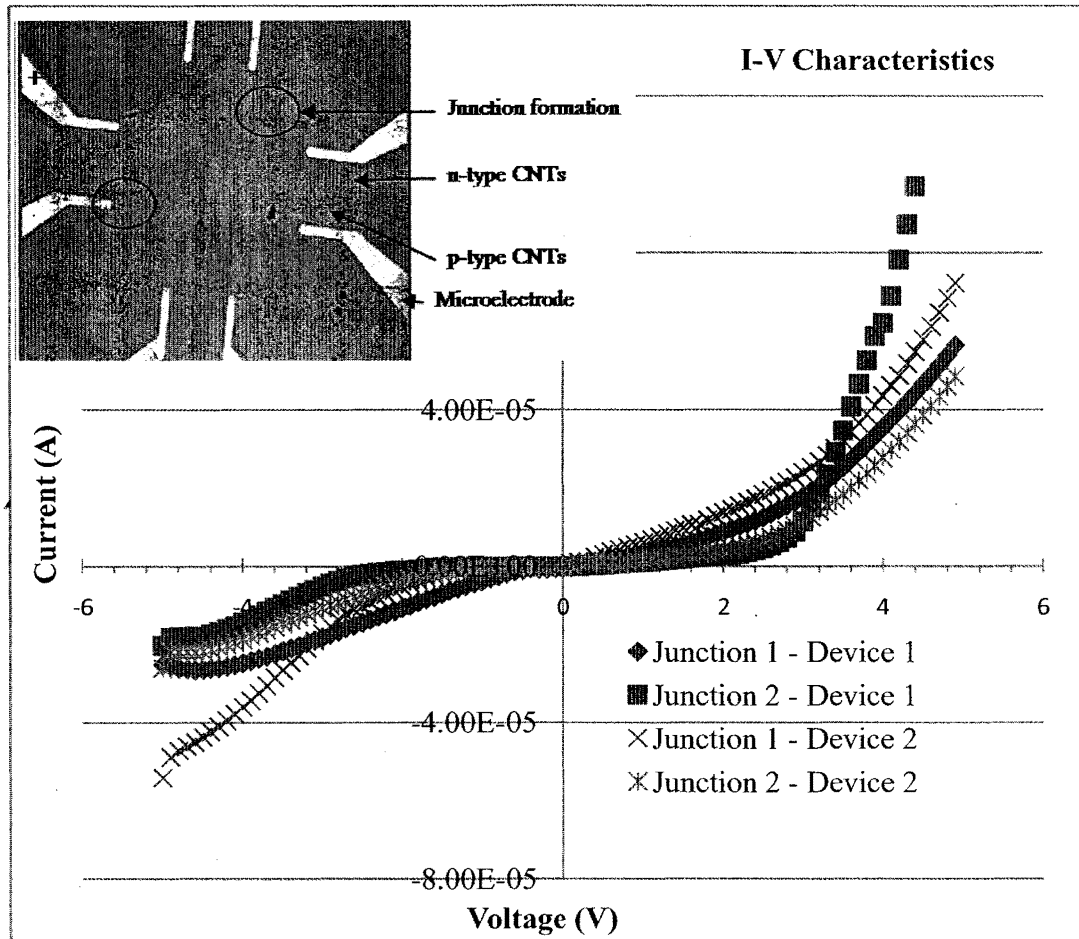


Figure 4.16: The data illustrates formation of P-N ionic junction when patterned and assembled using CTAB-CNTs and SDS-CNTs. The S-curve observed using I-V characteristic shows rectifying forward junction behavior with a turn ON voltage at 2.5 V.

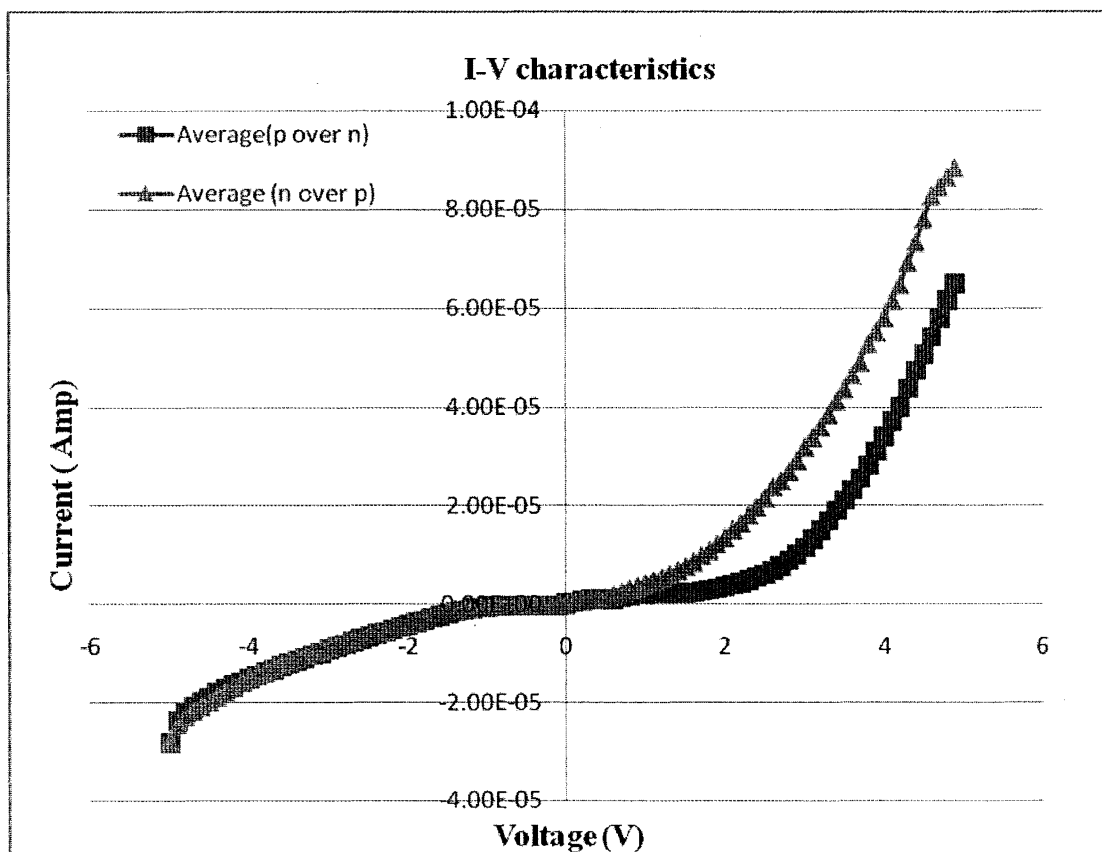


Figure 4.17: The graph illustrates the junction behavior irrespective of P-type or N-type stamped earlier. In the I-V graph, each data point is a duplicate of a single junction formation on different devices. The color red I-V data curve shows rectification behavior of junctions formed by imprinting SDS-CNTs followed by perpendicular imprinting of CTAB-CNTs. While as the junction formed by initial stamping of CTAB-CNTs and SDS-CNTs stamped later, in an alternative manner is shown by the green I-V data points.

4.5 Modeling Results

Carbon nanotube due to its unique inherent properties is considered one of the best nanomaterials for building fundamental functional blocks. With its improved electrical properties in terms of mobility and current carrying capacities, many researchers are building basic diode nanodevices. Among these various research group, John Rogers group from university of Illinois demonstrated carbon nanotube based diode by patterning CNTs with p-type and n-type dopant materials [97]. The nanodiode fabricated consists of thin strip of carbon nanotube between two metal electrodes where half of the strip is exposed to PMMA and the other half by PEI. These diode fabricated by coating method showed a very high built in voltage of 4.6V [97]. Similarly, in my devices, when carbon nanotubes coated with CTAB and SDS surfactant are patterned, a high built in potential of approximately 2.5 V is recorded. Reason for high built in potential is the ionization energies of dopants atoms that play an important role for generating the electric field at the junctions [86]. In crossbar junction devices, nanotubes are doped by positive and negative surfactant ion, these ions lead to formation of ionic junction at the interface of the p-type and n-type CNTs. This ionic junction leads to a built-in electric field in the vicinity of the junction and due to the high ionization potential associated with these ions, these ionic junctions are characterized by a high junction resistance. As a result, the amount of the energy required to move the charge carrier freely across the junctions is high, leading to a high turn on voltage. In addition, the sodium and bromide ions of the surfactants are associated with the charge transport through the device, electron-hopping effect

through these ions should also be considered as the rationale for high turn on voltage [98, 99].

Looking at the reverse characteristics, the reverse current shows combined behavior of resistive and saturation effect. The bulk carbon nanotube consists of 30% of metallic nanotubes during synthesis process [97]. When voltage is applied across the positive and negative electrodes, charge carrier sees low resistive path and flows through these metallic conductive CNT path. Thus, on application of negative voltage, resistive effect is added and thereby increasing the current in the reverse bias region. In addition, the semi log plot of the crossbar junction device shows a high ideality factor, which is inconsistent with the Sah-Noyce-Shockley theory. The Sah-Noyce-Shockley theory states that an ideality for the ideal diode should be in the range of 1 to 2. However, Shah et. al [100] proposed the theory for the high ideality factor. According to his theory, the externally measured ideality factor of a p-n junction diode is the sum of the ideality factors of the individual rectifying junctions. In the CNT crossbar junction, dense sheet of p-type and n-type CNTs are patterned to form a p-n junction. Multiple series junctions are possibly formed at the interface. I believe that adding up the ideality factor of these junctions has resulted in high ideality factor. To calculate an ideality factor, a fit curve is plotted using diode equation.

In an ideal diode, the current–voltage curve is described by the following equation

$$I = I_S \left(e^{V_D/(nV_T)} - 1 \right);$$

where, I_S is the reverse bias saturation current,

n is ideality factor depending on the fabrication process and semiconductor material.

$$V_T = \frac{kT}{q},$$

$$k = 1.3807 \times 10^{-23} \text{ J}\cdot\text{K}^{-1},$$

$$q = 1.6 \times 10^{-19} \text{ C}$$

where, k and T are Boltzmann constant and temperature, respectively. The thermal voltage V_T is approximately 25.85 mV at 300 K, a temperature close to “room temperature.” The fit is to the diode equation given with the ideality factor in the range 35 to 42 and $I_s = 1.7 \text{ }\mu\text{A}$. The simulation for theoretical fit was performed using Matlab. In figure 4.18, by comparison, it is found that the measured I - V curves exhibit a good similarity to the fit line plotted using an ideal diode equation with high ideality factor of 35.

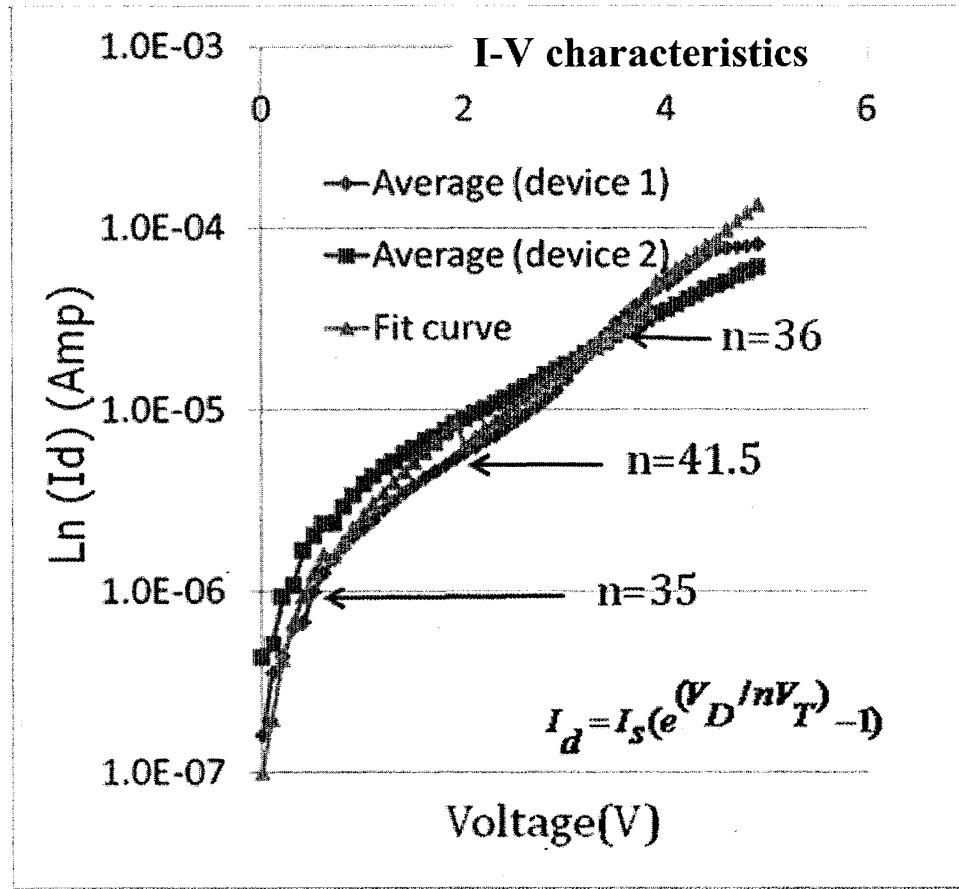


Figure 4.18: Semi log plot of I-V characteristics of a SWNT ionic junction when chemically doped to form a crossbar p-n junction. Comparison of fit curve vs experimental curve is illustrated.

Figure 4:19 shows the I-V plots of the crossbar junctions having high ideality factor that fits best to the polynomial equation compared to a diode exponential equation. The trendline was plotted using Microsoft Excel where the linear regression is performed to fit the I-V curves. The third order polynomial trendline equation plotted for each I-V curve shows that the R squared factor approaches the value one. The closer the R squared factor to unity the better is the fit. Using ideal diode equation

with ideality factor 1.5 was plotted and the polynomial trendline was fitted to it. It was found that R squared factor for the ideal diode plot is 0.985 in compared to 0.988, 1 and 0.991 for device 1, device 2 and fit curve respectively. In conclusion, we found that the crossbar junction with high ideality factor could be best represented by the polynomial equation. Finally, the nanodevices with these junction characteristics can be used for sensor applications as explained in the motivation section.

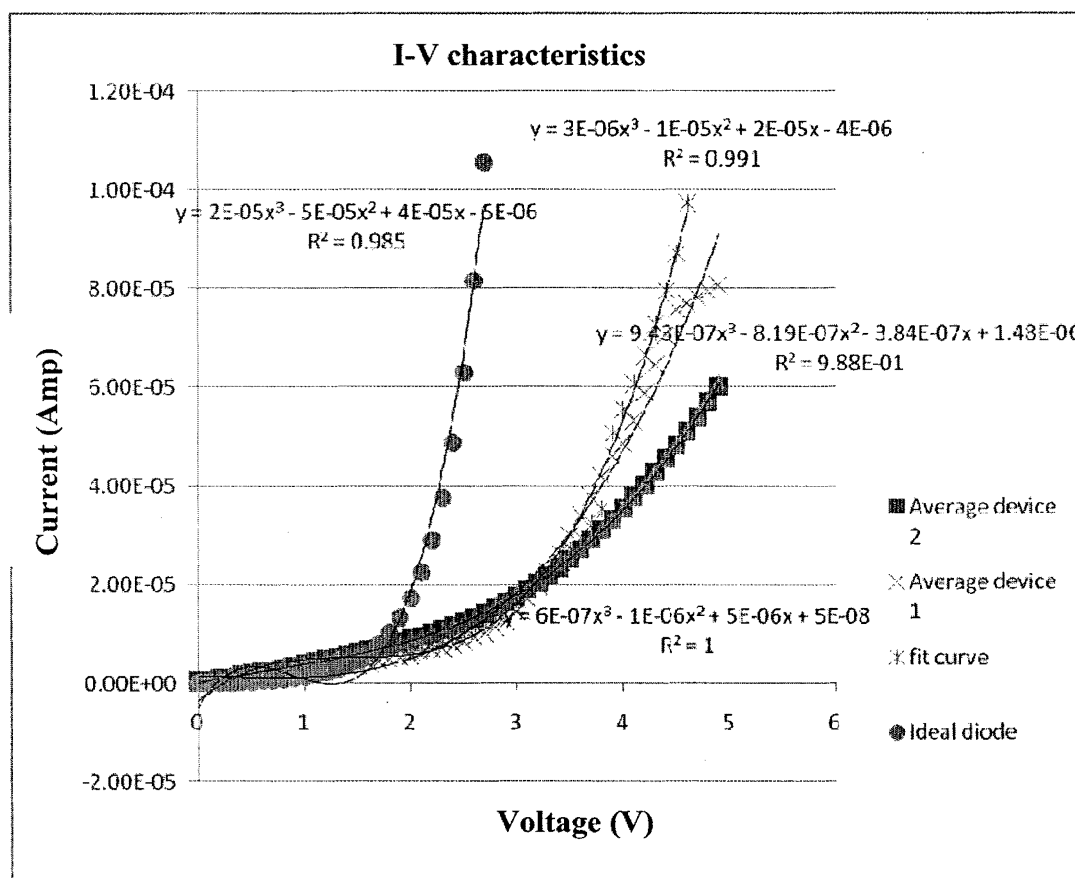


Figure 4.19: I–V characteristics showing polynomial trendline with equation for crossbar junctions, fit curve and ideal diode curves.

Here, I have integrated the advantages of microscale patterning printing and organic chemical doping of nanomaterials to rapidly form crossbar junction arrays comprising

of extrinsic ionically doped nanomaterial. I have demonstrated the ability to pattern such nanomaterials to form functional crossbar junctions with the potential of working as functional building blocks in nanoelectronic devices.

Analogous to the electrons and holes transport in a semiconductor p-n junction, ionic charge transfer occurs through the ionic junction. When anionic and cationic SWCNTs are patterned to form crossbar ionic junction across base electrode, ion transfer between two electrodes is observed due to transport of ions through SWCNT grid, as well as ionic tunneling and ionic charge transfer between two adjacent SWCNTs. Cations/anions diffuse across the junctions creating a depletion region and the region extends from $-x_{SDS}$ to $+x_{CTAB}$. As the ions diffuse, an electric field is created and the built-in potential opposes further diffusion of ionic charge. The built-in potential across the depletion region is equal to the difference between two Fermi energy levels E_{fSDS} and E_{fCTAB} (where E_{fSDS} and E_{fCTAB} represent the Fermi energy level of anionic SWCNTs and cationic SWCNTs respectively). At thermal equilibrium, the ionic charge diffusion is balanced by the ionic drift current. Figure 4.20 shows the structural representation of the ionic junction and the band bending at the interface due to ionic charge transfer. Therefore, due to a built in the potential across the P-N junction and the tuning of Fermi energy level, rectification is observed in an ionic junction similar to a semiconducting junction. The I-V characteristics obtained from such devices obey the rectifying forward bias junction behavior similar to the MWCNTs device characteristics.

Here, microcontact-patterning technique associated with softlithography polymer based processes, typically used for generating microtextured substrates in biotechnology applications was implemented for generating nanomaterial patterns towards building functional crossbars. This technique has helped to overcome some of the issues associated with the use of standard electron beam lithography techniques that are currently being adopted for patterning of individual discrete components of nanomaterials. These include connectivity between nanomaterial, number of functional junctions per array. In addition, this technique reduces the time required for fabricating functional arrays as well as the cost per array. We have demonstrated the formation of crossbar P-N junction arrays using ion doped SWCNTs by adopting microcontact printing technique.

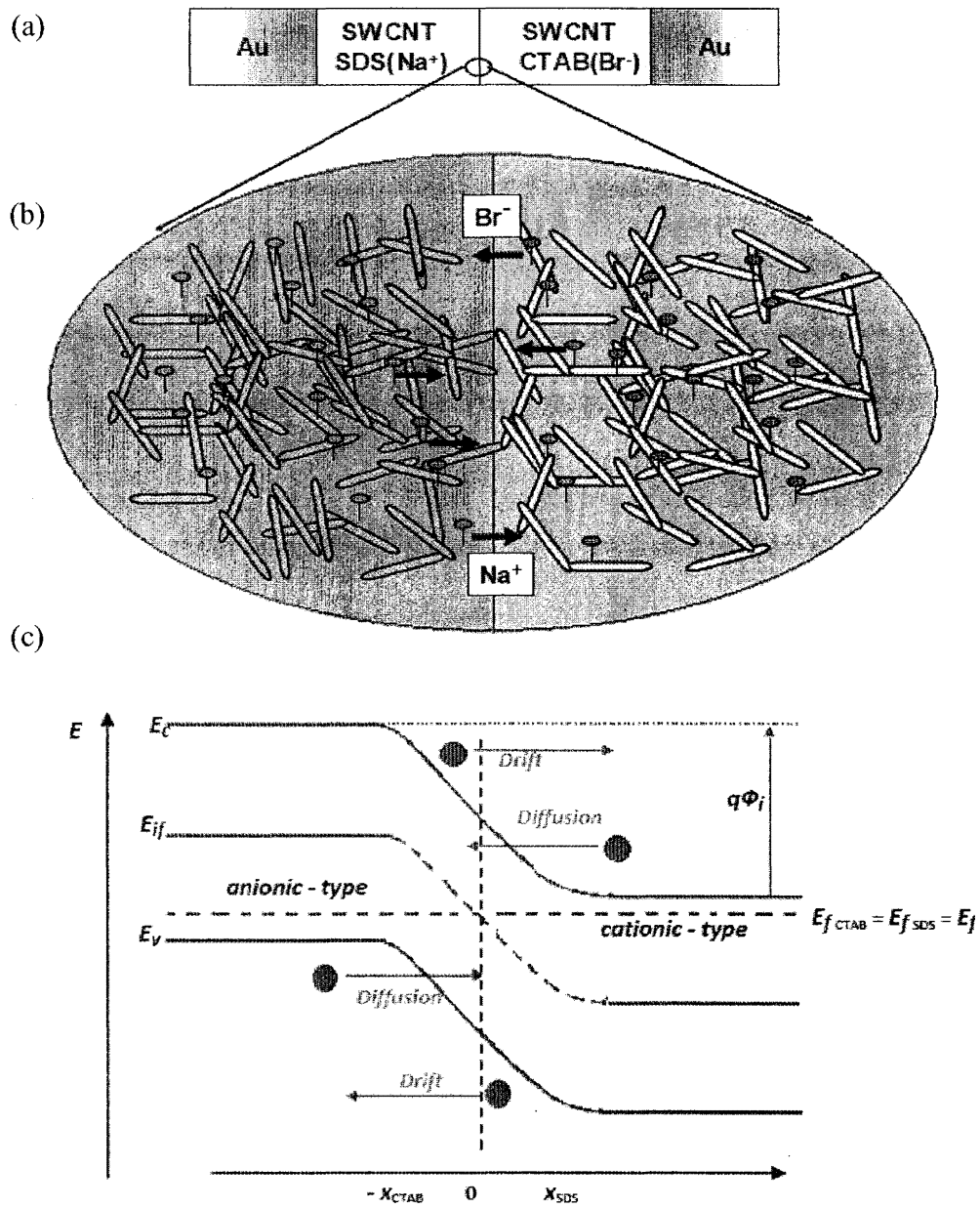


Figure 4.20: Schematic representation of P-N junction and band energy diagram. (a) Schematic representation of the formation of the ionic p-n junction, (b) Counter Flow of Na^+ and Br^- ions results in the generation of the built-in potential across the interface. (c) Band energy diagram of ionic junction at thermal equilibrium showing

band bending due to drift and diffusion of ions at the interface of anionic and cationic SWCNT junction.

The results indicate that the microcontact printing technique and the extrinsic chemical doping process can be used to form functional crossbar junctions that may have potential in device applications. The fundamental issue is the efficacy of the junction functionalization and the refresh rates associated with the functionalization. However, aging of the surfactants is dependent on their concentration. The surfactant being non volatile in nature, the functionalization of SWCNTs maintained as long as the concentration of surfactant solution is greater than 1% by volume. Once functionalized CNTs are patterned and the ions are intercalated, devices formed show junction characteristics consistently. If the concentration of surfactant is less than 1% weight by volume, the surfactant molecules floats in the liquid solution, thereby having mixtures of intrinsic SWCNTs in ionic medium. Thus, device fabricated demonstrates resistive behavior.

The demand for fabrication of high-density devices has resulted in the exploration of nanomaterials as device components. A number of nanoscale fabrication, patterning techniques, and alignment techniques have been explored for obtaining high throughput device architectures. Microcontact patterning technique associated with softlithography polymer based processes was implemented for simultaneous and rapid assembly of nanomaterials. The microcontact printing technique was adopted towards assembling high-density, crossbar junction devices. I have demonstrated the formation

of crossbar junction arrays using CNTs by implementing microcontact printing technique. This fundamental study integrates CNTs with microstructures in the patterned manners such that they can be easily probed for electrical characterization. This device is a good example of multidimensional integration of CNTs with metallic microelectrodes. These microelectrodes can be probed using standard lead based address lines associated with IC technology. The results indicated that the microcontact printing technique has wide applications in the future development of prototyping rapid and inexpensive nanoscale devices. In addition, this technique provides the capability of simultaneous patterning of both similar and disparate nanomaterials. Thus, it is a faster technique than the standard nanolithography techniques for nanodevice fabrication. Finally as the observed I-V characteristics were similar to those observed from nanodevices fabricated by standard lithography techniques, but at reduced cost per device, so this technique can provide more cost effective devices.

CHAPTER 5

CONCLUSION AND FUTURE WORK

In conclusion, we have demonstrated a simple, low cost and rapid prototype technique for developing crossbar MWCNT junction arrays. Similar to printing color ink onto piece of paper, in my research, using flexible polymeric stamp having microrelief structures, CNTs are inked and patterned on base Si substrate with microelectrode array to form a nanoelectronic crossbar junction device.

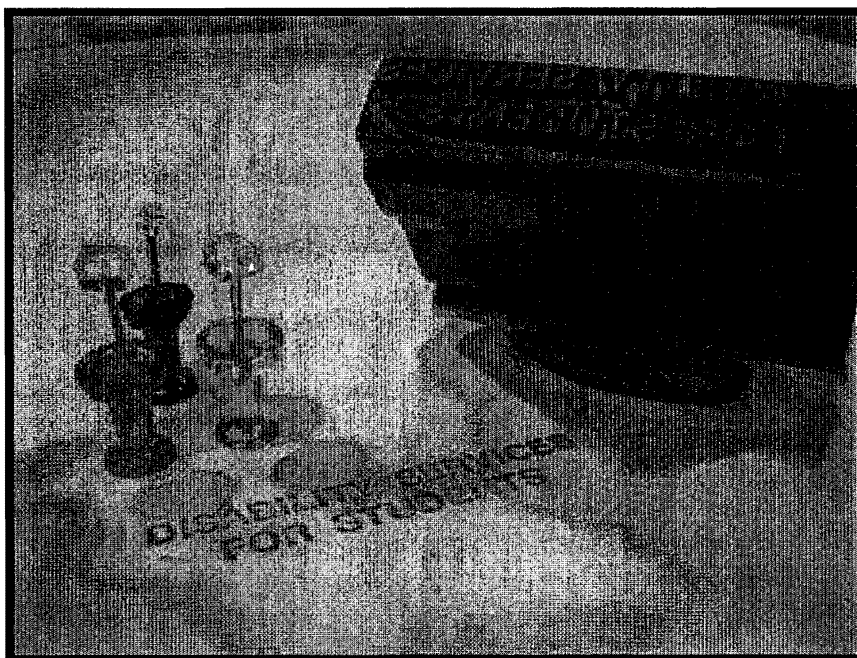


Figure.5.1: A pictorial representation of a generic approach for assembling and patterning nanomaterial using microcontact printing.

These studies provide a generic approach for assembly and patterning nanomaterial via microcontact printing which is shown in figure 5.1. In addition, we have integrated

bottom-up and top-down technology to develop these devices. The I-V characteristics and the data values suggest the formation of crossbar junction arrays with characteristics comparable to those formed using more complex nanofabrication techniques. The crossbar junction shows promising results towards the future development of crossbar junction diodes. Lastly, high density nanostructured sensor platform can be implemented by using simple micro and nanoarray devices, which can be used for biochemical sensors. We believe that fabrication of high-density nanoarray devices using the nanoprinting technique will provide a wide scope for future nanomaterials-based sensor devices. This could be a new asset to the world of nanosensor.

In addition, I have demonstrated a method for chemically modulating the electrical properties of nanomaterials and implemented a simple, low cost and rapid prototyping technique for developing crossbar ionic P-N junction arrays. This study shows generic a approach for patterning and assembling nanomaterial via microcontact printing. Secondly, simple extrinsic doping technique has been adapted in which dopant agent has been introduced which alters the intrinsic semiconducting property of nanomaterial. The rectification characteristics graph suggested formation of P-N ionic junction using microcontact printing similar to that of semiconductor p-n junctions formed using complex nanofabrication techniques. Lastly, the electrical characteristics of the assembled crossbar P-N junction shows promise towards the formation of a junction diode array which can be used for the detection of biological and chemical species in atmosphere or process gases and is of a great concern in relation to

environmental pollution, industrial emission monitoring and process control, medical diagnosis, public security, agriculture and a variety of industries. I believe that the chemical modulation method and microcontact printing techniques will have a wide scope for development of nanomaterial-based devices.

One of the advantages of this technique is the ability to pattern homogeneous as well as heterogeneous material on to the same substrate to form multi functional building blocks of a wide range of geometries. . The nanomaterial patterns produced using this technique can be generated at a much faster rate than the standard nanolithography techniques for nanodevice fabrication. Despite the advantages described earlier in fabricating the crossbar junction there are still considerable limitations in aligning single CNTs in an array due to the size mismatch between the master mold and the diameter of the single CNTs. It is extremely difficult to achieve alignment with precision. This limitation need to be overcome to improve the efficiency of the devices. The reproducibility of the device arrays is still an issue as this technique is based on microscale patterning of nanoscale materials. This results in the deposition of arrays/bundles of CNTs as opposed to a sequence of single tubes. These issues can be improved by incorporating nanoimprinting techniques. Also, due to the limitation of photolithography, where the smallest dimension that can be achieved is 5 μ m, another alternative plan is the use of electron beam lithography or focus ion beam techniques to create structures for the alignment of nanomaterials. In addition, the contact resistance, as well as the junction resistance is large and can be decreased by improving the interfacing techniques by using back contact electrodes during the

fabrication of the microelectrode array structures. In addition, improvement in performance of junction characteristics is also possible by optimizing the relief structure width and passivation of these nanostructures.

REFERENCES

- [1] M. S. Fuhrer, Nyg, aring, J. rd, L. Shih, M. Forero, Y.-G. Yoon, M. S. Mazzoni, nbsp, C, H. J. Choi, J. Ihm, S. G. Louie, A. Zettl, and P. L. McEuen, "Crossed Nanotube Junctions," *Science*, vol. 288, pp. 494-497, April 21, 2000 2000.
- [2] R. Martel, T. Schmidt, H. R. Shea, T. Hertel, and A. Ph, "Single- and multi-wall carbon nanotube field-effect transistors." vol. 73: AIP, 1998, pp. 2447-2449.
- [3] S. K. Padigi, R. K. Reddy, and S. Prasad, "Carbon nanotube based aliphatic hydrocarbon sensor," *Biosensors and Bioelectronics*, vol. 22, pp. 829-837, 2007.
- [4] D. Whang, S. Jin, Y. Wu, and C. M. Lieber, "Large-Scale Hierarchical Organization of Nanowire Arrays for Integrated Nanosystems," *Nano Letters*, vol. 3, pp. 1255-1259, 2003.
- [5] N. A. Melosh, A. Boukai, F. Diana, B. Gerardot, A. Badolato, P. M. Petroff, and J. R. Heath, "Ultrahigh-Density Nanowire Lattices and Circuits," *Science*, vol. 300, pp. 112-115, April 4, 2003.
- [6] K. Takuya, A. Masashi, F. Akira, Y. Kenji, O. Yukinori, I. Hiroshi, and T. Yasuo, "Single-electron device using Si nanodot array and multi-input gates," in *Solid-State and Integrated Circuit Technology, 2006. ICSICT '06. 8th International Conference on*, 2006, pp. 1062-1064.

- [7] K. Takuya, O. Takahide, A. Masashi, T. Yasuo, and C. Jung-Bum, "Multifunctional Device Using Nanodot Array," *Jpn J Appl Phys* vol. 45, pp. 5317-5321, 2006.
- [8] P. D. K. A. S. B. L. Allen, "Carbon Nanotube Field-Effect-Transistor-Based Biosensors," *Adv. Materials*, vol. 19, pp. 1439-1451, 2007.
- [9] A. Bachtold, P. Hadley, T. Nakanishi, and C. Dekker, "Logic Circuits with Carbon Nanotube Transistors," *Science*, vol. 294, pp. 1317-1320, November 9, 2001.
- [10] W. Hui, L. Dandan, and P. Wei, "Fabrication, assembly, and electrical characterization of CuO nanofibers," *Appl. Phys. Lett.*, vol. 89, p. 133125, 2006.
- [11] Y. Cui, Z. Zhong, D. Wang, W. U. Wang, and C. M. Lieber, "High Performance Silicon Nanowire Field Effect Transistors," *Nano Letters*, vol. 3, pp. 149-152, 2003.
- [12] J. B. Jackson, J. Sun-Gon, D. Kapoor, and M. S. Miller, "Integrated silicon nanowire diodes," in *Microelectronics and Electron Devices, 2006. WMED '06. 2006 IEEE Workshop on*, 2006, p. 2 pp.
- [13] G. Goncher, R. Solanki, J. Carruthers, J. Conley, and Y. Ono, "p-n junctions in silicon nanowires," *Journal of Electronic Materials*, vol. 35, pp. 1509-1512, 2006.
- [14] M. P. Anantram and F. onard, "Physics of carbon nanotube electronic devices," *Reports on Progress in Physics*, vol. 69, pp. 507-561, 2006.

- [15] C. C. Intelligence, "**Organic semiconductors - an emerging industry**," *Display Technology Investor*, 2005.
- [16] L. Boyang and H. Seng-Tiong, "Sub-100 nm Nanolithography and Pattern Transfer on Compound Semiconductor Using Sol-Gel-Derived TiO₂ Resist," *J. Electrochem. Soc.*, vol. 155, pp. P57-P60, 2008.
- [17] F. o. Microfabrication, *Fundamentals of Microfabrication* 1st ed.: CRC-Press, 1998.
- [18] P. Gargini, "Silicon Nanoelectronics and Beyond," *Journal of Nanoparticle Research*, vol. 6, pp. 11-26, 2004.
- [19] S. Miya, S. Muramatsu, N. Kuze, K. Nagase, T. Iwabuchi, A. Ichii, M. Ozaki, and I. Shibasaki, "AlGaAsSb buffer/barrier on GaAs substrate for InAs channel devices with high electron mobility and practical reliability," *Journal of Electronic Materials* vol. 25, pp. 415-420, 1996.
- [20] S. Bollaert, A. Cappy, Y. Roelens, J. S. Galloo, C. Gardes, Z. Teukam, X. Wallart, J. Mateos, T. Gonzalez, B. G. Vasallo, B. Hackens, L. Berdnarz, and I. Huynen, "Ballistic nano-devices for high frequency applications," *Thin Solid Films*, vol. 515, pp. 4321-4326, 2007.
- [21] M. C. McAlpine, R. S. Friedman, S. Jin, K. h. Lin, W. U. Wang, and C. M. Lieber, "High-Performance Nanowire Electronics and Photonics on Glass and Plastic Substrates," *Nano Letters*, vol. 3, pp. 1531-1535, 2003.

- [22] S. Ju, A. Facchetti, Y. Xuan, J. Liu, F. Ishikawa, P. Ye, C. Zhou, T. J. Marks, and D. B. Janes, "Fabrication of fully transparent nanowire transistors for transparent and flexible electronics," *Nat Nano*, vol. 2, pp. 378-384, 2007.
- [23] H. J. Levinson, *Principles of Lithography*, 2nd ed.: SPIE Publications, 2005.
- [24] G. A. DeRose, L. Zhu, J. K. S. Poon, A. Yariv, and A. Scherer, "Periodic sub-wavelength electron beam lithography defined photonic crystals for mode control in semiconductor lasers," *Microelectronic Engineering*, vol. 85, pp. 758-760, 2008.
- [25] M. Hatzakis, "Electron beam processing systems (a state of the art review)." vol. 14, 1974, pp. 516-517.
- [26] G. M. W. Younan Xia, "Soft Lithography," *Review*, vol. 37, pp. 550-575, 1998.
- [27] Fern, xe, S. ndez, xe, C. nchez, xe, sar, V. J. Cadarso, M. Darder, Dom, xed, C. nguez, and A. Llobera, "Patterning High-Aspect-Ratio Sol–Gel Structures by Microtransfer Molding," *Chem. Mater.*, vol. 20, pp. 2662-2668, 2008.
- [28] Y. X. G. M. W. Xiao-Mei Zhao, "Fabrication of three-dimensional micro-structures: Microtransfer molding," *Advanced Materials*, vol. 8, pp. 837-840, 1996.
- [29] E. Kim, Y. Xia, and G. M. Whitesides, "Micromolding in Capillaries: Applications in Materials Science," *J. Am. Chem. Soc.*, vol. 118, pp. 5722-5731, 1996.

- [30] A. Blümel, A. Klug, S. Eder, U. Scherf, E. Moderegger, and E. J. W. List, "Micromolding in capillaries and microtransfer printing of silver nanoparticles as soft-lithographic approach for the fabrication of source/drain electrodes in organic field-effect transistors," *Organic Electronics*, vol. 8, pp. 389-395, 2007.
- [31] S. J. Park, J. Zheng, T. S. Anderson, M. Lu, B. T. Cunningham, and J. G. Eden, "Transparent, Flexible Microplasma Arrays Fabricated by a Micro Replica Molding Process," in *Plasma Science, 2007. ICOPS 2007. IEEE 34th International Conference on*, 2007, pp. 219-219.
- [32] J. G. M. R. L. N. H. V. D. Losic, "Rapid Fabrication of Micro- and Nanoscale Patterns by Replica Molding from Diatom Biosilica," *Advanced Functional Materials*, vol. 17, pp. 2439-2446, 2007.
- [33] T.-K. Shih, C.-F. Chen, J.-R. Ho, and F.-T. Chuang, "Fabrication of PDMS (polydimethylsiloxane) microlens and diffuser using replica molding," *Microelectronic Engineering*, vol. 83, pp. 2499-2503, 2006.
- [34] A. K. H. A. B. E. K. a. G. M. W. James L Wilbur, "Microcontact printing of self-assembled monolayers: applications in microfabrication," *Nanotechnology*, vol. 7, p. 452, 1996.
- [35] Y. Chen, A. Lebib, F. Carcenac, H. Launois, G. Schmidt, M. Tormen, G. Müller, L. W. Molenkamp, M. Liebau, J. Huskens, and S. N. Reinhoudl, "Microcontact printing and pattern transfer with a tri-layer processing," *Microelectronic Engineering*, vol. 53, pp. 253-256, 2000.

- [36] P. Yang, "Nanotechnology: Wires on water," *Nature*, vol. 425, pp. 243-244, 2003.
- [37] F. K. Peidong Yang, "Langmuir-Blodgett Assembly of One-Dimensional Nanostructures," *ChemPhysChem*, vol. 3, pp. 503-506, 2002.
- [38] J. R. Heath, "Superlattice Nanowire Pattern Transfer (SNAP)," *ASAP Acc. Chem. Res*, 2008.
- [39] A. Tafazzoli, C. Pawashe, and M. Sitti, "Atomic force microscope based two-dimensional assembly of micro/nanoparticles," in *Assembly and Task Planning: From Nano to Macro Assembly and Manufacturing, 2005. (ISATP 2005). The 6th IEEE International Symposium on*, 2005, pp. 230-235.
- [40] T. Yoshinobu, W. C. Moon, A. Nishikawa, J. Suzuki, and H. Iwasaki, "Patterning of Biomolecules on Silicon by AFM Oxidation," *IEEE*, vol. 11, pp. 336-337.
- [41] M. Senthil Kumar, S. H. Lee, T. Y. Kim, T. H. Kim, S. M. Song, J. W. Yang, K. S. Nahm, and E. K. Suh, "DC electric field assisted alignment of carbon nanotubes on metal electrodes," *Solid-State Electronics*, vol. 47, pp. 2075-2080, 2003.
- [42] Y. Huang, X. Duan, Q. Wei, and C. M. Lieber, "Directed Assembly of One-Dimensional Nanostructures into Functional Networks," *Science*, vol. 291, pp. 630-633, January 26, 2001 2001.
- [43] A. Grüneis, C. Kramberger, D. Grimm, T. Gemming, M. H. Rummeli, A. Barreiro, P. Ayala, T. Pichler, C. Schaman, H. Kuzmany, J. Schumann, and B.

- Büchner, "Eutectic limit for the growth of carbon nanotubes from a thin iron film by chemical vapor deposition of cyclohexane," *Chemical Physics Letters*, vol. 425, pp. 301-305, 2006.
- [44] H. H. Solak, C. David, J. Gobrecht, V. Golovkina, F. Cerrina, S. O. Kim, and P. F. Nealey, "Sub-50 nm period patterns with EUV interference lithography," *Microelectronic Engineering*, vol. 67-68, pp. 56-62, 2003.
- [45] L. Jing and J. K. Lumpp, "Electrical and mechanical characterization of carbon nanotube filled conductive adhesive," in *Aerospace Conference, 2006 IEEE*, 2006, p. 6 pp.
- [46] C. P., J. Poole, and F. J. Owens, *Introduction to Nanotechnology* Wiley-Interscience 2003.
- [47] X.-F. Wang, Z.-J. Xu, and Z.-Y. Zhu, "Reversible mechanical bistability of carbon nanotubes under radial compression," *Chemical Physics*, vol. 334, pp. 144-147, 2007.
- [48] M. Samec, "Electron Dynamics of Single-Walled Carbon Nanotubes," *Journal of Young Investigators*, vol. 9, 2003.
- [49] Y. Cheng and O. Zhou, "Electron field emission from carbon nanotubes," *Comptes Rendus Physique*, vol. 4, pp. 1021-1033, 2003.
- [50] J. Hone, M. Whitney, C. Piskoti, and A. Zettl, "Thermal conductivity of single-walled carbon nanotubes," *Physical Review B*, vol. 59, pp. R2514 - R2516, 1999.

- [51] Y. A. Kim, H. Muramatsu, T. Hayashi, M. Endo, M. Terrones, and M. S. Dresselhaus, "Thermal stability and structural changes of double-walled carbon nanotubes by heat treatment," *Chemical Physics Letters*, vol. 398, pp. 87-92, 2004.
- [52] R. Martel, V. Derycke, J. Appenzeller, S. Wind, and A. Ph, "Carbon nanotube field-effect transistors and logic circuits," in *Proceedings of the 39th conference on Design automation* New Orleans, Louisiana, USA: ACM, 2002.
- [53] C. Po-Wen and C. Chien-Hua, "High-performance carbon nanotube network transistors for logic applications," *Appl. Phys. Lett.* , vol. 92, p. 063511, 2008.
- [54] A. Javey, H. Kim, M. Brink, Q. Wang, A. Ural, J. Guo, P. McIntyre, P. Mceuen, M. Lundstrom, and H. Dai, "High- κ dielectrics for advanced carbon nanotube transistors and logic gates," *Nature*, vol. 1, pp. 241-246, 2002.
- [55] A. G. Mamalis, L. O. G. Vogtländer, and A. Markopoulos, "Nanotechnology and nanostructured materials: trends in carbon nanotubes," *Precision Engineering*, vol. 28, pp. 16-30, 2004.
- [56] T. Rueckes, K. Kim, E. Joselevich, G. Y. Tseng, C.-L. Cheung, and C. M. Lieber, "Carbon Nanotube-Based Nonvolatile Random Access Memory for Molecular Computing," *Science*, vol. 289, pp. 94-97, July 7, 2000.
- [57] S. Akita and Y. Nakayama, "Manipulation of Nanomaterial by Carbon Nanotube Nanotweezers in Scanning Probe Microscope," *Jpn. J. Appl. Phys.*, vol. 21, pp. 4242-4245 2002.

- [58] P. Kim and C. M. Lieber, "Nanotube Nanotweezers," *Science*, vol. 286, pp. 2148-2150, December 10, 1999.
- [59] J. Li, Y. Lu, Q. Ye, L. Delzeit, and M. Meyyappan, "A Gas Sensor Array Using Carbon Nanotubes and Microfabrication Technology," *Solid-State Lett.*, vol. 8, pp. H100-H102 2005.
- [60] F. Villalpando-Páez, A. H. Romero, E. Muñoz-Sandoval, L. M. Martínez, H. Terrones, and M. Terrones, "Fabrication of vapor and gas sensors using films of aligned CNx nanotubes," *Chemical Physics Letters*, vol. 386, pp. 137-143, 2004.
- [61] M. Shiraishi, T. Takenobu, A. Yamada, M. Ata, and H. Kataura, "Hydrogen storage in single-walled carbon nanotube bundles and peapods," *Chemical Physics Letters*, vol. 358, pp. 213-218, 2002.
- [62] C. V. Nguyen, Q. Ye, and M. Meyyappan, "Carbon nanotube tips for scanning probe microscopy: fabrication and high aspect ratio nanometrology," *Meas. Sci. Technol.*, vol. 16, pp. 2138-2146, 2005.
- [63] L. Forró and C. Schönenberger, "Carbon nanotubes, materials for the future," *Europhysics News*, vol. 32, 2001.
- [64] H. S. Gokturk, "Electrical properties of ideal carbon nanotubes," in *Nanotechnology, 2005. 5th IEEE Conference on*, 2005, pp. 677-680 vol. 672.
- [65] M. Balkanski, "Physical Properties of Carbon Nanotubes, Edited by R. Saito, G. Dresselhaus and M.S. Dresselhaus, Imperial College Press, London, 1998," *Materials Science and Engineering B*, vol. 76, pp. 241-242, 2000.

- [66] L. Duclaux, "Review of the doping of carbon nanotubes (multiwalled and single-walled)," *Carbon*, vol. 40, pp. 1751-1764, 2002.
- [67] T. McNeish, G. Gumbs, and A. Balassis, "Model of plasmon excitations in a bundle and a two-dimensional array of nanotubes," *Phys. Rev. B* vol. 77, 2008.
- [68] J.-C. Charlier, A. De Vita, X. Blase, and R. Car, "Microscopic Growth Mechanisms for Carbon Nanotubes," *Science*, vol. 275, pp. 647-649, January 31, 1997 1997.
- [69] "Nanowires, nanowhiskers and green LEDs," *III-Vs Review*, vol. 19, pp. 43-46, 2006.
- [70] P. Y. Y. Xia, "Guest Editorial: Chemistry and Physics of Nanowires," *Advanced Materials*, vol. 15, pp. 351-352, 2003.
- [71] K. Takayanagi, Y. Kondo, and H. Ohnishi, "Suspended Gold Nanowires: Ballistic Transport of Electrons," *JSAP International*, vol. 70, pp. 3-8, 2001.
- [72] A. Facchetti, "Semiconductors for organic transistors," *Materials Today*, vol. 10, pp. 28-37, 2007.
- [73] A. L. Paul, P. K. Gary, and H. K. Zakya, "Efficient, single-layer molecular organic light-emitting diodes," vol. 90, p. 023511, 2007.
- [74] X. Jiangeng and R. F. Stephen, "Organic thin-film transistors based on bis(1,2,5-thiadiazolo)-p-quinobis (1,3-dithiole)," vol. 79, pp. 3714-3716, 2001.
- [75] L. Rubin and J. Poate, "Ion Implantation in Silicon Technology," *The Industrial Physicist*, vol. 9, pp. 12-15, 2003.

- [76] T. Burakowski and T. Wierzchon, *Surface Engineering of Metals: Principles, Equipment, Technologies* 1st ed.: CRC, 1998.
- [77] S. Sienz, B. Rauschenbach, A. Wenzel, A. Lell, S. Bader, and V. Härle, "In-situ stress measurement during the ion implantation-induced doping of gallium nitride," *Thin Solid Films*, vol. 415, pp. 1-4, 2002.
- [78] T. S. Jeong, M. S. Han, J. H. Kim, C. J. Youn, Y. R. Ryu, and H. W. White, "Crystallinity-damage recovery and optical property of As-implanted ZnO crystals by post-implantation annealing," *Journal of Crystal Growth*, vol. 275, pp. 541-547, 2005.
- [79] A. D. Korotaev and A. N. Tyumentsev, "Amorphization of metals by ion implantation and ion mixing methods," *Russian Physics Journal*, vol. 37, pp. 703-724, 1994.
- [80] M. Abbas, H. Kerkow, and R. Wedell, "Heavy Ion Channeling Implantation Processes in Single Crystals," *physica status solidi* vol. 159, pp. 597-608, 1990.
- [81] M. C. Tringides, *Surface Diffusion: Atomistic and Collective Processes* 1st ed.: Springer, 1997.
- [82] R. Kelly, "Bubble Diffusion and the Motion of Point Defects near Surfaces. (Diffusion Theory for Discrete Media, Part IV)," *physica status solidi* vol. 21, pp. 451-459, 1967.

- [83] A. B. Artyukhin, M. Stadermann, R. W. Friddle, P. Stroeve, O. Bakajin, and A. Noy, "Controlled Electrostatic Gating of Carbon Nanotube FET Devices," *Nano Letters*, vol. 6, pp. 2080-2085, 2006.
- [84] Y. Nosh, Y. Ohno, S. Kishimoto, and T. Mizutani, "The effects of chemical doping with F4TCNQ in carbon nanotube field-effect transistors studied by the transmission-line-model technique," *Nanotechnology*, vol. 18, 2007.
- [85] C. Zhou, J. Kong, E. Yenilmez, and H. Dai, "Modulated Chemical Doping of Individual Carbon Nanotubes," *Science*, vol. 290, pp. 1552-1555, November 24, 2000.
- [86] J. U. Lee, P. P. Gipp, and C. M. Heller, "Carbon nanotube p-n junction diodes," *Applied Physics Letters* vol. 85, pp. 145-147, 2004.
- [87] V. Derycke, R. Martel, J. Appenzeller, and P. Avouris, "Carbon Nanotube Inter- and Intramolecular Logic Gates," *Nano Letters*, vol. 1, pp. 453-456, 2001.
- [88] A. Javey, R. Tu, D. B. Farmer, J. Guo, R. G. Gordon, and H. Dai, "High Performance n-Type Carbon Nanotube Field-Effect Transistors with Chemically Doped Contacts," *Nano Letters*, vol. 5, pp. 345-348, 2005.
- [89] J. Appenzeller, L. Yu-Ming, J. Knoch, C. Zhihong, and P. Avouris, "Comparing carbon nanotube transistors - the ideal choice: a novel tunneling device design," *Electron Devices, IEEE Transactions on*, vol. 52, pp. 2568-2576, 2005.

- [90] X. Duan, C. Niu, V. Sahi, J. Chen, J. W. Parce, S. Empedocles, and J. L. Goldman, "High-performance thin-film transistors using semiconductor nanowires and nanoribbons," *Nature*, vol. 425, pp. 274-278, 2003.
- [91] Y. Huang, X. Duan, Y. Cui, and C. M. Lieber, "Gallium Nitride Nanowire Nanodevices," *Nano Letters*, vol. 2, pp. 101-104, 2002.
- [92] M.-F. Yu, O. Lourie, M. J. Dyer, K. Moloni, T. F. Kelly, and R. S. Ruoff, "Strength and Breaking Mechanism of Multiwalled Carbon Nanotubes Under Tensile Load," *Science*, vol. 287, pp. 637-640, January 28, 2000.
- [93] T. K. a. X. W. X Chen, "Effects of initial stress on wave propagation in multi-walled carbon nanotubes," *Physica Scripta*, vol. 78, p. 015601, 2008.
- [94] C. Richard, F. Balavoine, P. Schultz, T. W. Ebbesen, and C. Mioskowski, "Supramolecular Self-Assembly of Lipid Derivatives on Carbon Nanotubes," *Science*, vol. 300, pp. 775-778, May 2, 2003 2003.
- [95] C. Bagdassarian, W. M. Gelbart, and A. Ben-Shaul, "Liquid crystalline states of surfactant solutions of isotropic micelles," *Journal of Statistical Physics*, vol. 52, pp. 1307-1313, 1988.
- [96] H. Dai, "Carbon Nanotubes: Synthesis, Integration, and Properties," *Acc. Chem. Res.*, vol. 35, pp. 1035-1044, 2002.
- [97] Y. Zhou, A. Gaur, S.-H. Hur, C. Kocabas, M. A. Meitl, M. Shim, and J. A. Rogers, "p-Channel, n-Channel Thin Film Transistors and p-n Diodes Based on Single Wall Carbon Nanotube Networks." vol. 4, 2004, pp. 2031-2035.

- [98] C. H. W. Cheng, S. W. Boettcher, D. H. Johnston, and M. C. Lonergan, "Unidirectional Current in a Polyacetylene Hetero-ionic Junction." vol. 126, 2004, pp. 8666-8667.
- [99] D. A. Bernards, S. Flores-Torres, H. D. Abruna, and G. G. Malliaras, "Observation of Electroluminescence and Photovoltaic Response in Ionic Junctions." vol. 313, 2006, pp. 1416-1419.
- [100] M. S. Jay, Y. L. Li, G. Th, and E. F. Schubert, "Experimental analysis and theoretical model for anomalously high ideality factors ($n \gg 2.0$) in AlGaIn/GaN p-n junction diodes." vol. 94: AIP, 2003, pp. 2627-2630.

APPENDIX A
Operating Instructional Manual

OPERATING INSTRUCTIONAL MANUAL

SPIN COATER - P6700 Series, Specialty Coating System Inc.

Initial State Check

If the display on the front of the spinner is blank turn power ON using the POWER switch located on the rear panel of the spinner.

- After five seconds the display will change to *Message mode* where RECIPE #, RPM, TIME, AND PRESS START/ TO INITIATE will appear.
- The computer response is delayed after entering commands by several seconds. Enter each command then wait for display to change.
- Enter the programming mode by pressing **CHG PRE**. This changes the display screen to a parameters display. A flashing cursor will be in the left column, at the word RECIPE.
- Press **ENT** to move cursor to the right column.
- To change the recipe number use the + key to count up or the – key to count down.
- To accept the changes and return to *Operation mode*, Press **MSG**.
- Recipes

Editing a Recipe

- Enter the programming mode by pressing **CHG PRE**. This changes the display screen to a parameters display. A flashing cursor will be in the left column, at the word **RECIPE**.

- To locate a specific parameter line, press the + or – keys. This moves up or down to the desired parameter. (But only if the cursor is in the *left* column.)
- To access the parameter numbers, press **ENT**. This moves the cursor to the right column where the numbers are.
- To select parameter digit, press <- to move the cursor left or -> to move the cursor right. To raise or lower a value, use the + or – keys. The number will count up or down. (But only if the cursor is in the *right* column.)
- To accept the new setting press **ENT**. The cursor will move back to the left column.
- Repeat steps until you are done making changes. Additional information on creating a recipe is located in the Specialty Coating Systems P6700 Spinner Operator's Instruction Manual on pages 11-15.
- To accept and return to operation mode, press **MSG**.

Starting a Program

- Place the substrate on the vacuum chuck (substrate must be centered for proper operation).
- Manually dispense your desired coating solution onto the center of the substrate using a pipette.
- Press **START** (Green light illuminates). The instrument will take a few seconds to check the vacuum. If the vacuum is present, spin coater will start. Spin rate is indicated on the display. The time remaining to complete the process will also be

indicated on the display. When the cycle is complete, the Start LED will extinguish.

- Note: The process can be stopped at any time by pressing the STOP button.
- Remove bowl cover.
- Remove substrate from vacuum chuck.

SPUTTER COATER - 208HR, Cressington Scientific Instruments Ltd

Initial Set up

- Lift the top-plate and remove the glass cylinder.
- Remove the dark space shield by loosening the M3 cap screw using a 2.5 hexagon key.
- Unscrew the clamp ring with the top-plate close to the horizontal position.
- Using this position allows the target to remain in the clamp ring when it is completely removed from the target holder.
- FOIL TARGETS: Remove the clamp ring with spacer ring and foil target.
- Au TARGET: Remove the clamp ring and place the Au target
- Load the sample, close the chamber top-plate, and press POWER. The unit will start up in AUTO. Select CYCLE.

Starting program

- The unit will proceed through its standard cycle of:-
pump to 0.05mb

open argon flush valve for 3 seconds, then close

pump to 0.15mb

open argon flush valve for 3 seconds, then close

open leak valve

pump to 0.15mb and continue pumping for further 20 seconds

set MTM-20 to ZERO

switch on sputter supply at preselected current

switch off sputter supply at preselected time/thickness.

- And each step in the process is shown by the indicator lights over the manual control buttons.
- Remove the target from the clamp ring
- Remove the deposit from inside the glass cylinder by wiping with a lint-free tissue or cloth. A 50:50 mixture of acetone and propan-2-ol (isopropanol) is suitable

MASK ALIGNER - Hydralign Series 200 IR, Optical Associates Inc

Initial Setup

- Turn on the vacuum pump and open the vacuum valve on top of the pump.
- Turning on and warming up the lamp
- Plug in the blower that exhausts ozone from the lamp. The blower is housed in the hood with the spincoater.

- To “ignite” the lamp, depress the “Start” switch momentarily, releasing when the lamp ignites (you can tell when this happens because the voltage drops and the power supply makes a high pitched sound).
- The lamp needs to warm up for at least five minutes.
- Switch the intensity-power selector to “mW/cm²”. It should read near zero. Now that the lamp is warm, perform an intensity reading with the OAI UV Powermeter. Note the intensity reading on the meter. The intensity has been set at 35 mW/cm² and your reading should be close to that value.

Loading the mask and substrate

- Move the microscope to the back of the aligner by pressing in on the button on the main supporting arm (that slides on a rail in the base of the aligner) and pushing the whole stage back.
- Place your chip on the cross in the middle of the vacuum chuck. The chip must cover the entire cross, otherwise it will not be held down properly when vacuum is applied.
- You are now ready to expose your substrate.
- Check or set the desired exposure time (in seconds) on the left of the front panel of the aligner.
- Press the button on the handle of the alignment module and slide it under the lamp housing. After about one second, the shutter will automatically open, expose your sample and close.

- Slide the alignment module back to the alignment position.
- You can now remove the substrate.
- Shutting down the system
- After allowing the lamp to cool for a few minutes, turn of the exhaust blower.
- Close the vacuum valve and turn off the vacuum pump.